The SPIRAL radioactive ion beam facility

N. Alamanos, Y. Blumenfeld, H. Doubre, D. Guillemaud-Mueller, A.C.
Mueller, N. Schultz, Y. Schutz, J.C. Steckmeyer, J.P. Thibaud, M.
Toulemonde, et al.

The

SPIRAL

Radioactive

Ion

Beam

Facility

May 1994
GANIL R 94 02

SPIRAL
GANIL
Laboratoire commun CEA / DSM - CNRS / IN₂P₃

The SPIRAL Radioactive Ion Beam Facility

May 1994

GANIL R 94 02

SPIRAL
GANIL
Laboratoire commun CEA / DSM - CNRS / IN2P3

FOREWORD

GANIL has been for ten years at the forefront of the physics with medium energy heavy ions beams. The growing interest in the worldwide scientific community for the physics with radioactive beams has prompted our laboratory to engage major efforts in this direction.

This document describes the scientific goals as well as the technical choices of the SPIRAL project (Système de Production d'Ions Radioactifs et d'Accélération en Ligne). This does not intend to be a contractual document but it may serve as a guideline as the main options of the project will remain unchanged.

Our efforts have been recognized by NuPECC which has considered that the domain of nuclei with extreme N/Z ratios and at high energy was well covered by the proposed GANIL facility. Therefore the Committee has recommanded the construction of this facility with a high priority as a European users Laboratory for accelerated radioactive beams.

The SPIRAL project has been officially approved by the french funding agencies and an agreement has been signed in October 1993 by the DSM-CEA, IN2P3-CNRS and the Region of Basse Normandie. The first beam is expected for 1998.

The realization of SPIRAL will be led by M. Lieuvin and several laboratories will be involved in the construction.

Two International Committees have been appointed to follow the project, a Scientific Committee chaired by B. Mottelson and a Technical Committee chaired by M. Prome.

The Human Capital and Mobility program of the European Union has already granted GANIL the role of European host facility. The aim of GANIL is to pursue in that direction and become a center for international exchange in the domain of radioactive beams. This project will be achieved only through a large collaboration with other institutes and any laboratory willing to join in is naturally welcome as our goal is to get the european community strongly involved at any stage of the project.

S. HARAR
Director

D. GUERREAU
Deputy Director

CONTIBUTORS

SCIENTIFIC OBJECTIVES :
N. Alamanos Y. Blumenfeld, R. Dayras, H. Doubre, D. Guillemaud-Mueller, A.C. Mueller, N. Schultz, Y. Schultz, J.C. Steckmeyer, J.P. Thibaud, M. Toulemonde.

TECHNICAL DESIGN :
R. Anne, E. Baron, P. Bertrand, D. Bibet, C. Bieth, M.P. Bourgarel, P. Bricault, B. Bru, A. Chabert, M. Duval, A. Joubert, R. Leroy, Ch. Ricaud, P. Sortais, M. Van den Bossche.

EVALUATION OF THE BEAM PERFORMANCES :
N. Alamanos, Y. Blumenfeld, R.Dayras, J. Fermé, B. Fernandez, D. Guerreau, D. Guillemand-Mueller, A.C. Mueller, N. Schultz, Y. Schultz, J.C. Steckmeyer, J.P. Thibaud, M. Toulemonde, G. Walter.

EVALUATION OF THE TECHNICAL OPTIONS :
J.L. Belmont, J. Fermé, M. Gouttefangeas, M. Promé, G. Ryckewaert.

PROGRESS STUDIES :
M. Bajard, L. Bex, M. Bisch, Y. Bourgoin, G. Chamoin, F. Clapier, M. Di Giacomo, F. Daudin, P. Dolegieviez, M. Dufour, G. Dugay, J. Faure, Y Huguet, A. Laisné, P. Leconte, M. Lemaitre, M. Lewitowicz, C.F. Liang, M. Loiselet, T.T. Luong, J. Obert, M. Ozille, P. Paris, J.C. Putaux, F. Ripouteau, G. Ryckewaert, M.G. Saint-Laurent, M. de Saint Simon, A. Tkatchenko, G. Tousset, C. Tribouillard.

EDITOR :
M. Bex.

CONTENTS

PART 1 :

PHYSICS WITH SECONDARY ION BEAMS

PART 2 :

THE SPIRAL PROJECT

PART 3 :

DETAILED TECHNICAL DESCRIPTION
OF THE SPIRAL PROJECT

CONTENTS

We give an account in the following of the work carried out by the GANIL study group and by several units of the CEA/DSM and of the CNRS/IN2P3 from October 1992 to November 1993.

PHYSICS WITH SECONDARY ION BEAMS

I. INTRODUCTION

The unique properties of the atomic nucleus stem from the finite number of constituents and the interactions between them. The shell model provides an excellent description of different nuclear configurations, but it is clear that these configurations (and hence the order in which the shells are filled) can change dramatically when the number of neutrons or protons varies by only a few units. Although some dynamical aspects can be described in classical terms, the nucleus is a quantum system. Very schematically (and grossly oversimplifying) a few valence nucleons and their correlations are responsible for nuclear structure and dynamics and each nucleus is different from its neighbours. This is why so many new phenomena have been discovered by investigating nuclei far from the valley of stability.

The possibility of accelerating these nuclei has opened up new forms of exploration in nuclear physics by providing a number of new situations for the investigation of nuclear structure and reactions. The availability of such secondary beams will also provide for advances in related fields such as astrophysics and condensed matter physics.

After the pioneering efforts of ISOLDE at CERN, the development of the physics of nuclei far from stability now urgently needs the new tool which nuclear physicists are preparing for, namely "Accelerated Secondary Nuclear Beams". Owing to the work of several groups of physicists, the French scientific community has explored the theoretical and practical concerns of the prospects of the physics of secondary nuclear beams. As many general and exhaustive reports have already appeared or will soon be published on this subject, we summarize here only the major points most specific to the GANIL project.

II. NUCLEAR STRUCTURE

Our current understanding of nuclear systems stems mostly from the systematic investigation of properties (mass, momentum, decay modes, etc.) of their ground state. Investigation in the field of exotic nuclei, i.e., far from the valley of β-stability, have led to the discovery of many unexpected phenomena. Tightly connected to the technical progress in accelerators and instrumentation, the advances and surprises in this field of research can be found in the proceedings of the Conferences on "Nuclei Far From Stability" [NFFS 66-92].

However, in the case of nuclei at the limits of β-stability, which open up perhaps the most exciting area of exploration, current knowledge is limited, since each measurement is a major experimental challenge. It is for this reason that nuclear models have rarely been tested except in areas relatively close to stability. Indeed, it is far from stability that new phenomena are expected, such as the onset of new degrees of freedom. It is also worthwhile noting that the behaviour of nuclei far from isospin equilibrium, which is fundamental in nuclear physics, also plays a key role in stellar evolution (see Section VI).

In this context, an accelerator for secondary nuclear beams would enable physicists to perform many new and exciting experiments and hence open up new perspectives on the nuclear system.

II.1 MASS MEASUREMENTS

Once a given nucleus has been shown to be stable (against particle emission) its mass is the first piece of quantitative information which is of interest. Indeed, the binding energy of a nucleus provides fundamental information on its structure. It reflects the subtle balance between nuclear and Coulomb forces and may shed light on the configuration of the nucleons. Data on the mass of the nuclei at the border line of stability challenge theoretical approaches (as in the case of ^{26}O) which draw their predictive power from general considerations. The configurations populated in exotic nuclei are, however, rarely the ones we expect to find. The ingredients for the calculations are determined from stable nuclei, but it is obvious that for exotic N/Z ratios, some characteristics of the effective nuclear forces remain little or entirely unknown, as is shown by the comparison between the predictions of the best theoretical calculations [BER92] and those of systematics when no experimental values are available.

Calculations are needed which contain no free parameters and are based on reliable effective nucleon-nucleon interactions that encompass a vast amount of knowledge of these nuclei. To progress in this area, the experimental data base must be extended to extreme values of isospin.

When direct measurement is not feasible, the mass of exotic nuclei can be calculated with the isobaric multiplet mass equation (IMME). Recent findings [BOR92] show that this equation retains an excellent predictive power for A ≥ 30. Nevertheless, the structure of nuclei located at the drip-line is still too poorly known for predictions to be reliable. Indeed, these systems are so loosely bound that three-body effects can play a major role. A recent study [COM88] illustrates these difficulties by revealing a systematic discrepancy between predictions by local mass formulae and experimental values for nuclei located at the proton drip-line. The observed effect strongly affects the location of the proton drip-line and, consequently, the possible occurrence of one- and two-proton radioactivity. In contrast, an error in the mass prediction indicates a misunderstanding of the underlying nuclear structure, for example, the relative position of poorly known shells. The extreme sensitivity of the r-process path (which takes place far from stability) to nuclear masses has recently been demonstrated [ARN90].

From an experimental standpoint, two different operating modes of the SPIRAL accelerator can provide new data on masses far from stability. The nucleus to be studied may be accelerated by SPIRAL or produced in a reaction induced by a SPIRAL beam. In the first case, the nucleus is synthesized in the SPIRAL ion source and its subsequent acceleration allows an excellent determination of its mass through measurements of flight- time and magnetic rigidity. Such experiments are feasible, after post-acceleration, with the SPEG spectrometer [GIL86] or in SPIRAL itself, used as an "accelerator mass spectrometer" [AUG91]. As compared to other methods, such as ion traps or storage rings, this method has the advantage of only requiring a few nuclei and being applicable to nuclei with relatively short half-lives.

In a second category of experiments, nuclei on the proton drip-line up to A ≈ 200 are synthesised in fusion-evaporation reactions induced by neutron deficient beams of SPIRAL. Measurements of the β-decay can provide the mass of the isobaric analog states and, in turn, by using the IMME, the mass of the ground state of these nuclei (see for example the case of ^{28}S [POU89]). The case of N=Z nuclei up to A = 100 immediately comes to mind, but one may also consider nuclei whose stability has recently been demonstrated such as ^{22}Si, ^{46}Fe, ^{50}Ni, etc.

II.2 RADIOACTIVITIES AND HALF-LIVES

II.2.1. Direct radioactivity

Two islands of proton radioactivity have been discovered in the regions A = 110 and 150 [HOF89b]. The Coulomb barrier of these unbound nuclei is high enough to increase their lifetime well beyond the characteristic time of the strong interaction. The decay process is simpler than the one associated with α-radioactivity, since it does not require the existence of a pre-formed structure within the nucleus. This simplicity is useful in particular in investigating the roles of orbital angular momentum and deformation. Hence, a new (critical) examination of the ordering of the shells at the limits of nuclear stability becomes possible. It is shown below how fusion-evaporation reactions induced by neutron deficient beams supplied by SPIRAL may lead to the discovery of unknown regions of proton radioactivity.

Ground-state proton radioactivity

This phenomenon is predicted for several light nuclei such as ^{39}Sc, ^{42}V, ^{55}Cu, ^{65}As, ^{69}Br, etc., where many emitters of β-delayed particles are known. So far, however, it has not been observed. These nuclei, whose structure is relatively simple, have already been produced at GANIL and MSU. A measurement of their mass would be a major step forward because the lifetime depends critically on the Q-value for the decay. In the neighbourhood of ^{100}Sn, calculations [OGA84] predict the half-lives of the isotopes listed in Table I. The proton radioactivities of ^{109}I and ^{113}Cs have already been observed [HOF89b] with half-lives on the order of 0.1 to 500 μs, compatible with these predictions. These nuclei should provide valuable information on energy and shell ordering at the limits of stability (where no general method can predict them), on violations of isospin and on the presence of deformations (of major important in this region).

Beyond $Z \geq 35\text{-}40$ it is no longer possible to produce these nuclei by fusion-evaporation induced by stable projectiles.

Initial state	Final state	Qp (MeV)	$T_{1/2}$ (s) (exp.)	$T_{1/2}$ (s) (theory)
^{97}In (9/2$^+$)	^{96}Cd (0$^+$)	1.38		4.7 10^{-9}
^{96}In (8$^+$)	^{95}Cd (9/2$^+$)	1.44		0.96 10^{-9}
^{93}Ag (9/2$^+$)	^{92}Pd (0$^+$)	1.10		0.12 10^{-6}
^{92}Ag (2$^+$)	^{91}Pd (9/2$^+$)	1.09		0.10 10^{-6}
^{89}Rh (9/2$^+$)	^{88}Ru (0$^+$)	0.88		6.0 10^{-6}
^{105}Sb (3/2$^+$)	^{104}Sn (0$^+$)	0.86		5.4 10^{-6}
^{109}I (5/2$^+$)	^{108}Te (0$^+$)	0.83	(109±17).10^{-6}	77.0 10^{-6}
^{113}Cs (5/2$^+$)	^{112}Xe (0$^+$)	0.96	(33±7).10^{-6}	8.4 10^{-6}

Table I. Proton radioactivity in the neighbourhood of ^{100}Sn [OGA84]

Proton radioactivity of high-spin isomeric states

This property, characteristic of neutron-deficient nuclei in the $g_{9/2}$ shell, has also been predicted [OGA84] in isotopes near the N=Z line: ^{95,97}In[25/2$^+$], ^{96}Cd[16$^+$], ^{95}Cd[23/2$^+$] and ^{95}Ag[23/2$^+$]. In fact, proton emission from these states is slowed down by the high angular momentum of the emitted proton and the small amplitude of the associated spectroscopic factor. The study of this decay mode (up to now only observed for ^{53m}Co) serves to assess penetrability through Coulomb and centrifugal barriers and yields information on simple (aligned) configurations of several particles.

Two-proton radioactivity from the ground state

In some even-Z nuclei, which are stable against proton emission, the pairing effect makes the direct emission of two protons energetically possible. This should provide the most direct source of information on the correlations between protons in the emitter nucleus. Calculated half-lives are extremely sensitive to the available decay energy [DET90], which makes it difficult to choose the most promising candidate. Those mentioned by Détraz et al. [DET90] correspond to light nuclei, but this phenomenon can also be sought in heavier nuclei, such as some isotopes in the vicinity of ^{100}Sn: ^{87,89,90}Pd, ^{94}Cd, ^{97,98}Sn [OGA84] or ^{132}Gd and ^{138}Dy. It has not

been possible to produce these nuclei with stable beams, but they could be produced by secondary beams supplied by SPIRAL, for example:

$$^{64}\text{Zn}(^{74}\text{Kr},2p4n)^{132}\text{Gd with } \sigma=760 \text{ } \mu\text{b at } E_{inc}= 380 \text{ MeV}$$

$$\text{or } ^{64}\text{Zn}(^{73}\text{Kr},2p3n)^{132}\text{Gd with } \sigma=6.3 \text{ } \mu\text{b at } E_{inc}= 350 \text{ MeV}.$$

Cluster emission

Before closing this section on proton radioactivity, it is worth mentioning that the probability of cluster emission, from alpha to heavier nuclei such as ^{14}C, should increase in the neighbourhood of the proton drip-line. More experimental data, particularly in this region are necessary to obtain a better description of this phenomenon.

II.2.2. Beta decay of very exotic nuclei

β-decay and electron-capture of nuclei far from stability provide access to many spectroscopic features of daughter nucleus states, such as the excitation energy, spin and parity of occupied levels and partial decay widths (radiative or from delayed particle emission). Aside from the inherent interest in nuclear structure, these data are also crucial to astrophysics. Finally, a few specific transitions may shed light on different aspects of the weak interaction.

Gamow-Teller transitions

Exotic nuclei provide unique opportunities to study the distribution of G-T strength (and its quenching down) over a considerably wider energy domain. So far the confrontation of experiment and theory has been particularly disappointing [TOW87]. One of the difficulties theory is faced with, is the construction of a transition operator which fits the data on the weak interaction and takes into account the presence of exchange currents and the truncated configuration space. Even with an operator adjusted to experimental data on nuclei close to stability, the results have been disappointing. The feeding of unbound states leads to the emission of β-delayed charged particles. From observed spectra, one can deduce accurate quantitative data on level densities at high excitation energy. For neutron-deficient nuclei with A $\geq$ 60, indications on the lifetimes of these states can be obtained [DES87, DES88, MIE91]. As a general rule, for light nuclei in the s-d shell, the experimental distribution is well reproduced, provided a general quenching factor of $\approx$ 0.6 is applied to the theoretical predictions. For heavier nuclei, the size of the configuration space makes the situation even more confusing.

By making it possible to reach particularly pure configurations, secondary beams will serve to search for the origin of these disagreements. They will also permit a better study of the characteristics of weak interaction in the nuclei, for example in β-transitions (of extremely weak intensity) which violate the conservation of parity, to be undertaken. Lastly, "exotic" types of β-delayed emissions may be searched for, such as β^+ - 2p emission observed for ^{39}Ti, ^{43}Cr, ^{49}Ni [BOR92].

Fermi transitions

Studies of superallowed transitions are always particularly well suited to test basic interactions in the nucleus. High precision measurements of eight superallowed β-

transitions $0^+ \rightarrow 0^+$ have demonstrated [HAR90] the universality of the interaction once Coulomb and radiative corrections have been taken into account. The extension of these measurements to heavier nuclei (^{58}Cu, ^{62}Ga, ^{66}As, ^{70}Br, ^{74}Rb or even nuclei with T=2) would provide a way to assess the magnitude of isospin violations in this mass region and to better estimate the corrections to the Fermi matrix element due to the charge of the nucleus. Reduced-probability measurements of isospin forbidden ($\Delta T = 1$) Fermi transitions will allow further tests as to whether isospin remains a good quantum number. A violation is expected in the region of mass A = 64 to 96, for N = Z nuclei close to the drip-line. This point may be related to the violation of isospin in halo nuclei shown by recent calculations [HAN93]. In addition, $\beta - \gamma$ decay measurements in this mass region will enable investigations of the shell structure, which is extremely sensitive to the neutron number, to be undertaken. Such measurements will also lead to a better understanding of the rapid shape transitions and tri-axiality observed in this region. It is known that this region could reveal different deformations for neutrons and protons [BON85].

II.2.3. Contribution of SPIRAL

As in the case of mass measurements, two types of experiments need to be considered : post-acceleration of nuclei very far from stability, produced in the target irradiated by the primary beam and use of more intense radioactive beams (closer to stability) producing still more exotic nuclei by a secondary reaction. A number of examples are given below.

Post acceleration of beams far from stability

The spectroscopic analysis of nuclei produced by a thick target/ion source combination is often complicated by contamination due to isobars closer to stability. An efficient purification (several orders of magnitude) of these beams can be obtained when their energy is above 10 MeV/nucleon by exploiting the simple Z dependence of energy losses in matter, possibly followed by an analysis of magnetic rigidity. This method can therefore be used with SPIRAL beams up to the nickel region. Secondly, the velocity gained by post-acceleration allows to tag each nucleus in the beam. Experiments using recoil separators, in particular LISE, have demonstrated the value of identifying the nuclei far from stability "event-by-event". That is, it is possible to combine time-of-flight and position measurements for incident nuclei with similar information on time-of-flight and emission angle (as well as the nature) of particles after disintegration. This results in a considerable reduction of background, which greatly facilitates measurements of half-lives as well as studies of decay schemes.

Production of proton-rich nuclei by secondary reactions

Nucleon exchange and multi-nucleon transfers

Reactions of this type have already been observed at high incident energy, at GANIL and GSI. It would be worthwhile checking whether reactions such as,

$$^{38}\text{Ca} + \text{target} \rightarrow {}^{39}\text{Ti} + \text{X} \qquad (+2p, -1n)$$
$$^{56}\text{Ni} + \text{target} \rightarrow {}^{55}\text{Cu} + \text{X} \qquad (+1p, -2n)$$
$$^{80}\text{Rb} + \text{target} \rightarrow {}^{79}\text{Y} + \text{X} \qquad (+2p, -3n)$$
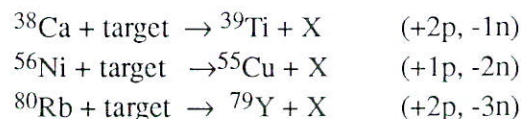
can provide a competitive alternative for the production of such nuclei of interest.

Fusion-evaporation reactions

Cross-sections predicted from statistical codes for the synthesis of nuclei far from stability, through fusion-evaporation reactions from radioactive beams such as^{14}O, ^{30}S ^{56}Ni and from stable beams such as ^{16}O, ^{32}S and ^{58}Ni, have been compared. Some values of cross-sections for the most favourable reactions, at the optimal incident energy, are presented in Table II.

The cross-sections expected with radioactive beams are higher than those obtained with stable beams, in some cases by two orders of magnitude. Moreover, aside from production cross-sections, secondary beams result in a much better signal/background ratio when the nucleus under study belongs to the main exit channel. In many cases this advantage will overcompensate for the decrease in production with a low-intensity secondary beam.

Reaction	^{49}Fe	^{51}Co	^{62}Ga	^{66}As	^{80}Zr
^{16}O+^{40}Ca	3 μb	5 μb			
^{14}O+^{40}Ca	180 μb	300 μb			
^{32}S+^{40}Ca			5 mb	3 mb	
^{30}S+^{40}Ca			15 mb	10 mb	
^{58}Ni+^{24}Mg					90 μb*
^{56}Ni+^{24}Mg					500 μb

Table II. Cross-sections predicted by the statistical model for some fusion-evaporation reactions.

* The experimental value is 10μb.

For the formation of heavier nuclei, which are possible proton emitters and impossible to produce by fusion-evaporation reactions with a stable beam, the following values have been estimated :

$$\sigma = 135 \ \mu b \ for \ ^{40}Ca \ (^{70}As, \ 2p3n)^{105}Sb \ and$$
$$\sigma = 400 \ \mu b \ for \ ^{92}Mo \ (^{68}As, \ 2p3n)^{155}Ta.$$

II.3. NUCLEAR STRUCTURE STUDIES VIA REACTIONS INDUCED BY UNSTABLE NUCLEI

The use of nuclear reactions to study nuclear structure is one of the main reasons to develop post-accelerated unstable beams. This experimental method has been frequently used with secondary beams produced by projectile fragmentation and the halo phenomenon (large spatial extension) of the last weakly bound neutrons in light nuclei located at the neutron drip-line was discovered this way [TAN91, ANN90]. However, the energy of these beams typically cannot be less than $\approx$ 20 MeV/nucleon and without "cooling", the quality is quite poor. As an example, the estimated emittance of the beam provided by the SISSI device is about 17 π mm.mrad. On the contrary, SPIRAL will directly provide beams with energies close to the Coulomb barrier (note that the effects connected to the halo are most apparent at low energy). Its excellent optical qualities (estimated emittance of SPIRAL beams is 5π mm.mrad) should allow one to perform much more precise

experiments and to take full advantage of the qualities of spectrometers and other available detectors. Elastic (and inelastic) scattering, Coulomb-excitation and transfer-reaction experiments can be carried out under such conditions and the prospects for each are discussed below.

II.3.1. Elastic scattering

The cross-sections for elastic scattering, which are fundamental quantities in nuclear physics, provide information on the nuclear potential when the two interacting nuclei come into contact. These cross-sections are relatively large and are among some of the first quantities to be measured.

Conceptually, the simplest is to study [MOO92] elastic scattering of a radioactive beam on a light target (p,d or α). In the case of the halo, orbiting of the light nucleus around the heavy nucleus is expected, causing a peak in the angular distribution at large angles and, at higher incident energy, the so-called nuclear rainbow. These two effects (which are clearly manifest only for reactions on very light nuclei) can be used to deduce accurately the density of nuclear matter over a wide radial range.

Elastic scattering can also be studied on heavier targets such as ^{12}C, for a series of isotopes containing neutron-rich nuclei, in order to compare the strong absorption radii. The goal here is to search deviations from the $A^{1/3}$ dependence of the radius parameters, indicative of a neutron excess at the surface of the nucleus. Elastic scattering measurements are now in progress with secondary beams produced by projectile fragmentation [KOL92, LEW93] and seem to indicate, in accordance with theoretical predictions [SAT91], that the optical potential associated with a neutron-halo nucleus contains a long-range imaginary part. These results are, however, somewhat ambiguous since the relatively poor qualities of the beam prevent any separation between elastic and inelastic scattering. A precise study of elastic scattering implies a vast improvement in angular and energy resolutions, which may be achieved by coupling beams from SPIRAL with the SPEG spectrometer.

II.3.2. Inelastic scattering and Coulomb excitation

At incident energies close to the Coulomb barrier, inelastic scattering, and in particular Coulomb excitation, allows the study of excited states of moderate energy to be undertaken and thus may enhance our knowledge of the structure of nuclei far from stability. From an experimental standpoint, it is possible to separate bound states, whose γ-decay can be detected, from continuum states, which decay mainly by particle emission.

The excitation energies, and, better still, the B(E2) transition probabilities of the first 2^+ states excited by the Coulomb interaction provide information on the deformation of the ground state and on the collectivity of the excited states, which are key tests for nuclear models. These measurements would be extremely valuable for proton-rich nuclei with $60 \leq A \leq 100$. Indeed large prolate deformations have been observed for these nuclei, which can be accounted for by the presence of new energy

gaps for the one-particle orbits when both N and Z are close to 38. This is a region where sudden shape transitions are predicted [BON85], in particular along the N=Z line. The production and acceleration of N=Z nuclei will serve to better grasp the interplay of collective and shell effects and to study the role of n-p correlations in the T = 0 states, since neutrons and protons, present in the same orbits, act together to stabilize the nuclei in a given shape.

For these measurements, which only require a low-intensity beam, magic-nucleus targets (eg.^{208}Pb) will be bombarded by a beam of the nuclide of interest delivered by SPIRAL. Thanks to the high efficiency of the new generation of γ-detector array (e.g. of the EUROGAM type), experiments are feasible with beam intensities of 10^6 or even 10^5 pps and the granularity of the detector serves to correct for the large Doppler effect. A concrete demonstration of the feasibility of such experiments on E1 excitation has recently been obtained at the LISE spectrometer at GANIL, where the γ-decay of the first excited state of ^{11}Be was clearly observed [ANN93] in a measurement of a few hours despite a low-intensity ^{11}Be beam (5 x 10^4 pps) and considerable Doppler broadening.

The energies available from SPIRAL will be particularly well suited to the excitation of continuum states at low energy, especially for nuclei close to the drip lines. For these nuclei, in particular for those exhibiting a neutron halo, numerous calculations [SAG90, FAY91] predict a concentration of the strength, not only the dipole one but also of all the other multipolarities, just above the neutron emission threshold (pygmy resonance). Up to now, information on these excitations has been collected with beams obtained by projectile fragmentation, but the optical qualities and energies of SPIRAL beams, in association with state-of-the art spectrometers and large detector arrays should provide for a major quantitative step forward in the accuracy of the results and hence in the detailed study of the properties of the halo.

Two experimental methods can be used for these studies. Because the ejectile is detected with a spectrometer, one must observe either the decay neutron (implying a neutron detector array) or the target recoil nucleus, since it is crucial to reconstruct the kinematics of the reaction. The cross-sections for populating these excited states are high (calculations predict more than 1 b/sr for l=2 multipolarity in the ^{11}Be + ^{12}C reaction at 10 MeV/nucleon), thus implying that the relatively low intensities of the secondary beams available will not be an obstacle.

II.3.3. Transfer reactions

Transfer reactions are among the main reaction channels at energies around the Coulomb barrier and serve to probe one- or multiple-particle components of the wave functions of nuclear states. The study of one-nucleon transfer reactions provides information on the occupancies of the shell model orbitals, which may be directly linked to the "magicity" of a shell closure, (eg. in the neighbourhood of N = 20, (N,Z) = 28 and (N,Z) = 40). These measurements, if performed for example on the carbon-isotope chain, would give access to the occupied configurations, the order of filling of the shells and the evolution of nuclear shapes for very light nuclei. Similarly, when studied systematically on a long isotopic chain, one-nucleon transfer would serve to deduce the fragmentation of orbitals and provide a stringent test to

predictions of the shell model. Transfer reactions can also provide accurate information on the radial extension of specific orbits, which would be particularly valuable in the case of systems as weakly bound as halo nuclei. Analysis of such experiments shows that the values for the radii of orbitals deduced in this way generally agree with the values obtained by other methods [WOO81], such as for example, the magnetic scattering of electrons. These measurements, which rely on stripping and pick-up reactions, can be carried out at energies which are either below or above the Coulomb barrier.

It should be noted that the use of transfer reactions makes it possible to determine the low-energy level scheme of nuclei far from stability and to obtain high-precision mass measurements. Indeed this is the only method in the cases of levels unbound against particle emission. This method, which is used intensively at the VICKSI accelerator facility [NFFS92] with beams of ^{13}C and ^{14}C could certainly be extended with beams farther from stability available from SPIRAL.

III. REACTIONS INDUCED BY VERY NEUTRON-RICH EXOTIC NUCLEI

III.1. FUSION AROUND THE COULOMB BARRIER

Observations in the sixties of resonances in the excitation functions of the fusion cross-sections of some light nuclei and the demonstration ten years later of large fluctuations as a function of the number of neutrons involved, revealed the shortcomings of the one-dimensional barrier model and attracted attention to the key role of nuclear structure in the fusion process. These observations hold for the entire periodic table [STE86]. Above the Coulomb barrier, fusion ceases to be the main process and must compete with inelastic and transfer-reaction channels, which are highly sensitive to the structure of the interacting nuclei. This coupling results in the replacement of the original barrier by a whole distribution of barriers of variable heights, the lowest of which play a key role. One major consequence could be [HUS91] the increase (by several orders of magnitude) of the fusion cross-section through the excitation of the pygmy resonance (see II.3.2.). Such an effect is illustrated in Fig. 1 for ^{11}Li + ^{208}Pb. As a result, the fusion induced by neutron-rich secondary beams could provide a means of synthesizing very heavy nuclei (Z ≥ 100).
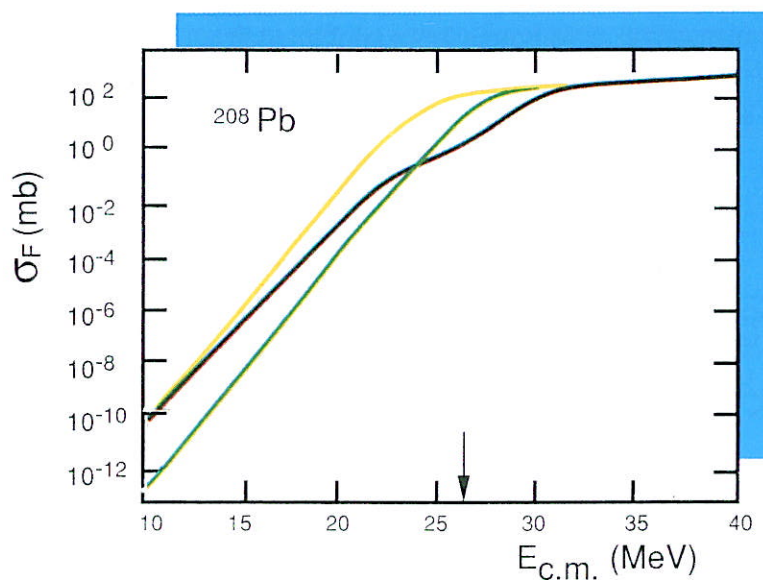
Figure 1 : Theoretical predictions for the fusion cross-section for the system ^{11}Li + ^{208}Pb (green line : without pygmy resonance, yellow line : with pygmy resonance, black line : with pygmy resonance and halo dissociation). Taken from [HUS92].

III.2. SYNTHESIS OF VERY HEAVY AND SUPERHEAVY NUCLEI

The limits of nuclear charge provide information on the persistence of shell effects. As early as 1966, the presence of an island of stability based on proton and

neutron shell closures, was predicted at $Z = 114$ and $N = 184$ - the so-called superheavy nuclei.

Even though very heavy elements (up to $Z = 109$) have been observed [MUN89], experimental attempts have failed to synthesize the superheavy elements. This failure emphasizes the need to try other methods. Theoretical advances and, moreover, the advent of secondary beams open up many new possibilities in this area. Present models, which include a variety of multipolar deformations [MOL86, PAT89], predict that the island of stability centered at $Z = 114$ and $N = 184$ corresponds to spherical nuclei and is only the extremity of the "peninsula" of very heavy nuclei whose ground states are deformed and are stabilized by shell effects. The partial decay width of most of these nuclei are below that of fission [BON86] with corresponding lifetimes which are longer than a microsecond. These encouraging predictions deserve verification.

The heaviest nuclei have been produced so far by fusion of stable neutron-rich projectiles (Ti, Cr, Fe) with targets close to ^{208}Pb. It is estimated that the production cross- section for very heavy nuclei ($Z \geq 109$) by this method (cold fusion) is of the order of a picobarn, the current limit of detection capabilities. The use of more asymmetric systems, with targets in the actinide region, makes it possible to take advantage of higher fusion cross-sections. Moreover, this effect can be enhanced with the use of neutron-rich beams, as has been suggested in recent works on complete fusion below the barrier (Fig. 2) [TAK90]. It is believed that several orders of magnitude could be gained in the yield in this way. On the other hand, the higher excitation energy of the compound nucleus may lead to fission or to dissipation by neutron emission. The strong shell effects predicted for these nuclei, however, reduce the excitation energy, thus resulting in a net gain in the cross-section.
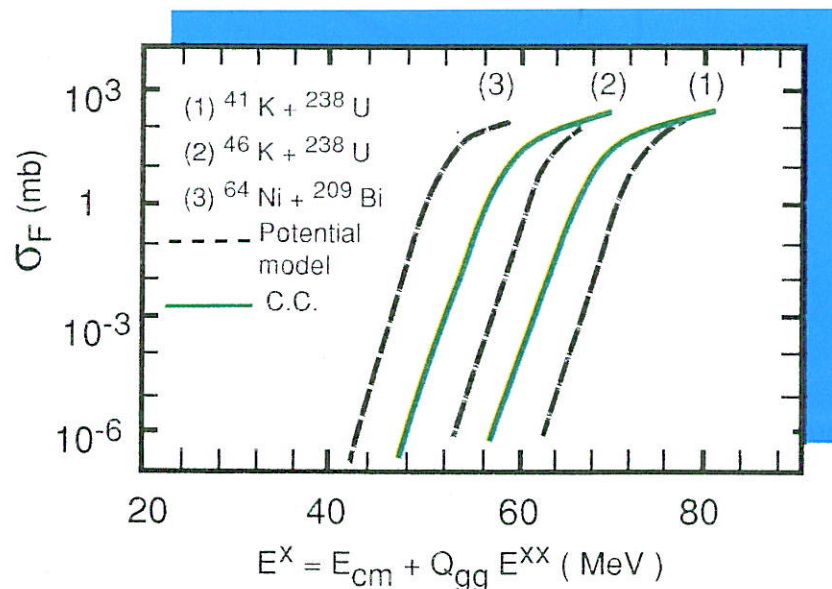

Figure 2 : Excitation functions for the fusion cross-section of isotopes of element $Z = 111$, calculated using an interaction potential and the coupled channel method. Excitation energy, on the abscissa accounts for incident energy, Q-value and extra-push.energy. Taken from [TAK90].

For nuclei that are closest to the center of the peninsula of stability, measurements of lifetimes, masses and decay modes (α-decay, internal conversion and fission) are feasible with only about a hundred or more nuclei. With several thousand it is possible to locate the first excited states, the height of the fission barrier and, possibly, demonstrate the existence of fission isomers or the emission of clusters. Furthermore, the atomic properties of these elements are interesting because of relativistic effects on the atomic electrons. The long lifetimes of the most neutron-rich isotopes may even allow investigations of very heavy chemical elements.

III.3. INFLUENCE OF ISOSPIN ON DEEXCITATION MODES

At excitation energies below 10 MeV, deexcitation of nuclei remains sensitive to shell effects. However, structure effects specific to exotic nuclei can considerably modify the deexcitation channels. For instance, the emission of nucleons or clusters (for example di-neutrons) can compete with γ-emission at very low excitation energies. Indeed deformations of exotic nuclei can considerably modify the emission barriers for charged particles, and hence the probabilities and emission characteristics. With neutron-deficient projectiles, fusion can go beyond the stability limit in protons and a new form of pre-equilibrium particle emission is predicted [BES89] with highly specific features (energy spectra and angular distributions).

In the case of fission, the shapes of exotic nuclei may be used to extend the study of phenomena which have seldom been explored up to now. The case of the fission of Fermium is illustrative of this. The evidence for the existence of two fission valleys, associated with compact and prolate configurations respectively, should obviously be paralleled to the superdeformations observed in γ-spectroscopy. The experimental consequences are spectacular, as shown in Fig. 3, for fission mass distributions which can have radically different shapes for two neighbouring isotopes.
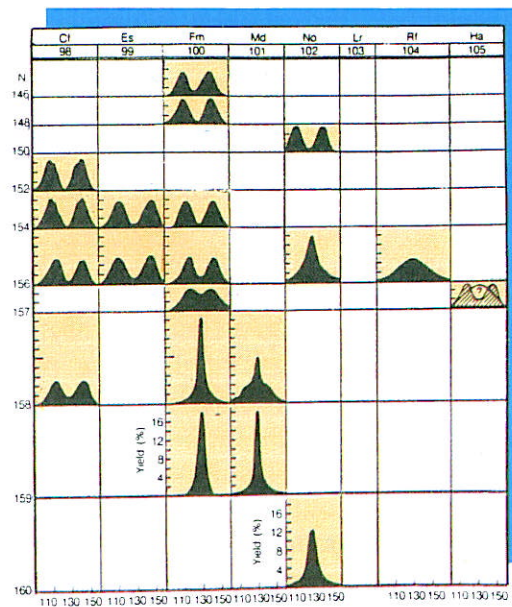
Mass yield curves for SF

Figure 3 : Schematic diagram of fission fragment mass distributions. Taken from [HOF89a]

29

Other unexpected findings have also been obtained for fragment kinetic energies, which considerably exceed theoretical predictions as well as systematics. The shell effects resulting in these properties are perhaps those linked to the potential-energy surface at the saddle point. However, this interpretation cannot be refined without studies on other weakly excited nuclei in the region. This can be carried out with exotic beams within studies of superdeformation performed with γ-spectrometry. In this way, a program could be devoted to extending the study of isomeric fission to exotic nuclei in the region of masses A = 150 - 200.

In this context, up-to-date fission barrier calculations, extending over the whole range of accessible nuclei, would be very useful. Such calculations need to be made for a very restricted range of excitation energy. Indeed, for intermediate-mass nuclei, the fission channel competes with particle emission because of the high barrier. However, these nuclei can be studied at fairly high angular momentum to compensate for the height of the barrier. Once again, this physics is very close to that of high-spin isomers.

IV. ISOMERIC BEAMS

Isomeric states may be considered as "reservoirs" of spin and excitation energy. They open up fascinating new prospects for the whole area of physics described above. Up to now, only targets of an isomeric state, ^{178m2}Hf ($_{\tau 1/2}$ = 31 years, E_x = 2.45 MeV and J^{π}= 16$^+$), have been used [OGA91]. However, producing a nucleus in its isomeric state and accelerating it should make it possible to avoid problems of chemical separation, which is the main difficulty encountered with this type of target (at least for short half-lives).

Our interpretation of nuclear reactions generally relies on the use of the optical model, with the tacit hypothesis that the nucleon-nucleus or nucleus-nucleus interaction potential (determined by elastic scattering between nuclei in their ground states) is independent of the state of excitation of the nucleus. However, the existence of an isomeric state generally implies a configuration very different from that of the ground state. Indeed the orbits involved have different spatial extensions, leading to a redistribution of the nuclear matter at the surface. This can result in a modification of the optical potential (nucleon-nucleus or nucleus-nucleus), which can be detected either by comparative measurements of the cross-sections for elastic scattering of the ground and isomeric states, or by measurements of fusion cross-sections. These measurements are the basis for the study of the role of spin in these reactions.

By means of transfer reactions, accelerated isomeric beams may provide a means to populate configurations of certain particular (mostly high-spin) states which are not accessible from the ground state. It may also be assumed that collective excitations built up on certain isomeric states could be observed by Coulomb excitation.

The deexcitation of an isomeric state in the presence of an external field is an interesting area of investigation. Observations have shown that thermal neutrons scattered on a nucleus in an isomeric state can take on the excitation energy of the state (super-elastic scattering) in the form of kinetic energy. It is likely that similar effects would be observed with other projectiles. This phenomenon could lead to the so-called high-density materials. A good understanding of the mechanisms of population and deexcitation is, therefore, necessary.

Carrying out such a program would first call for the ability to produce isomeric nuclei to be developed - this has only been achieved for a few cases. For isomers whose lifetimes are much longer than that of the ground state, satisfactory purification is obtained after decay of the ground state. In contrast, in the other cases, purification of the beam by classical methods will be necessary and may well prove difficult if not impossible (mass resolution $\geq 10^5$ typically required).

V. NUCLEAR STRUCTURE AT HIGH ANGULAR MOMENTUM

In the last ten years heavy-ion beams have played a major role in the study of nuclear structure. They have served to extend the degrees of freedom of the nucleus, such as spin and isospin, to extreme values and hence often reveal totally unpredicted characteristics of the atomic nucleus.

So far available techniques for beam production and detection have not allowed for the simultaneous variation of the isospin and spin degrees of freedom of reaction products. Exotic nuclei have been studied at low angular momentum and the study of very high spins has been limited to extremely restricted areas of the chart of nuclides. Superdeformation and octupolar deformation are currently amongst the most highly debated topics in high-spin physics. While radioactive beams may serve to extend and complete studies of nuclear structure at high angular momentum, they are also key tools for the investigation of regions which have been inaccessible up to now for example heavy nuclei in the valley of stability. Their availability, coupled with sophisticated detectors such as EUROGAM or the future EUROBALL [BEC92] will allow the further extention of these investigations, and will also provide for the study of the novel situation where nuclei far from the valley of stability will be submitted to rapid rotation.

Minima in the potential energy surfaces result from gaps in single-particle energies, which show up at different deformations. Extreme deformations correspond to ellipsoids whose axis ratios are close to 2:1 (superdeformation) or 3:1 (hyperdeformation). Whereas superdeformed proton-rich nuclei have been observed at high angular momentum in the regions about A = 130,150 and 190 and at low angular momentum in the region of fission isomers, other regions of extreme deformation can only be explored with radioactive projectiles (Fig. 4). For example, neutron-rich beams provide an additional possibility of stabilizing the residual nucleus against fission by using fusion-evaporation reactions. On the other side of the valley of stability, neutron-deficient nuclei can be reached by combining Coulomb excitation and the transfer of one or several nucleons to those orbits that induce deformations. This method would allow one to search, in particular, for the superdeformed and hyperdeformed rotational bands predicted in the Rn and Ra nuclei with masses near 200, which can only be formed by fusion-evaporation due to the high fission probabilities.

Specific attention will be devoted to N=Z nuclei, whose formation at high angular momentum calls for exotic beams. The study of these nuclei will help specify the role of intruder orbitals (increasingly bound with increasing deformation, to such a point that their energies become comparable to those characteristic of the lower major shell) whose behaviour is crucial for the moments of inertia of superdeformed nuclei. Additionally, pairing effects between nucleons affect the shape of the nuclei and give rise to excitations of quasi-particles. By producing at high spin N=Z nuclei, where the

same intruder orbitals act for protons and for neutrons, it will be possible to observe these pairing effects.
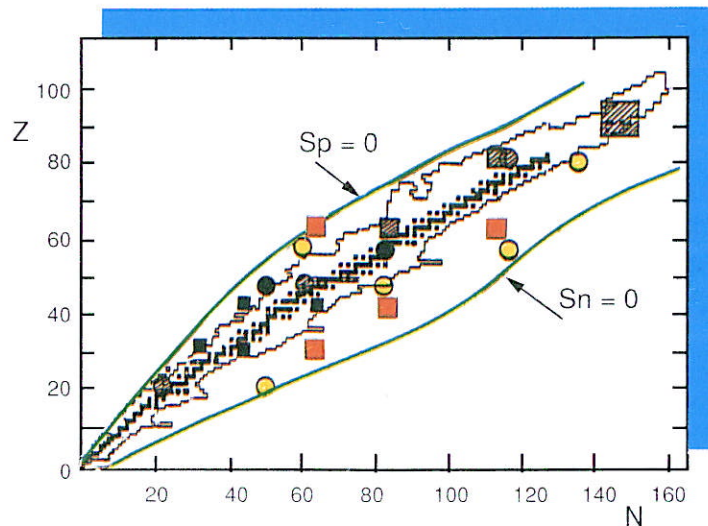

Figure 4 : Different superdeformation (squares) and hyperdeformation (circles) zones. The shaded zones can be reached with stable beams, those in red with radioactive beams.

The study of extreme deformations casts new light on research for new symmetries. Individual energies of non-intruder orbitals, plotted as a function of the nuclear deformation, group in multiplets characteristic of underlying quantic numbers [DRA91, DUD88]. The different super and hyperdeformed configurations result from the existence of these multiplets. This could be confirmed experimentally by the discovery of extreme shapes, for example the hyperdeformation of proton-rich nuclei in the Er-Yb region. The observation of identical superdeformed bands in neighbouring nuclei [BYR90] can also be understood within the framework of the same symmetries. The mechanism responsible for these bands should be studied only in relatively light nuclei (A ≈ 60 or 90) where the previous hypotheses reach the limits of their validity.

Other phenomena related to extreme deformations which have never been observed could be revealed by means of exotic beams. For example, the degeneracy of normal, superdeformed and hyperdeformed states for the same spin value is predicted in the region of the light actinides [WER92] and in superdeformed structures of proton-rich nuclei with N = 86 (^{165}Yb and ^{158}Hf). The superdeformed rotational bands could have a superdeformed "twin" structure without octupolar deformation and with a weaker nuclear elongation.

In nuclei where the total deformation is not very large, other aspects of octupolar deformation deserve further investigation. For example, the study of heavy isotopes of Ra and Th formed by reactions using neutron-rich carbon and oxygen beams may serve to assess whether the octupolar deformation at low and moderate spin disappears at high angular momentum [NAZ87]. Radioactive beams may also produce nuclei presenting exotic octupolar deformations ($a_{3\mu} \neq 0$). Such experiments may also serve to specify the band structure and transition probabilities associated with each mode $\mu = 1, 2$ or 3.

VI. NUCLEAR ASTROPHYSICS

Although our understanding of the universe has benefited considerably over the last fifteen years from a close cooperation between nuclear physics and astrophysics, many questions remain unanswered. Their experimental as well as theoretical investigation represents a major challenge to modern physics [ARN90, BAR88].

Nuclear astrophysics deals with two key (and closely related) issues :

1) The production of energy in different astrophysical sites, from "quiet" stars (like the Sun) to explosive events, in particular novae, supernovae and X- and γ-ray bursts.

2) The production of nuclides observed in the Universe (and in particular in the solar system) which began with the Big Bang and continues today in stars. The comparison of abundances predicted from nuclear data and astrophysical models with observed abundances provides information on the physical properties of these sites.

These issues lead to two types of studies in nuclear physics. The first one is the measurement of the cross-sections for nuclear reactions at energies of astrophysical relevance. The second one is concerned with nuclear data such as the masses or β-decay half-lives of unstable nuclei.

The first type of studies requires low-energy beams ($\cong 0.2$ to 1 MeV/ nucleon). In contrast, the second-type measurements will draw to a greater extent on a large range of available energies. The SPIRAL project will provide beams in the energy range 1.8 - 25 MeV/nucleon. Covering lower energies would require additional dedicated equipment which is not included in the present project.

Measurements of reactions relevant to particular astrophysical sites have recently made a spectacular step forward at Louvain-la-Neuve with the study of the ^{13}N (p,γ) ^{14}O reaction, thanks to the development of an intense and relatively pure ^{13}N beam. Such measurements have truly opened up a "new frontier" in nuclear astrophysics.

VI.1. OUTLOOK ON NUCLEAR REACTIONS OF ASTROPHYSICAL INTEREST

Nuclear reactions which occur in stars are either thermonuclear reactions or spallation reactions. The latter are not discussed in this report, as radioactive species do not play an important role in spallation. The former deal with proton, α-particle or neutron capture by a variety of stable or unstable nuclei.

The determination of the rates of these reactions is a major experimental challenge. During the non-explosive phases of stellar evolution, temperatures are low and the corresponding reaction cross-sections are extremely small (of the order of picobarns to nanobarns). In contrast, during stellar explosions, the temperatures are

much higher (some 10^8 to 10^9 K) and the corresponding cross-sections range from microbarns to millibarns. However, this advantage is counterbalanced by the large number of unstable nuclei which play a role in the modelling of stellar explosions. The scarcity of existing data on reactions involving these nuclei make the modelling less reliable as well as the subsequent nucleosynthesis calculations.

Two types of measurements may be considered :
- direct measurements, which deal with reactions actually taking place. These are illustrated, for example, by the $^{13}N (p,\gamma)^{14}O$ reaction cited above.
- indirect measurements, which are a frequent and essential substitute. Different approaches have been used such as (i) obtaining spectroscopic data on the resonant nuclear states, by populating these states with reactions that differ from those occuring in the stellar environment and (ii) the study of inverse reactions, in particular Coulomb disssociation (for radiative capture). These latter measurements, which are extremely promising, may already begin to be explored with the sophisticated SISSI system at GANIL.

For light nuclei with low level density, a small number of major reaction channels can be identified. In contrast, for heavy nuclei, many reactions can occur, involving nuclei with high level densities. Specific models (for example the Hauser-Feshbach model) are thus used for these reactions. A small number of carefully selected cases should be studied to obtain reliable data on the optical potentials, level densities and features of the giant dipole resonances.

VI.2 ISOLATED RESONANCES - NUCLEOSYNTHESIS VIA HOT PROCESSES.

A few proton and α-particle capture reactions which are of major importance in astrophysics are of interest here. The direct measurement of the cross-sections are considered in the case of light nuclei (A<40). In these measurements, hydrogen or helium targets are bombarded by beams of radioactive ions.

VI.2.1. Astrophysical sites and corresponding reactions of importance

Nucleosynthesis in the inhomogeneous Big Bang
Some recent studies suggest the presence of inhomogeneities in the distribution of hadronic matter after the quark-hadron phase transition. Under such conditions, elements with $A \geq 7$ could be created with primordial abundances much higher than those predicted by the standard model. One of the crucial reactions in this scenario is $^8Li (\alpha, n) ^{11}B$.

Hot proton-proton chains
The existence of these chains, which could replace the usual p-p chains in novae explosions or in hypothetical pregalactic stars, is a function of the rates of reactions such as $^7Be(p,\gamma)^8B$, $^7Be(\alpha,\gamma)^{11}C$, $^8B(p,\gamma)^9C$, $^{11}C(p,\gamma)^{12}N$.

Hot CNO and NeNa-MgAl cycles
A major modification in the classical CNO cycle takes place when the $^{13}N (p,\gamma)$ ^{14}O reaction becomes more probable than the β-decay of ^{13}N. The corresponding hot

CNO cycle then plays a key role in novae and certain supermassive objects. Several reactions with unstable nuclei are involved in this cycle, in particular the ^{19}Ne (p,γ) ^{20}Na reaction.

A comparable evolution of the NeNa-MgAl cold cycles towards hot cycles is based on the rates of reactions such as ^{20}Na(p,γ)^{21}Mg, ^{22}Na(p,γ)^{23}Al. The measurement of the reaction rate for ^{26m}Al(p,γ)^{27}Si, which requires the development of an isomeric beam of ^{26m}Al, would represent a first in experimental nuclear astrophysics.

The rp- and αp- processes
The hot CNO and NeNa-MgAl reaction cycles can give way to rp and αp processes when the ^{15}O(α,γ)^{19}Ne and ^{14}O(α,p)^{17}F reactions become more probable than β-disintegrations of ^{15}O or ^{14}O. This may be the case in some type-I supernovae or in the events leading to "X bursts". This situation could be clarified by studying reactions such as ^{15}O(α,γ)^{19}Ne and ^{14}O(α,p)^{17}F, as well as ^{26}Si(p,γ)^{27}P, ^{31}S(p,γ)^{32}Cl, ^{35}Ar(p,γ)^{36}K, ^{39}Ca(p,γ)^{40}Sc and ^{43}Ti(p,γ)^{44}V.

VI.2.2 Experimental requirements

Direct reactions
The radioactive beams will bombard a hydrogen or helium targets. Table III summarizes the characteristics of some major reactions. In cases where the counting rate is below a hundred counts per hour, or in the presence of low-energy γ-rays, the detection of the recoil nuclei is necessary to obtain a satisfactory signal-to-noise ratio. The features of the radioactive beams necessary for these direct measurements are the following :

- energies between 0.2 to 1 MeV/nucleon for ions with masses lower than 40 (not available from the present project),
- a variation of the incident energies around the resonance energies,
- an energy resolution of the order of 10^{-3},
- purification of the beam, the magnitude of which will depend on the experimental setup and will be analyzed for each case.

Transfer reactions
Transfer reactions are one of the indirect ways used to determine spectroscopic properties of resonant states. These reactions are crucial for the measurement of proton or α widths of bound states, which are necessary for the evaluation of the cross-sections for direct radiative capture. This type of measurement can be illustrated by the ^{8}B (p,γ) ^{9}C reaction, where one would measure the differential cross-section for the reaction ^{3}He (^{8}B,d)^{9}C. The use of SPEG at small angles should result in counting rates of several counts per second. For such an experiment, a beam energy of about 10 MeV/nucleon and an emittance on the order of 5 π mm.mrad are needed and are well within the design parameters of the SPIRAL project.

Reactions	astrophysical site	Beam	$T_{1/2}$	Estimated $\omega\gamma$ (eV)	Ebeam (MeV/ nucleon)	Reaction rate for 10^9 pps (counts/h)
$^{13}N(p,\gamma)^{14}O$	hot CNO	^{13}N	10mn	1.8	0.6	7200
$^{14}O(\alpha,p)^{17}F$	hot CNO	^{14}O	71s	-	0.5	40
$^{15}O(\alpha,\gamma)^{19}Ne$	hot CNO	^{15}O	122s	0.060	0.3	15
$^{17}F(p,\gamma)^{18}Ne$	hot CNO	^{17}F	64s	<1	0.6	<3600
$^{19}Ne(p,\gamma)^{20}Na$	hot CNO	^{19}Ne	17s	0.008	0.5	40
$^{27}Si(p,\gamma)^{28}S$	rp process	^{27}Si	4s	0.010	0.6	40
$^{31}S(p,\gamma)^{32}Cl$	rp process	^{31}S	3s	0.013	0.6	90

Table III : Direct measurements. The calculated reaction rates are for 10^9 incident pps, and thick targets of gazeous CH_2 or He. Beam energy corresponds to the energy of the dominant resonance.

VI.3 SYNTHESIS AND PROPERTIES OF EXOTIC NUCLEI: THE p-, rp-, AND r-processes

Various astrophysical sites have been proposed for the p-, rp-, and r-processes. Detailed studies on the explosion of O-Ne shells in the progenitors of Type-II supernovae have shown that the production of p-type nuclei is primarily based on the photodisintegration of preexisting s- and r-process nuclei. It is impossible to obtain measurements of the yield of r-process reactions, which are likely to develop in the explosive phases of the supernovae type and which involve thousands of neutron-rich unstable nuclei [RAY87, THI86]. The same problem emerges for the rp-process which involves proton-rich nuclei. A common feature of all three processes (p,r, and rp) is the high density of states in the nuclei along the pathway of the process.

The accuracy of calculations of these cross-sections will depend on experimental efforts to determine the optical potentials used in the calculation of the transmission coefficients, level densities and electromagnetic transition strengths.

Knowledge of other nuclear data is fundamental to a reliable modelling of the different nucleosynthesis mechanisms, in particular the r-, rp- and p-processses [MAT90]. This is the case for the masses, deformations, and β-decay modes of thousands of exotic nuclei. Fig. 5 shows the importance of the values of nuclear masses in the calculation of the r- process. More generally, the study of nuclear properties along capture paths and, in particular, in the neighbourhood of expected waiting points, is crucial for the modelling of the r-process and should be considerably enlarged with the availability of secondary beams.

So far it has been possible to measure at ISOLDE several spectroscopic quantities (masses, half-lives, Q_β) in the region of the waiting points around ^{80}Zn and ^{130}Cd and at GANIL by using projectile fragmentation and the LISE separator in

many nuclei along the rp-process pathway (and also r-process nuclei where A $\geq$ 70-80). SPIRAL should provide the following advantages :

- better production yields for short-lived isotopes in thinner targets than those used with proton beams,

- access to many different elements by coupling the production target to an ECR source,

- the possibility of separating isobars, using a thin degrader, up to masses 60 or 70. Hence the study of neutron-rich nuclei of the r-process and the production of nuclei of the rp- and p- processes with a greater flexibility than is found at existing facilities will be possible.

Measurements of half-lives and of β-delayed neutron emission probabilities would be made at low energies, without deep implantation and with good beam quality. Similarly, the precision of the direct mass measurement with SPEG will benefit from the lower velocities of the reaccelerated nuclei. This is particularly important for high masses. The nuclei of the rp-process may also be produced via fusion-evaporation reactions induced with a ^{30}S beam, for example, with cross-sections on the order of a millibarn.
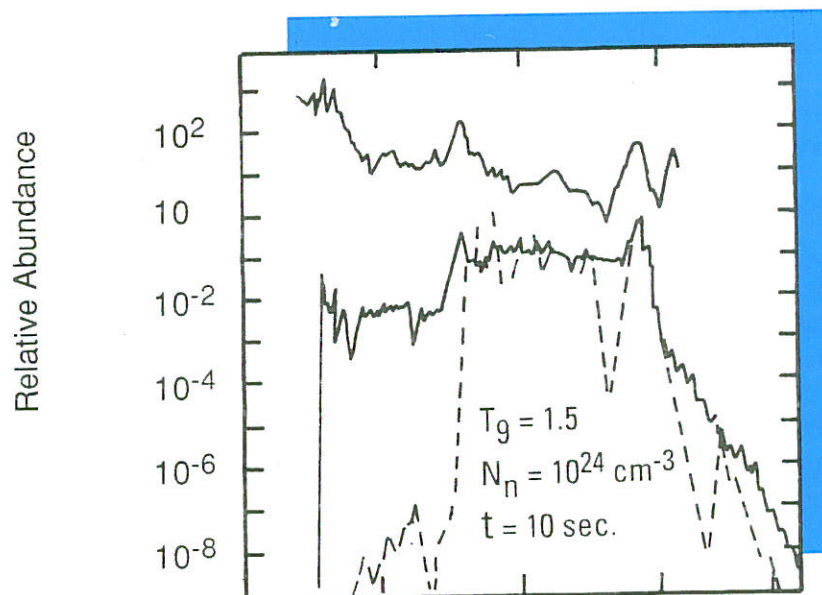
Figure 5 : A comparison between abundances of r-process nuclides observed in the solar system and predictions of a canonical model [GOR91] under the following astrophysical conditions : T_9 (temperature in $10^9 K$), Nn (neutron flux) and τ (duration of the neutron irradiation). The results using masses obtained from Liquid Droplet Model (solid lines) and Microscopic model (dotted lines) are shown

VI.4 GAMOW-TELLER FORCES FOR UNSTABLE NUCLEI A $\approx$ 60

A realistic modelling of the structure of the core of the progenitor of a supernova requires reliable knowledge of the rate of electron capture on nuclei with A $\approx$ 60 . The electrons of the medium have energies comparable to those in Gamow-Teller resonances [AUF90]. The measurement of the Gamow-Teller decay in unstable nuclei in the region of Fe, Co and Ni, produced by fusion-evaporation reactions and studied by β-decay will hence be of major interest in the understanding of supernovae.

VII. SOLID STATE PHYSICS

VII.I. INTRODUCTION

Since 1983, GANIL has been interested in particle-matter interactions (swift particles) and its impact on material science. The latter is difficult because it requires many techniques to characterize the material. Here the use of radioactive beams can provide decisive complementary information, as a radioactive isotope provides a probe at the atomic level. Its nuclear properties are affected by the spatial distribution of electrons in its surrounding. The study of surfaces, interfaces, grain boundaries and thin layers and the investigation of semiconductor, organic and even biological matter thus becomes feasible using nuclear methods associated with radioactive nuclei.

Because the data acquisition rate depends on the radioactive decay lifetime rate $(1/T_{1/2})$, the study of the material takes place with low fluxes (10^8-10^{12} atoms/cm^2), provided short-lived radioactive nuclei are used. These low fluxes significantly decrease the damage of the material. Hence it becomes possible to study the structure of the defects induced by the ion itself. On the other hand, the study of the initial undamaged material needs the development of annealing methods faster than those presently in use.

VII.2. RADIOACTIVE ISOTOPES AS LOCAL PROBES

Channeling and blocking

Once the radioactive ion has been implanted, the crystallographic directions, in which the decay products (e^+, e^-, α) may or may not be observed, can be determined. These allow the position of the embedded impurity to be located. By implanting at low temperature, and after annealing, the movement of the impurity in the matrix can be studied [HOF91].

Mössbauer spectrometry

Analysis of a Mössbauer spectrum - isomeric shift, quadrupolar and magnetic splittings - provides access to the electronic density, the gradient of the electric field and the magnetic field seen by the nucleus. The magnitude of the resonant absorption measures [WEY81] the mean vibration amplitude of the probe nucleus. The Doppler effect is also useful for deducing the mean velocity of the probe nucleus in its site and, in some cases, its diffusion mode.

Perturbed angular correlations

Another hyperfine interaction technique, the study of perturbed angular correlations probes [SCH87] the influence of the hyperfine magnetic field and the electric field gradient which exists around the probe radioactive nucleus. It should be noted that this experimental technique does not apply to solids only.

VII.3. RADIOTRACERS

One direct application of radiotracers is the superficial activation of layers in which a very small number of radioactive isotopes have been implanted. The loss of activity is then detected layer by layer as a function of the mechanical, thermal or chemical treatment that the surface undergoes. This method [MAL89].has considerable advantages compared with direct activation as it can be used for the study of materials with low atomic numbers for which there are no radioactive isotopes with sufficiently long lifetimes (for example, polymerous organic materials or light ceramics such as SiC).

VII.4. OUTLOOK

The different subjects presented below are derived from letters of intent from various laboratories. They deal with the study of surfaces, interfaces, thin layers and multi-layers.

Study of surfaces, interfaces and grain boundaries

The surface breaks the symmetry of a crystal: it presents highly different chemical and physical properties from those of the bulk of the material. In addition, it interacts with the environment of the material (for example, oxygen and sulfurous anhydrides of the atmosphere, ionized atoms of a plasma, water and sodium in nuclear reactors, etc.). To study these surfaces, interfaces and grain boundaries, only local probes with short lifetimes can be used. Among the radioactive beams envisaged, ^{19}O and $^{121,125}Xe$ appear so far to be the most promising. Oxygen, in particular, would enable one to study all the features of surface oxidation, a large-scale research program.

Thin and multi-layers

Oxygen is the basic element of all oxides. For example, depending on their oxygen stœchiometry, new oxides of type 1,2,3 ($YBa_2Cu_3O_{7-5}$) are either insulators or superconductors at high critical temperatures. The implantation of ^{19}O could be used to study the electronic environment in different cases.

Mössbauer spectrometry, in transmission or by use of electron conversion, could be developed to study the magnetism of thin layers. Radioactive beams such as ^{57}Mn, ^{67}Ga and ^{159}Gd would be of great value in studying these materials. In addition, a ^{61}Cu beam would make it possible to study all nickel-based materials.

The use of radioactive beams for condensed matter would be highly efficient provided a beam line is set up close to the target-source system, in order to use very low energy beams. Beams such as ^{19}O, ^{57}Mn, ^{67}Ga and ^{61}Cu appear to be the most useful.

REFERENCES

[NFFS 66-92]   Proceedings of the International Conferences on Nuclei Far From
               Stability :
               1) Lysekil 1966, (W.Forsling, C.J. Herrlander and H. Ryde ed.,
               Almqvist & Wiksell, Stockholm).
               2) Leysin 1970, CERN-Report 70-30, Vols. 1-2.
               3) Cargèse 1976, CERN-Report 76-13.
               4) Helsingør 1981, CERN-Report 81-09.
               5) Rosseau Lake 1987, AIP-Vol. 164 (I. S. Towner ed.)
               6) Bernkastel 1992 (J.Bonn, K.L.Kratz and G. Münzenberg ed., IOP
               Publishing), in press.
[ANN90]   R. Anne et al., Phys. Lett. B250 (1990), 19.
[ANN93]   R. Anne et al., Nouvelles de Ganil 45 (1993), 3.
[ARN90]   M. Arnould et al., Proc. Ecole Joliot Curie de Physique Nucléaire
               1990, Maubuisson (France) and references therein.
[AUF90]   M.-B. Aufderheide et al., Ap. J. 362 (1990) 241.
[AUG91]   G. Auger et al., J. Phys. G17 (1991), S463.
[BAR88]   C.A. Barnes, Research Reports in Physics : Nuclear Astrophysics
               (M. Lozano, M.I. Gallardo and J.-M. Arias ed., Springer Verlag,
               Berlin 1988).
[BEC92]   F.A. Beck, Prog. Part. Nucl. Phys. 28 (1992), 443.
[BER 92]   J.F. Berger, J.P. Delaroche et M. Girod, in NFFS 1992.
[BES89]   J. Besprovsvany and S. Levit., Phys. Lett. B217 (1989) 1.
[BON85]   P. Bonche et al., Nucl. Phys. A443 (1985), 39.
[BON86]   P. Bonche et al., Phys. Lett. B175 (1986), 387.
[BOR 92]   V. Borrel et al., Z.Phys. A344 (1992), 135.
[BYR90]   T. Byrski et al., Phys. Rev. Lett. 66 (1990), 1650.
[COM88]   E. Comay et al., Phys. Lett. B210 (1988), 31.
[DES87]   Ph. Dessagne et al., in NFFS 1987.
[DES88]   Ph. Dessagne et al., Phys. Rev. C37 (1988), 2687.
[DET90]   C. Détraz et al., Nucl. Phys. A519 (1990), 529.
[DRA91]   J.P. Draayer, Proc. AIP Conf. on Future Directions in Nuclear Physics
               with 4 π Gamma Detection Systems of the New Generation,
               Strasbourg (France) 1991 (J. Dudek and B. Haas ed.) p. 12.
[DUD88]   J. Dudek et al., Phys. Lett. B211 (1988), 252.
[FAY91]   S.A. Fayans, Phys. Lett. B267 (1991), 443.
[GIL86]   A. Gillibert et al., Phys. Lett. B176 (1986), 317.
[GOR91]   S. Goriely, Ph. D. Thesis, Oxford (1991), unpublished.
[HAN93]   P.G. Hansen, A.S. Jensen and K. Riisager, Nucl. Phys. A560 (1993), 85.
[HAR90]   J.-C. Hardy, Nucl. Phys. A509 (1990), 429.
[HOF89a]   C. Hoffman et al., Nucl. Phys. A502 (1989) 21c.
[HOF91]   H. Hofsass and O. Linder, Phys. Rep.201 (1991) 121.
[HOF89b]   S. Hofmann, Proc. Workshop Particle Emission from Nuclei, Raton,
               USA, 1989 (D. Poenaru and M. Ivascu ed., CRC-Press, Boca).
[HUS91]   M.S. Hussein et al., Nucl. Phys. A531 (1991), 191.
[HUS92]   M.S. Hussein et al., Phys. Rev. C46 (1992), 377.
[KOB89]   T. Kobayashi et al., Phys. Lett. B232 (1989), 51.
[KOL92]   J.J. Kolata et al., Phys. Rev. Lett. 69 (1992), 2631.
[LEW93]   M. Lewitowicz et al., Nucl. Phys. A562 (1993), 301.

[LI91]   X. Li et al., Phys. Lett. B271 (1991), 281.
[MAL89]   M.L. Mallort et al; NIM B40/41(1989),179.
[MAT90]   G.-J. Mathews et al., Nature 345 (1990) 491.
[MIE91]   Ch. Miché et al., Proc. Workshop Nucl. Shape and Nucl. Struct. at
              Low Excitation Energies, Cargèse, France, June 1991 (M. Vergnes,
              J. Sauvage, P. Heenen, H.-T. Duong ed., Plenum, New York)
[MOL86]   P. Möller et al., Zeit. Phys. A323 (1986), 41.
[MOO92]   C.B. Moon et al., Phys. Lett. B297 (1992), 39.
[MUN89]   G. Münzenberg, Nucl. Phys. A502 (1989), 571c.
[NAZ87]   W. Nazaezwicz et al., Nucl. Phys. A467 (1987), 437.
[OGA84]   K. Ogawa, Proc. AMCO 7, Darmstadt-Seeheim (Germany),1984
              (O. Klepper ed.) p.530.
[OGA 91]   Yu.T. Oganessian et al., Nucl. Phys. News 1 (1991), 28.
[PAG 92]   R.D. Page et al., Phys. Rev. Lett. 68 (1992), 1287.
[PAT89]   Z. Patyk et al., Nucl. Phys. A502 (1989), 591c.
[PER92]   Perspectives in Physics with Heavy-Ion Beams, GANIL report R92-08.
[POU89]   F. Pougheon et al., Nucl. Phys. A500 (1989), 287.
[RAY87]   M. Rayet, in Lectures Notes in Physics 287 : Nuclear Astrophysics
              (W. Hillebrandt ed., Springer Verlag, Berlin, 1987), p.210.
[SAG90]   H. Sagawa et al., Phys. Lett. B251 (1990), 17.
[SAT91]   G.R. Satchler et al., Nucl. Phys. A522 (1991), 621.
[SCH87]   G. Schatz et al, Hyp. Int. 34 (1987),555.
[SCH89]   N. Schulz et al., Phys. Rev. Lett. 63 (1989), 2645.
[STE86]   S.G. Steadman et al., Ann. Rev. Nucl. Sci. 36 (1986), 649.
[TAN91]   I. Tanihata, Nucl. Phys. A 522 (1991), 275 c.
[TAK90]   N. Takigawa and T. Shinozuka, Proc. of the 18th Int. Symp. on
              Physics with High-Intensity Hadrons Accelerators, Tokyo (Japan),
              1990,p. 223.
[THI86]   F.-K. Thielemann et al., in Advances in Nuclear Astrophysics
              (E. Vangioni-Flam ed., Editions Frontières, Gif/Yvette, 1986), p.525.
[TOW87]   I.S.Towner, Phys. Rep. 155 (1987), 263.
[WER92]   T. Werner et al., to be published.
[WEY81]   G. Weyer,NIM 186 (1981),201.
[WOO81]   P. Woods et al., Phys. Lett. B105 (1981), 339.

THE SPIRAL PROJECT

The project is divided into two independent parts :

- The first consists in providing the transport of the very high-intensity beams produced by the CO1 injector to the L3 beam line downstream of CSS2 (**THI** - Transport de Haute Intensité - High Intensity Transport). Among other work and modifications, the most important unit to be constructed is the medium-energy rebuncher (R2).

- The second is called **SPIRAL** (Separateur et Postaccélérateur d'Ions Radioactifs Accélérés en Ligne - Separator and Postaccelerator of On-line Produced Radioactive Ions). This consists of collecting and ionizing the radioactive ions formed by the interaction of the GANIL primary beam with a thick target, then separating them, subjecting them to postacceleration and, finally, reinjecting them in the spectrometer which is ahead of the beam distribution line going to the experimental areas.

In this section, we give a brief description of the projects (as more details of the technical developments are given in the third section) and discuss the planning, personnel and financial aspects.

1 - THE THI PROJECT

GANIL now produces beams with intensities reaching 1 to 2.10^{12} pps for the light ions at 95 MeV/nucleon, as the power is intentionally limited to 400 watts. The combination of the new ECR [1]4 source operating at 14.5 GHz and an injection stage at 100 kV, not only makes it possible to have the acceleration of higher intensities, but also to have a significantly improved transmission factor between this source and the cyclotron injector exit. This possibility entails the necessity of adapting the whole accelerator to high power beams (between 5 and 10 kW) both from the point of view of the adjustments and that of the protection and safety of the installation.

This operation is divided into two phases with equal financial requirements: the installation of a rebuncher (R2) in the L2 beam line, which conducts the beam from CSS1 to CSS2, and the adaptation of all of the machine to operating at a high intensity.

1.1. THE R2 REBUNCHER

The medium-energy rebuncher installed on the L2 line to reduce the phase extension of the bunches (and, consequently, increase the transmission in CSS2 which then reaches 100% for the internal light-ion beams) is a quarter wave type resonant cavity with two accelerating gaps operating in the 27 to 56 MHz frequency range.

1.2. ADAPTATION OF GANIL TO HIGH-INTENSITY OPERATION

A limited ion range extending from helium to argon will be used. The consequences of the intensity increase are described below.

1.2.1. Space charge

For an increase in intensity of the order of 15, the space-charge forces have an effect in the axial injection line up to the injector cyclotron. This complicates the transition between the adjustment phase of the machine, in which it must operate at a reduced intensity, and the high-intensity operating phase. The installation of an intensity reducer positioned as close as possible to the source and consisting of a pepper-pot shield appears to be the most satisfactory solution, in opposition with a high frequency chopping device which perturbs the stability of the beam control feedback systems.

1.2.2. Beam losses

The interception of the beam by any component of the accelerator can be partial or complete, local or distributed as well as transitory or lengthy.

1 *Electron Cyclotron Resonance*

Thermal aspect.

a) The accidental losses on the vacuum chamber walls as well as on components like the injection and ejection units of cyclotrons can lead, depending on the degree of focusing in these locations, to very rapid melting (a few milliseconds for elements that are not cooled). Thus, a detection system with an appropriate time response must be installed. For the injection/ejection units, the present entry diagnostics can be used for this objective, but they must be connected to a fast data processor (to be developed) which initiates the safety actions. As for the vacuum chambers which would be particularly endangered, especially the bending magnets, in addition to the necessity of equipping them with internal thermal shielding, it is proposed to install externally the system of ionization chambers adopted on the beam lines and the cyclotrons of the Paul Scherrer Institut at Villigen.

All the injection/ejection units are designed so that low but continuous losses can be tolerated except for the ejection of the CO1 injector which must be revised.

An on-line monitoring of certain current or voltage supplies (essentially those which control the bending magnets) is to be developed. It consists of monitoring the drift out of the desired values and specially the intensity of the beam delivered out off a given range.

Finally, considerable work must be carried out on the development of software for the automation of the adjustments, of the optimization and management of beam losses. This is required to ensure the stability of these high-intensity beams. This implies an increase of the ensemble of non-interceptive diagnostics based on the present model (or with slight modifications), in particular the position probes for monitoring the beam alignment.

b) The development of a non-interceptive radial transient probe at the ejection of CSS2 is required.

- The utilization on the L2 and L3 lines of residual gas ionisation profilers, developed at GANIL by the Experimental Area Division, makes it possible to regulate and measure high intensities. For the upstream lines, the spiral wire profiler, locally developed at the JINR at Dubna, is very suitable.

Radiological aspects

The increase in intensity evidently results in a radiation increase and in the activation of the irradiated components. The shielding must be reinforced in some locations of the CSS2 room, but above all, automated data processing systems must ensure the management of the losses measured by the instruments mentioned above as well as the spatial and temporal stability of the beam. For some of the critical components that are especially activated (defining slits, Faraday cups and beam stoppers) where a possible failure would obstruct the operation of the accelerator a demounting, handling and storage system must be developed which ensures an optimum protection of the personnel.

1.2.3. Lifetime of the stripping foils

The extrapolation of recent measurements of the lifetime of carbon foils used to

strip the beam at the energy of CSS1 gives an average value of 2.5 hours for a 10^{13} pps argon beam, focused as at present. Two methods are going to be tested to improve the performances of the solid stripper:

- Determine the limiting value of the beam diameter beyond which the increase in the beam emittance affects the current accepted in CSS2.

- Provide an arrangement for displacing the stripper in the beam so as to increase the total irradiated surface; obviously, the lifetime of the foils does not appear to be related to the heating, but, quite definitely, to modifications of the graphite structure.

1.3. REALIZATION PLANNING

The objective is to have finished the adaptation of GANIL to high-intensity operation at the beginning of 1996; in fact, it is only by this date that the R2 rebuncher will be in place and consequently, that the acceleration at high intensities will be possible.

Two constraints must be taken into account in the timetable :

- the multiyear apportioning of commitments presented at the Management Committee on 12/15/92.

- the shutdown periods of the machine, so that the additions or modifications of components do not perturb the normal operation.

1.4. PERSONNEL

The project can be carried out nearly completely with the GANIL personnel except that new capabilities will have to be developed, especially in the field of detectors and analogue signal processing (senior technician level).

Collaborations in parallel are required for the mechanical and radiofrequency studies, in particular for the R2 rebuncher (AGOR group of the IPN of Orsay and LNS of Saclay) and for the development of software for optimization and management of beam losses.

47

2 - THE SPIRAL PROJECT

2.1. GENERAL DESCRIPTION AND OBJECTIVES

The fundamental choices concerning the SPIRAL project result from the adequacy of the facilities available at GANIL, i.e. :
- intense high-energy heavy-ion beams,
- completely equipped experimental areas,
- technical teams with a great deal of experience about ECR sources and cyclotrons, with respect to the requests formulated by the experimenters.

2.1.1. The production method for radioactive ions

The radioactive elements result from interactions, within a thick target heated to a high temperature (1500 to 2000°C), between the nuclei of this target and the ions in the beam, referred to as "primary" and delivered by GANIL. They are produced in the form of atoms which diffuse out of the target.

The atoms are subsequently introduced into an electron cyclotron resonance (ECR) source and ionized. This source has been adapted to this function and to the ambient conditions. The high degrees of ionization that can be reached with this type of source have a direct effect on the possible type and size of the postaccelerator.

One of the main difficulties of this project is due to the great multiplicity of the elements and their isotopes which will be simultaneously produced and also to the fact that the desired beam intensity will be four to five orders of magnitude lower than that of the beams usually produced at GANIL.

2.1.2. The choice of the postaccelerator

We have chosen a compact cyclotron since :
- the high values of the charge-mass ratios (Q/A) of the ions from an ECR source allow the use of a cyclotron whose exit energy is, let us recall, proportional to the square of the Q/A ratio.
- the ranges of ions ($A \leq 100$) and of energies ($W \geq 6$ MeV/nucleon for $A \approx 100$ and $W_{max} \leq 25$ MeV/nucleon) requested by the experimenters are typical of a compact cyclotron, and also the required beam characteristics are well satisfied by this type of accelerator. In addition, a cyclotron is, essentially, a powerful mass analyzer. It will supply relatively pure beams, an essential quality in radioactive-ion physics.
- the GANIL technical groups have an in-depth knowledge of the design, construction and the operation of cyclotrons, which will result in a reduction of the delays in the realization and the commissioning.
- the cyclotron is, taking account of the beam characteristics specified for this project, the type of accelerator that has the lowest cost. The fact that it will be,

moreover, possible to install it, with all the other project facilities, within the limits of the present building is, of course, in accordance with this.

2.1.3. Use of the postaccelerated beam:

It will be possible to distribute the beam of postaccelerated radioactive ions to all of the present experimental rooms and thus, at this level, no specific additional investment is implied.

2.1.4. Interference with the normal operating mode of GANIL:

The accomplishment of this project will not result in any modification of the present operation of GANIL. Only a rearrangement and a short intervention will be necessary with respect to the high-energy spectrometer of the machine (α-spectrometer) to choose between the two possible operating modes : normal stable ions (present condition) or radioactive ions.
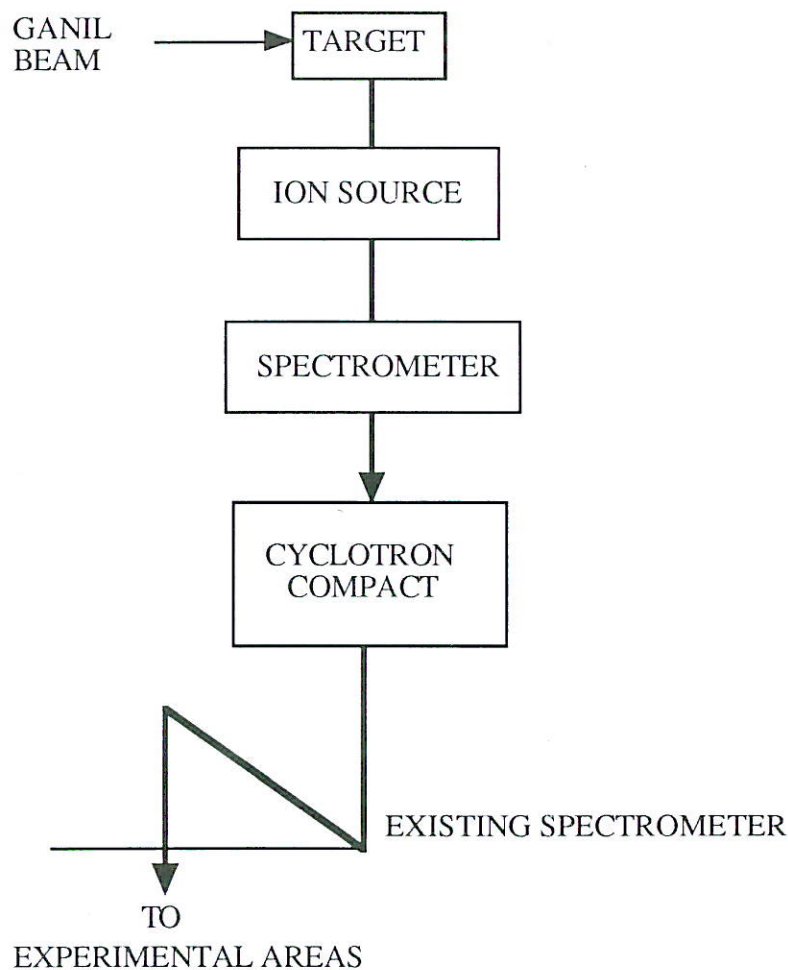
GANIL BEAM $\longrightarrow$ TARGET

ION SOURCE

SPECTROMETER

CYCLOTRON COMPACT

EXISTING SPECTROMETER

TO EXPERIMENTAL AREAS

Figure 6 : Schematic of the principle of the SPIRAL project

49

2.2. BRIEF DESCRIPTION

The constraints

The SPIRAL project is the result of compromises between different requirements, either environmental or technical, related to the putting into operation of the various components.

Thus, the implantation of the ensemble, in the northern end of the present machine building was designed so as not to result in any modification of the superstructures of this building.

In addition, certain constraints related to the future operation of the installation for the users have been taken into account as far as possible.

First, it is indispensable to plan for the installation of two target-source shielded caves knowing that, initially, only one cave will be equipped. This necessity is linked to the fact that the preparation of new radioactive beams will require a sustained research and development effort on the production and ionization and therefore, that a target-source cave must be available for this without interfering with the operation of the installation for the users. Moreover, a second cave would prove to be useful if, for safety measures, the first became temporarily unavailable. It is also for this reason that the two caves will be independent and, thus, accessible separately.

In addition, we wanted to respect three principles linked to the actual design of the production and ionization system:

a) The source axis (and, therefore, the direction of the radioactive beam) must be orthogonal to the arrival direction of the primary beam.

b) The source must be installed in the normal horizontal position to provide easier access for equipment and automated handling.

c) The primary and the secondary beams must not cross each other (complete independence of the vacuum chambers), their only common point being the target container.

Project structure

The SPIRAL project (figure 7) consists essentially of :

- A shielded cave in the basement housing the target-source ensemble and towards which the L3 high-energy beam line of the GANIL will be extended. This cave will be equipped with automated units to make it possible to demount and handle the activated components (targets, ion source vacuum chamber, etc.).

- A very low energy beam line (TBE) made up of a spectrometer ensuring a first level separation between the isotopes produced and subsequent division into two branches conducting the beam, one going to the experimental areas at this energy via a high-resolution spectrometer (which is not included in the first phase of the project), the other towards the postaccelerator.

- A postaccelerator which will be a compact cyclotron (K factor = 265) giving the radioactive ions an energy which depends on their atomic mass and their ionization state (from 2 to 25 MeV/nucleon).

- A medium-energy beam line (ME) conducting the beam extracted from the cyclotron to the focal point of the existing high-energy spectrometer (α spectrometer).
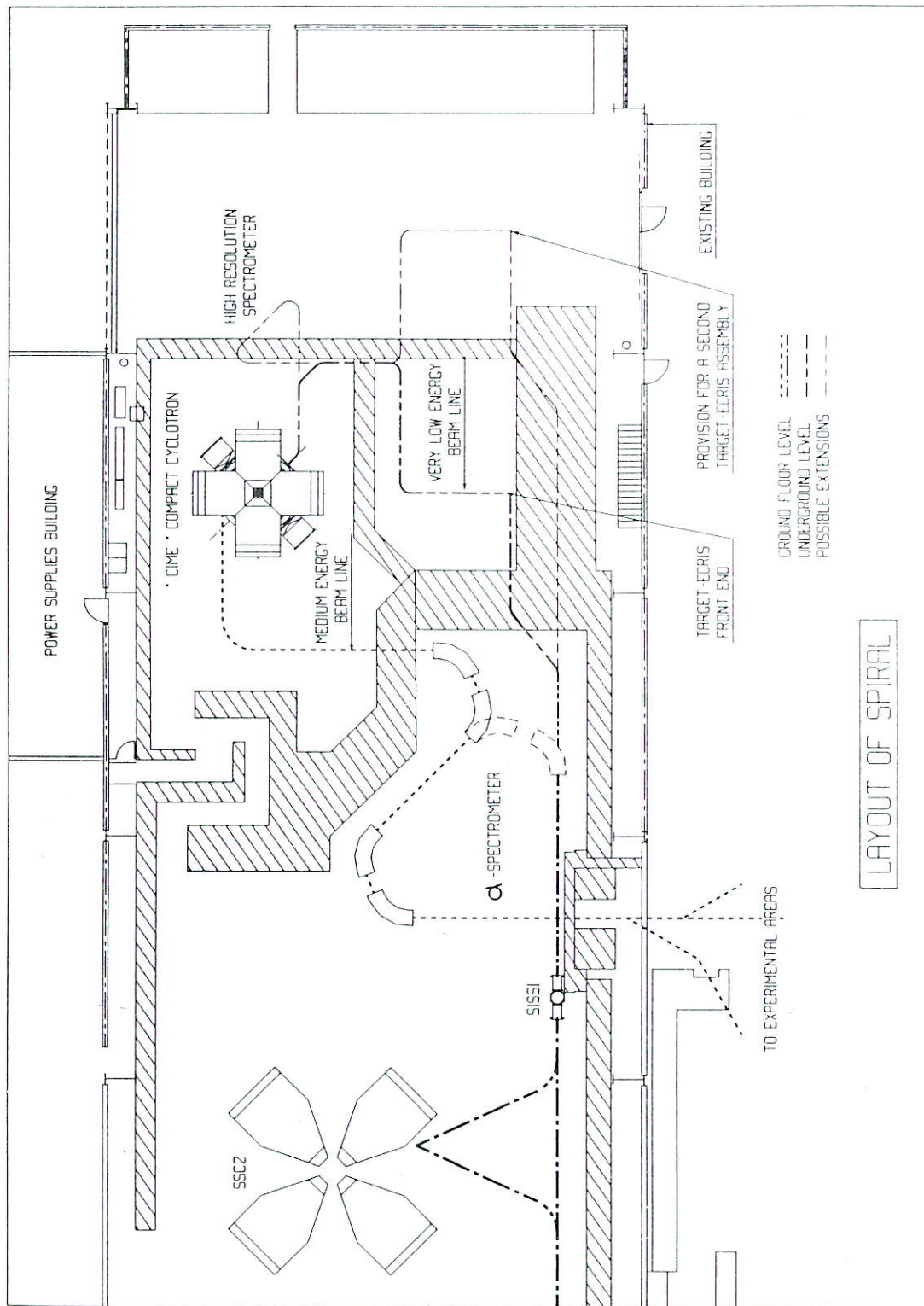
50

Figure 7 : SPIRAL project implantation schematic

The CIME (Cyclotron d'Ions à Moyenne Energie - Medium-energy ions cyclotron)

The principal discussions during the 7 months following the first presentation of the SPIRAL project (GANIL R92/11) have essentially concerned the following points :

- Characteristics of the beam delivered with respect to the physics requirements in collaboration with the performance evaluation group and the project group.
- Studies of the major components with long construction times (magnet, H.F.).
- Design of the ensemble.

The cyclotron parameters (figure 8) :

Let us recall that the basic specification for the postaccelerator is to obtain 6 MeV/nucleon for the masses A > 100. This implies that charge states such as Q/A ≥ 0.15 will be produced by the ECR source.
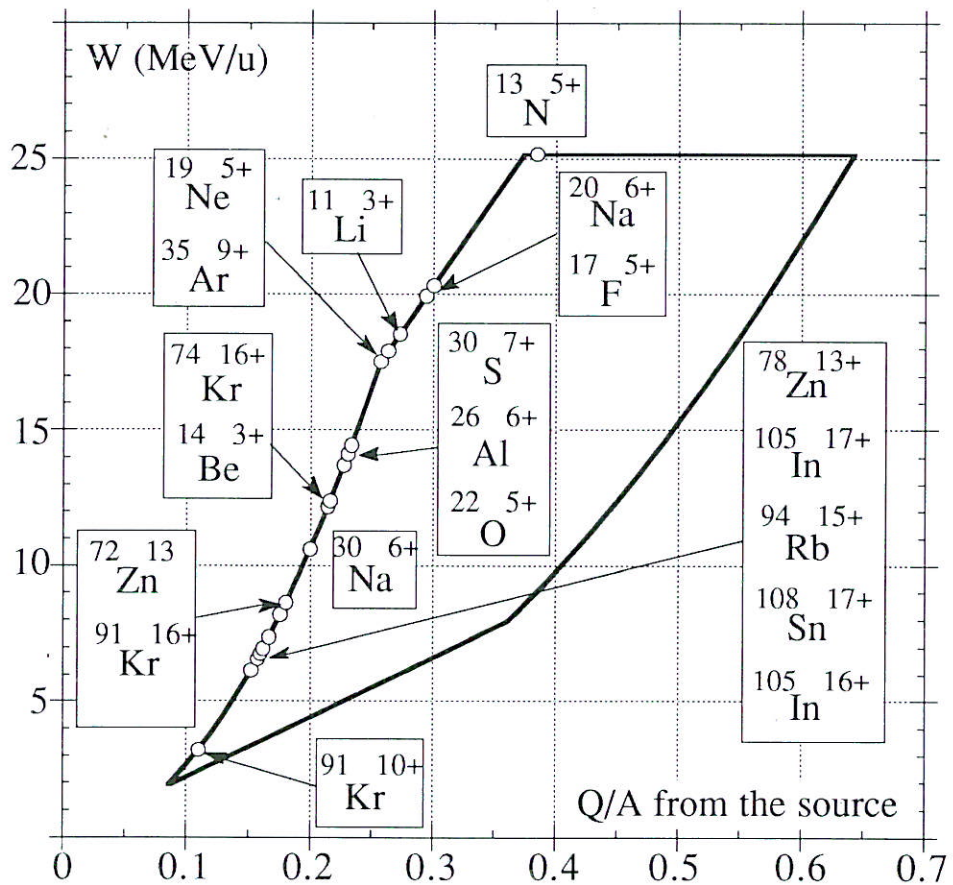

Figure 8 : Energy range of the CIME cyclotron

To attain this objective, the initially given k factor = 265 of the compact cyclotron is retained (BR_{ejec} = 2.344T.m with R_{ejec} = 1.50m).

The list of radioactive ions recommended by NuPECC shows that only a few light ions ($^{13}N^{5+}$, $^{7}Be^{3+}$, $^{14}O^{6+}$) that are already highly ionized, with Q/A ≥ 0.35, would be able to benefit from energies ≥ 20 to 30 MeV/nucleon. It was therefore agreed that the highest energy previously selected (29 MeV/nucleon) could be reduced.

On the other hand, there were strong requests that the low energy should be revised downwards : 2 MeV/nucleon is desired for the light ions. Technically, the cyclotron does not lend itself to very low energies due to difficulties in the construction of the RF system.

The following has, therefore, been proposed.

The energy range 2.7-25 MeV/nucleon, corresponding to the revolution frequency 2.4-7.25 MHz will be produced with the RF frequency range 9.6-14.4 MHz with the 2nd 3rd and 4th harmonics with the normal characteristics stated for the intensity, emittance and energy dispersion.

Energy as low as 1.9 MeV/nucleon will be obtained by working with the 5th harmonic on the condition that the beam intensity can be reduced (so as to reduce the emittance), which is not too detrimental with light ions, and a lower quality beam is acceptable for the users.

Mass separation

The cleaning of the beam, which is one of the basic requirements of the users, is obtained, downstream of the TBE spectrometer ($\Delta m/m = 4.10^{-3}$) by the complementary action of the acceleration by the cyclotron (in itself selective in the atomic charge-mass ratio $\Delta(Q/A) / (Q/A) \approx$ a few 10^{-4}) and the use of the stopping power of a thin carbon foil (which is atomic number selective) and which will make it possible, in association with the α spectrometer, to separate the isobars (within certain limits).

2.3. GENERAL PLANNING
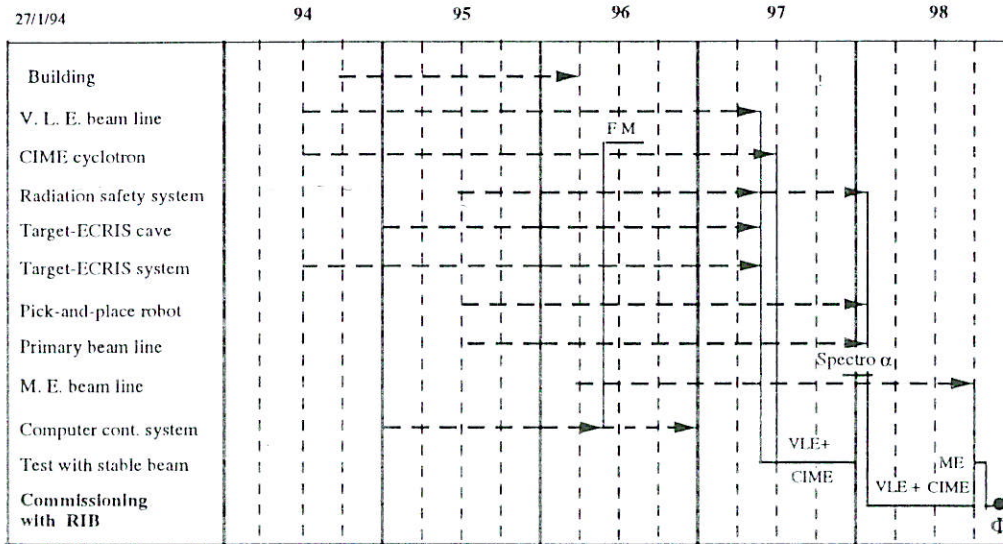
FM = Field mapping

2.4. PERSONNEL REQUIRED

Assuming an ideal situation in which there will be a closely knit group working full time and brought together at a single site, the overall requirements are, outside of subcontractors, estimated to be around 60 engineer.years and 80 technician.years (the most recent example of a similar sized project is that of AGOR).

As a consequence, it appears impossible to release the personnel required for a project the size of SPIRAL from GANIL. Some other projects already decided upon at GANIL are either in the first phase of operation (OAI, INDRA, data processing system for control of the machine), or in the course of realization (SISSI, THI, SIRa, renovating of the machine components and auxiliary equipment) and, above all, there is the considerable load of maintaining and operating GANIL and keeping the quality of this operation at the high level required by its users.

The solution can be found only through the intermediary of collaborations with other laboratories of the IN2P3[2], of the CEA/DSM[3] and of the CEA/DAM[4]

The first natural partners in this collaboration would be the AGOR group (IPN Orsay), the LNS (Saclay) and the DSM/DAPNIA (CEA, Saclay) which have already participated in preliminary studies carried out for this project. More recently a collaboration has also started with the DAM/Essais (CEA,Bruyères le Châtel).

---

[2] *Institut National de Physique Nucléaire et de Physique des Particules du CNRS*
[3] *Commissariat à l'Energie Atomique/Direction des Sciences de la Matière*
[4] *Commissariat à l'Energie Atomique/Direction des Applications Militaires*

TECHNICAL DESCRIPTION

OF THE SPIRAL PROJECT

1 - PRODUCTION AND IONISATION OF RADIOACTIVE ATOMS

1.1. PRODUCTION

1.1.1. Production methods

There are two main methods for the production of high energy radioactive ions: the fragmentation of the projectile in a thin target followed by a recoil spectrometer [MUE89] and the so-called ISOL [EIS92] method (Isotope Separator On-Line) followed by a post-accelerator.

The first method, employed extensively at GANIL and most notably at present in conjunction with the SISSI project, has its advantages and limits. The ISOL method, described here, forms the basis of the SPIRAL project and uses a complementary approach.

Classically in the ISOL technique a proton or a light ion beam is accelerated to a high energy and bombards a thick target producing radioactive nuclei by spallation reactions, fragmentation of the target and/or induced fission. Other reaction mechanisms, however, come into play with heavy ions. In particular, projectile fragmentation is the process of most importance. In all cases, the fragments are stopped in the target which is heated to a high temperature ($1500°$ to $2000°C$) to facilitate the migration of the radioactive atoms to the surface. Usually the target is located a short distance from the ion source and the radioactive ions effuse via a transfer tube to the plasma region where they are ionised and then accelerated. However, given the relatively short range of heavy ions (typically they stop in the production target) one could imagine locating the target itself in the ion source. Such a configuration would thus eliminate the losses due to sticking in the transfer tube - a major source of losses in systems presently in use . As the beam is ionised and accelerated in a manner identical to that for stable beams, the resulting radioactive beams are very pure, have good dynamic and optical characteristics and an energy which may be precisely adjusted.

The majority of the installations existing or in development use an intense high energy proton beam - ISOLDE at CERN, ISAC at TRIUMF, ISIS at the Rutherford Appleton Lab and the Isospin Laboratory project in North America. A few projects differ in that they use low energy light ions or protons- HHIRF at Oak Ridge and ARENAS 3 at Louvain-la-Neuve. The PIAFE project (ISN - Grenoble), in contrast, uses the high neutron flux of the ILL reactor to produce medium mass (A ~ 120) nuclei via thermal neutron fission of a Uranium target [ERB92].

The originality of the GANIL project lies in the use of an extended range of heavy ions, up to the maximum energies available at GANIL (eg. 95 MeV/nucleon for ^{12}C). Such an approach differs from the proton (or light ion) beam technique in that

the projectile rather than the target is varied in order to produce the different radioactive species, thereby allowing one to use the most resiliant and efficient production target for all cases.

1.1.2. The ISOL method with heavy ions

The production rate of exotic nuclei from heavy ions is:

$$\tau(A,Z) = I_P \int_0^{E_{max}} \sigma_f(A,Z,E) \, \varepsilon_c dE$$

where $\sigma_f(A,Z,E)$ is the total production cross section of the nucleus of mass A and atomic number Z at energy E, I_p the intensity of the primary beam (particles/s) and ε_c the range of the projectile in the target (paricles/cm^2).
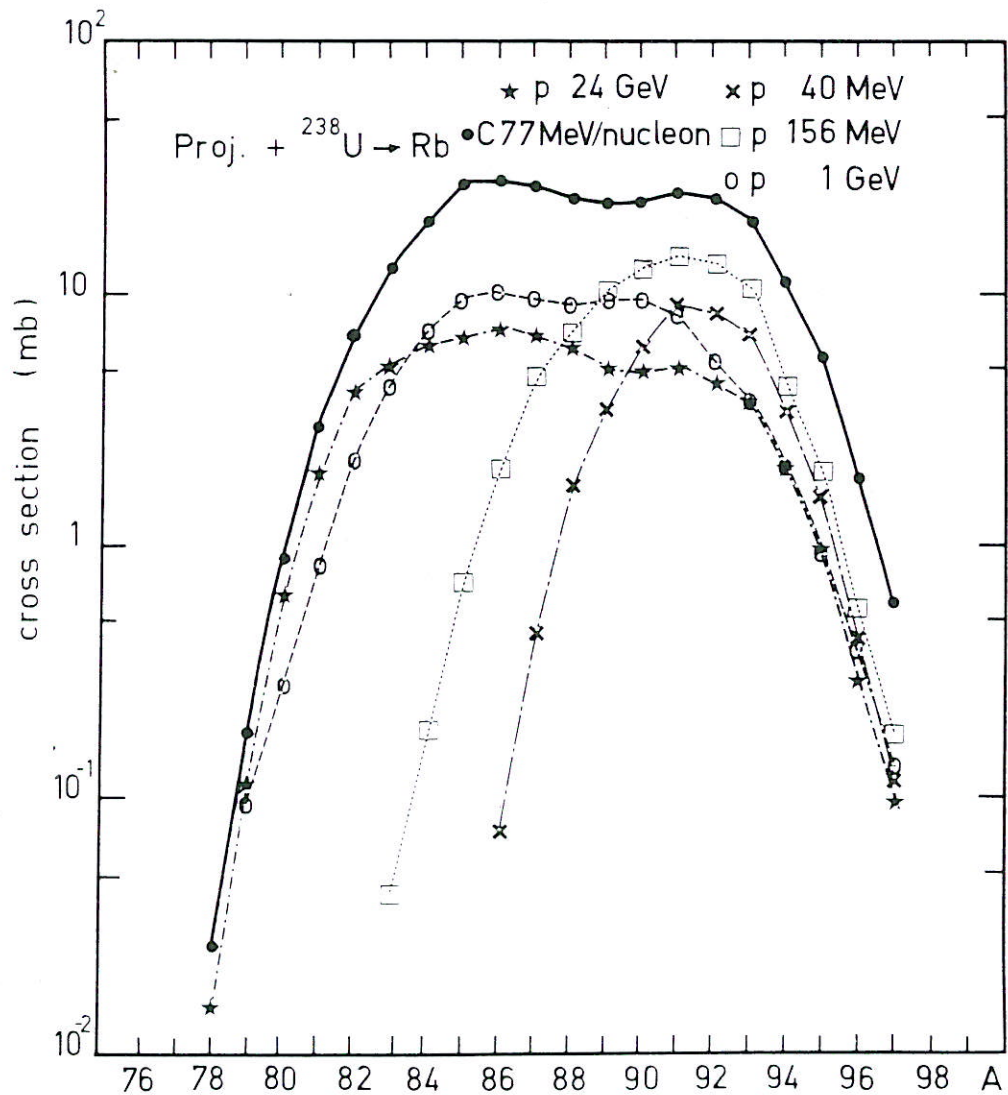

Figure 9a.

The total production cross section for a nucleus are generally higher for heavy ions than for protons. For example, the isotopic distributions of Rb and Cs nuclei obtained in the bombardment of a ^{238}U target by 77 A.MeV ^{12}C ions and by protons of different energies - 40 MeV, 156 MeV, 1 GeV and 24 GeV - are compared in figure 9. In the majority of cases the cross sections for ^{12}C exceed those for protons. This can be related to the size of the projectile and to the increase of the fission cross sections due to the angular momentum provided by the heavy ions. From the point of view of the production of exotic nuclei, the use of heavy ions compares favourably to that of high energy protons when the intensities are comparable.

The production yields for a number of nuclei were estimated and are summarised in table IV. It must be noted that these production yields do not account for the diffusion out of the production target or the effusion, ionisation, extraction (from the source), transport and acceleration efficiencies.
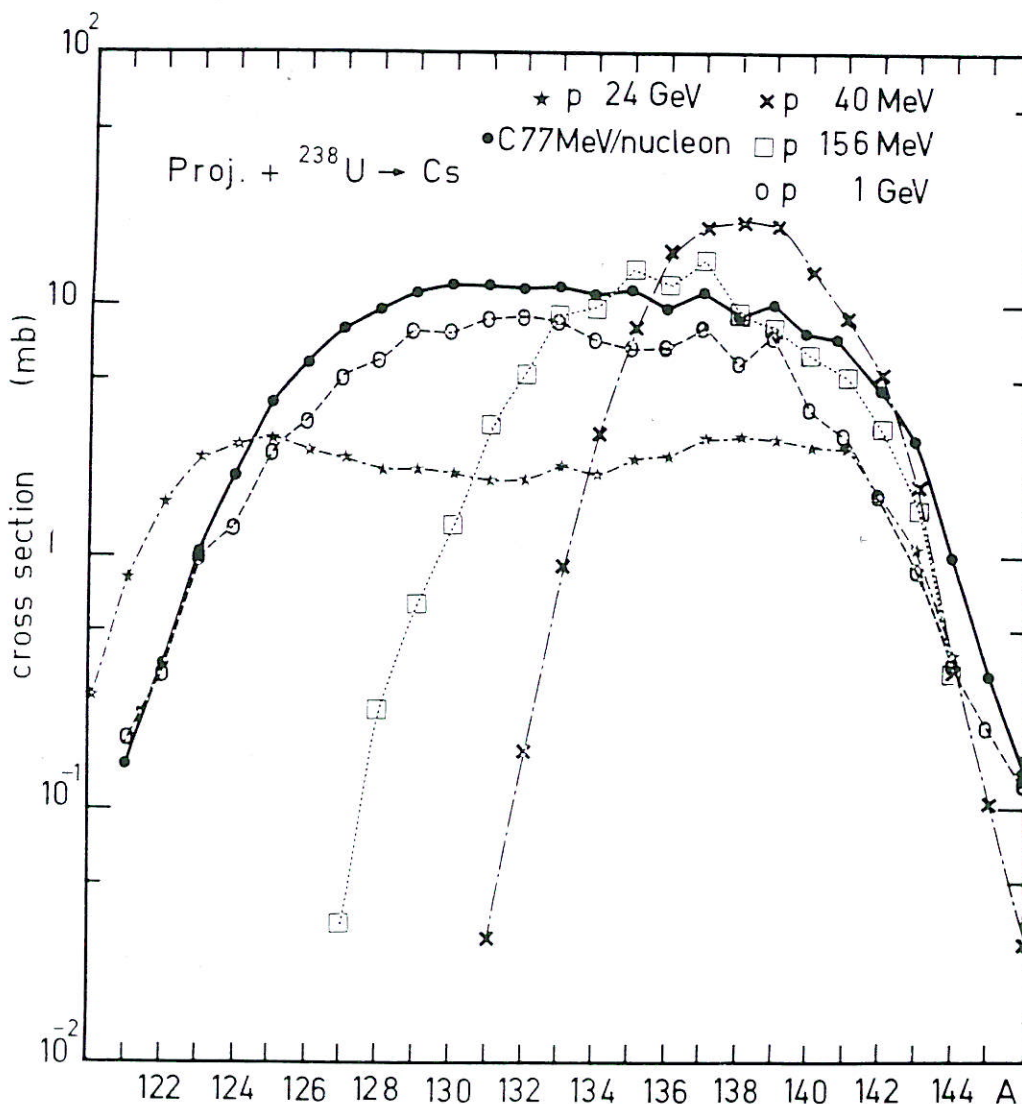

Figure 9b : Comparison of the isotopic distributions of Rb and Cs nuclei for the system ^{12}C+^{238}U with those obtained in the system p+^{238}U at different energies. [SAI82]

	CERN - ISOLDE (a)				GANIL				
	Reaction	Targ. thick. g/cm²	Production rates in target (1/s/10μA)	Half-life	Reaction	Targ. thick. g/cm²	σ (mb)	Estim. uncert. factor	Production rates in target (1/s/10μAp)
^{8}He	232Th(p.fg)	56	8×10^9	119 ms	^{11}B + ^{12}C	2.5	10	10	6×10^{10}
^{8}Li	Ta + p	122	4×10^{10}	842 ms	^{10}B + ^{12}C	3.5	25	4	2.5×10^{11}
$^9_3$Li	Ta + p	122	1.5×10^{10}	173 ms	^{11}B + ^{12}C	2.5	8	4	6×10^{10}
$^{11}_3$Li	Ta + p	122		8.7 ms	^{18}O + ^{12}C	1.3	0.01	1.5	4×10^7
^{7}Be	C + p	30		53 d	^{9}Be + ^{12}C ^{10}B + ^{12}C	4 3.5	23 19	4 4	2.9×10^{11} 2×10^{11}
^{11}Be	Ta + p	122	1.5×10^{10}	13.8 s	^{13}C + ^{12}C	2	5	2	3×10^{11}
^{14}Be				4 ms	^{18}O + ^{12}C	1.3	0.0025	1.5	1×10^7
^{9}C				127 ms	^{12}C + ^{12}C	2.5	2×0.3	3	4.7×10^9
^{16}C	18O + p	6	1.3×10^{10}	750 ms	^{18}O + ^{12}C	1.3	0.5	4	2×10^9
^{18}C					^{22}Ne + ^{12}C	1.1	10^{-2}	4	3×10^7
^{13}N	O + p	2	5×10^{10}	10 min	^{14}N + B	2.2	50	2	3×10^{11}
^{14}O	14N + p	10		70.5 s	^{16}O + ^{12}C	1.9	2	4	1.3×10^{10}
^{19}Ne	24Mg + p	3	3.6×10^{10}	17.2 s	^{20}Ne + ^{12}C	1.4	50	2	2.2×10^{11}
^{21}Na	Ti + p	40	9×10^{10}	22.5 s	^{23}Na + ^{12}C	1.2	30	4	1×10^{11}
^{29}Na	U + p	13	4×10^6	43 s	^{12}C + U ^{40}Ar + ^{12}C	4.0 .9	10^{-2} 5×10^{-3}	1.5 2	6×10^6 1.4×10^7
^{46}K	U + p	13	9×10^7	1.8 min	^{12}C + U ^{12}C + ^{48}CaO	4.0 4	.5 20	1.5 4	3×10^8 3×10^{10}
^{72}Zn	Ge + p	134	1.6×10^7 (b)	46 h	^{12}C + Au	4.9	20	2	2×10^{10}
^{80}Rb	Nb + p	50	1.9×10^{11}	30 s	^{12}C + U ^{12}C + ^{93}Nb	4.0 3.5	0.7 1.8	1.5 3	4×10^8 2.5×10^9
^{83}Rb	Nb + p	50	1.5×10^{11}	86.2 d	^{12}C + U ^{12}C + Nb	4.0 3.5	12 15	1.5 2	7.6×10^9 2×10^{10}
^{97}Rb	U + p	13	1.2×10^8	170 ms	^{12}C + U	4.0	0.6	1.5	3.8×10^8
^{119}Cs	Ta + p La + p	122 150	1.3×10^4 (c) 1.4×10^9	44 s	^{12}C + Ta ^{12}C + La	4.5 4.4	0.04 1.6	1.5 10	4×10^7 1.5×10^9
^{130}Cs	U + p	13 13	5×10^{10} 1.6×10^{10} (d)	29.9 min	^{12}C + U	4	12	1.5	9×10^9
^{145}Cs	U + p	13	2×10^8	59 s	^{12}C + U	4	0.3	1.5	2×10^8

a) Tested production yields, non corrected for ionization (b) and extraction (c) efficiencies.
d) Calculated from measured cross-sections.

Table IV.

1.2. IONISATION WITH AN ECR SOURCE

1.2.1. Transfer of radioactive atoms from the target to the ion source plasma

The diffusion of the radioactive products out of the target structure is a slow process whose speed is a function of the characteristic size of the target material (eg. grain size, foil thickness or fiber diameter) and the chemical affinity of the desired element. It is well known that, in the case of a granular material [FUJ81], the greater part of the time taken for the radioactive atoms to diffuse out of the target is the time

taken for each atom to escape from the grain where it was formed and not the time taken to travel between grains. For the other two target structures, the thickness of the foil or the diameter of fiber is the relevant dimension. Of course, the diffusion time is critically dependent on the target temperature.

Subsequent to the diffusion out of the target the atoms can be absorbed onto and released by any surface they come in contact with between the target and the plasma region (eg. target box, transfer tube, ion source chamber etc). The total time taken to reach the plasma region, thus, depends on the enthalpy of adsorption of the element and the temperature of the surfaces. This time, referred to as the effusion time, is almost certainly the "bottle neck" in the whole process. It should be noted that such effects can be neglected for noble gases. Of course, these losses increase as the half-life of the desired radioactive nucleus decreases. Thus it is essential that the target-plasma distance is as short as possible [KIR92].

1.2.2. Ion source

Ideally, the ion source must have two basic properties : a very good ionisation efficiency and small extracted beam emittance. The latter requirement is directly related to the mass resolution of the spectrometer which follows the source and the acceptance of the accelerator.

There are a great number of sources used in isotope separators. For several years ECR sources [ECR90] have been used on-line, notably at Louvain-la-Neuve and TRIUMF (Vancouver). These ECR sources have been, in general, optimised for the production of singly charged ions.

The GANIL project, SPIRAL, requires an ECR source with the following characteristics :
1) Charge-to-mass ratios, $Q/A \geq 0.10$,
2) emittance compatible with the axial injection of a cyclotron,
3) simple, compact and reliable,
4) low cost.

The first point has been demonstrated for stable gases. The total ionisation efficiency is approximately 40% over all ions in any charge state. For condensable materials, the presently performance of ECR sources at GANIL, is about 1% for a certain charge state. It can be implemented with some conceptual modifications of the ECR design and optimization of its performance. The second point refers to the design of the cyclotron for SPIRAL (CIME), which demands an emittance of 80π mm.mrad, independently of the extraction potential of the source. This point is perfectly compatible with presently available ECR technology. Points 3 and 4 are directly linked with the highly radioactivity environment which will be encountered around the target-source. The system should be compact in order to minimizes losses due to gas transfer, simple so as to allow remote handling and have a low cost, thus allowing the possibility of having several devices ready for use.

All these points point towards two solutions proposed for the SPIRAL project. The first one is called NANOGAN II, which is a low cost, on-line, ultra-compact multicharge ECR ion source with external target, based on the technology developed over many years at ISOLDE at CERN. The necessary magnetic field is provided by

permanent magnets as developed and tested with the original NANOGAN source at GANIL. The target is heated by the primary beam and/or by electron bombardment. The tranfer tube is as short as practically possible and is resistively heated. The whole system can be removable by remote control from the target-source cave. Figure 10 shows an schematic view of the proposed target-ion source device.
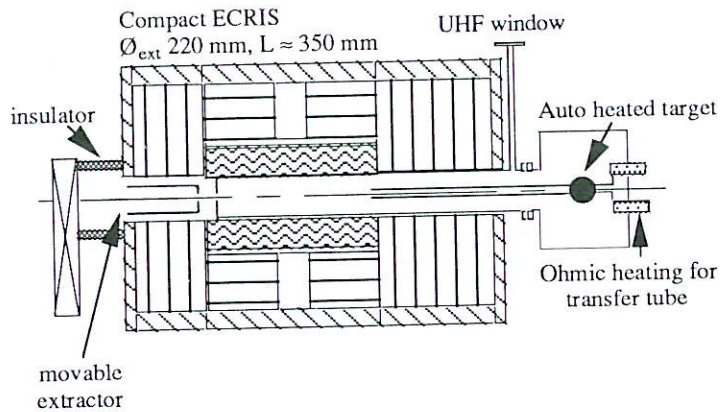

Figure 10 : NANOGAN II - 14.5 GHz

The second possibility for a target-ion source design involves the use of an internal target which would be well adapted to radioactive nuclei with short lifetimes. The device under consideration here at GANIL is called MAFIRa (MAchine à Faire des Ions Radioactifs) and is presented in figure 11. The goal of this design is to minimize the distance between the target and the plasma zone. Having the target inside the ECR increases significantly the diameter of the plasma chamber, thus requiring the use of coils for some magnetic elements instead of permanent magnets as in NANOGAN II. The possibility, yet to be studied, of having a double ECR resonance with two ECR frequencies, also offers the possibility of a significantly increased performance for condensable elements.
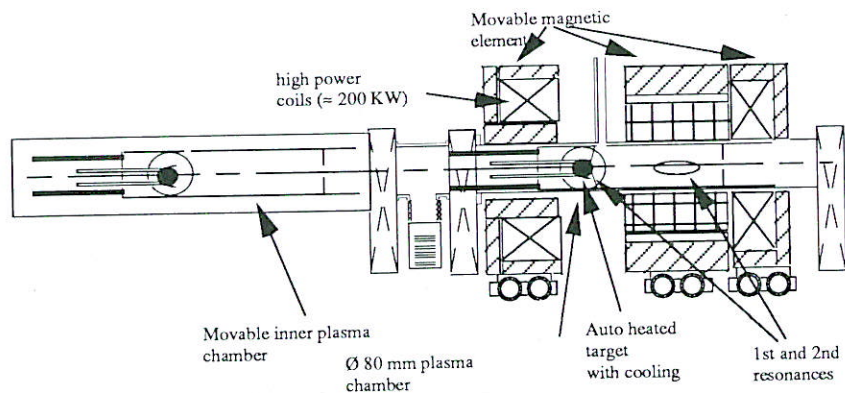

Figure 11: MAFIRA - 14.5 GHz

1.3. Research and development

1.3.1. Progress in 1991 and 1992 (collaboration with IPN, CSNSM and LPC)

The first separator was installed in experimental room D2, but under conditions that did not allow easy and reasonablly straightforward operation. Due to a very tight schedule and a limited budget it was not possible to displace the CYRANO reaction chamber which resulted in troublesome practical consequences. In particular, the target was not placed at an achromatic point and the position of the impact spot was therefore directly dependent on drifts in the beam. Additionally it was not possible to sufficiently shield the collection and detection systems, located in the same room, from the background generated by the primary beam. Thus, it was necessary to operate in a pulsed mode, using the dead time between pulses of the primary beam to identify the radioactive ions produced. To these disadvantages must be added that of having only just installed a new ECR source (NANOGAN), that was not sufficiently well tested and which had only mediocre extraction optics.

The collection system was made up of a metallised travelling tape collecting the ions and transporting them to two detection systems. The first consisted of two NaI (crystals) which were used to detect the two gammas emitted by positron annihilation, whilst the second consisted of a scintillator and a germanium detector.

Five experiments were carried out from March to September 1992 with four different primary beams and with targets of MgO, Al_3SiO_2 and CV. The following radioactive elements were detected : $^{10,11}C$, $^{18,19,23,24}Ne$ and ^{87}Kr. The following table gives the results obtained. After the last experiment in September 1992, the NANOGAN source was mounted on a test bench to ascertain the causes of the poor extraction and transport efficiencies observed and to measure the correction factors to be applied to the detected intensities to arrive at the actual production yields at the target level.

	Separator		ECR I. S.		Target	
	Yield meas. pps/pμA	Trans. eff.. %	Yield extract. pps/pμA	Ion. eff. %	Yield prod. pps/pμA	Yield Calc. pps/pμA
$^{19}Ne^{1+}$	$4.8\ 10^7$	3.5	$1.4\ 10^9$	25	$5.6\ 10^9$	
$^{19}Ne^{2+}$	$8.9\ 10^6$	3.5	$2.5\ 10^8$	7.5	$3.3\ 10^9$	
$^{19}Ne^{3+}$	$1.6\ 10^6$	3.5	$4.6\ 10^7$	4	$1.2\ 10^9$	
			$\Sigma 1.7\ 10^9$	40	$4.3\ 10^9$	$1.3\ 10^{10}$
$^{18}Ne^{2+}$	$1.9\ 10^6$	3.5	$5.4\ 10^7$	7.5	$7.2\ 10^8$	
$^{18}Ne^{4+}$	$1.9\ 10^5$	3.5	$5.4\ 10^6$	3.5	$1.5\ 10^8$	
			$*\ \Sigma 2.7\ 10^8$	40	$6.8\ 10^8$	$2.7\ 10^9$
$^{23}Ne^{1+}$	$6.3\ 10^5$	3.5	$1.8\ 10^7$	25	$7.2\ 10^7$	
$^{24}Ne^{1+}$	$1.5\ 10^5$	3.5	$4.3\ 10^6$	25	$1.7\ 10^7$	
$^{13}N^{1+}$	$3.8\ 10^5$	3.5	$1.1\ 10^7$	1(?)	$1.1\ 10^9$	

(*) with estimated yields of 1+ and 3+ charge states.

Table V

1.3.2. Progress in 1993 and the future

- The SIRa separator

After the first encouraging results obtained with the first separator, it was decided, in September 1992, that as soon as room D2 was completely free for the R & D for the radioactive ions, to construct a new separator called SIRa (Séparateur d'Ions Radioactifs) (figure 12). It was designed and constructed with the same collaboration as for the first separator (IPN and CSNSM-Orsay, LPC-Caen).
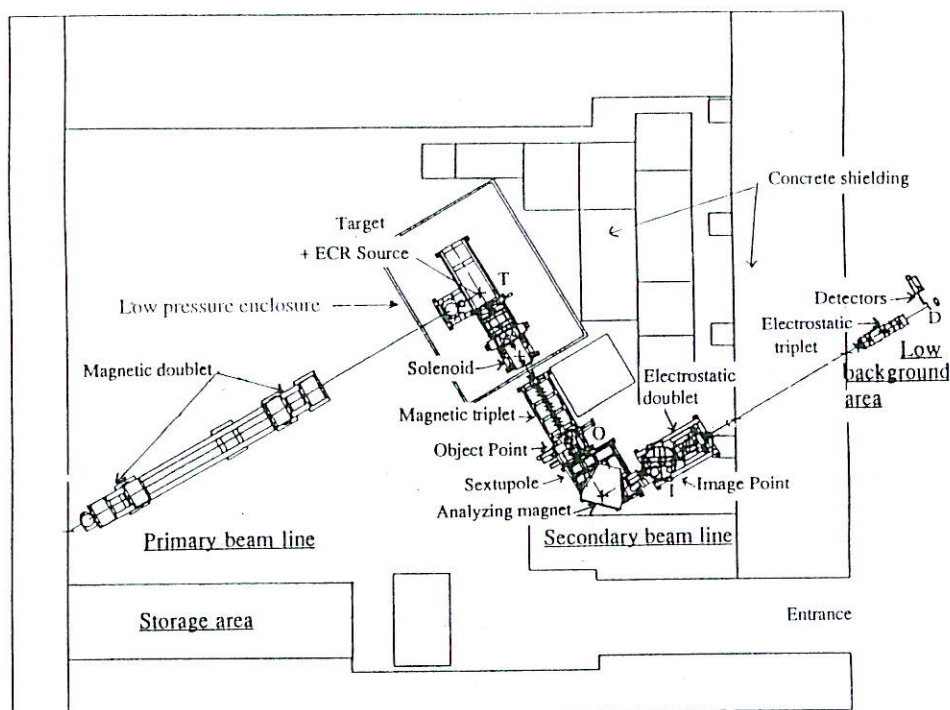

Figure 12 : Schematic diagram of the SIRa test bench facility

The study of the test bench facility was started in September 1992 and the first on-line test was conducted in November 1993. Some characteristics of SIRa of interest are :

- The production target is positioned at an achromatic focal point of the high energy line of room D2.

- The emitted atoms diffuse at 90° into an ECR source.

- A focusing system makes possible the beam matching from the exit of the source to the object point of the analysing dipole and also allows for the use of different types of sources with different source-object point distances.

- The focal point of the separator is in the detection system which is located outside D2. The detection system is thus well shielded (by concrete) from the primary beam induced backgrounds.

- The mass resolution (full width) of the separator is 1/250 .

A detailed description of this separator is given in the appendix.

- Experimental program

The first objective is to produce the gaseous radioactive nuclei ^{19}Ne, ^{34}Ar, ^{35}Ar and ^{77}Kr with good overall efficiency. As first approach we have utilised a very

flexible target box system, which allows us to control precisely the temperature of the target and measure the temperature at critical points. This target box is completly separeted from the ion-source itself and can be dismounted by remote control and placed in a shielded area far from the irradiation zone. This flexibility is very important during the first phase of R&D where we are testing performances of several components of the whole device. The target is connected to an ECR-3 source (the same type used for stable beams at GANIL) by a long transfer tube - approximately 60cm. This system is well adapted for performing the first on-line tests and exhibits good efficiencies for noble gases. We opted for using a well known ECR source in order to assure a good ionisation performance.

The first on-line test of SIRa was undertaken in November 1993. The target was carbon with a grain size of $4\mu m$ and a porosity of 8% . The first experiment had as its goal measurements of the overall efficiency of the separator for ^{35}Ar ($T_{1/2}$=1.77s) and the charge state distribution of ^{35}Ar ions produced produced by the ECR.

The overall efficiency of SIRa has been measured by implanting a known rate of ^{35}Ar ions produced by projectile fragmentation of a ^{36}Ar primary beam (95 MeV/nucleon) upstream from the target of SIRa. The secondary ^{35}Ar beam was selected by the α-spectrometer operated as a recoil separator and its rate was determinded using a Si detector located in front of the SIRa target. The ^{35}Ar released by the target at a high temperature (between 1200 and 1800 C) effuses threw to the ECR source, is ionised, extracted, selected by the separator and implanted in a plastic tape located ,as noted above, outside the experimental vault of SIRa itself. The γ-rays emmited by the decay of ^{35}Ar (1219 KeV) were detected using a Ge detector located just behind the tape.

The charge state distribution obtained for ^{35}Ar is compared in figure 13 with the same distribution for ^{40}Ar delivered from the same ion source. We can see that the performance of the ion source is the same off-line or on-line.

The overall efficiency of SIRa was measured as a function of the temperature. The maximum efficiency obtained so far was about 0.3% for ^{35}Ar. This efficency can
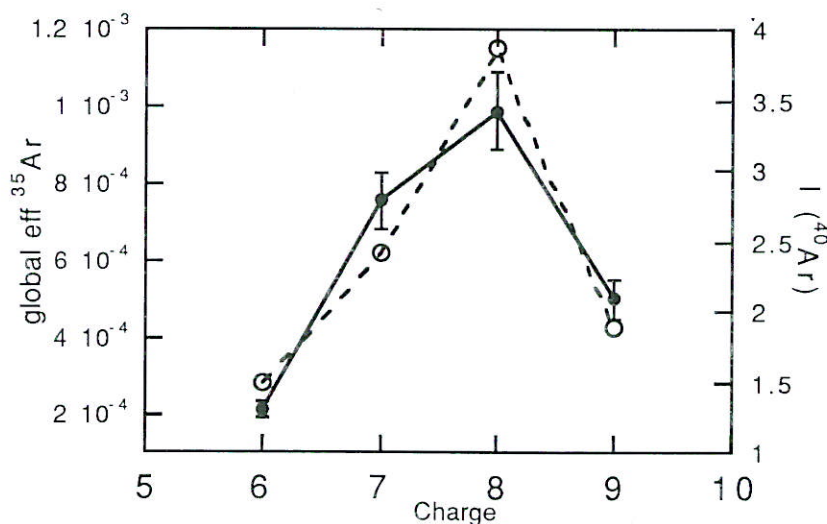

Figure 13 : Charge state distribution for ^{35}Ar and ^{40}Ar. The temperature of the target was 1500 ° C.

be attributed to several factors, which may be identified as follows.

1- The diffusion efficiency at 1800 degrees was about 30%. This value may be increased if we can work with target temperatures up to 2300 degrees. A gain of a factor 2 could thus be obtained. In this first test we could not increase the temperature beyond 1800 degrees due to a mechanical problem.

2- The gas transfer efficiency between the target and ion source was 20%. This low eficiency was due to a leak between the target and tranfer tube.

3- The ionisation efficiency for ^{35}Ar (8+) was approximately 10%. This can be enhanced of a factor two by changing the ionisation conditions of the ECR source.

4- The total transport efficiency of SIRa was approximately 50%. This may be ameliorated by improving the ion optics parameters. The total emittance acceptance of SIRa is 100 π mm mrad, which is, for the most part, sufficiently high to transport the full beam delivered by the ion source.

The goal of the next series of experiments is to increase the overall efficency for ^{35}Ar (8+) up to 12% by resolving all problems presented above.

In the second part of the tests carried out in November, the ^{36}Ar primary beam bombarding directly the target of SIRa was used to produce the ^{35}Ar nuclei . The intensity used was very small in order not to activate the target-source device in this first test. The results obtained are listed in the table VI, with the projected secondary beam for 1 pμA of ^{36}Ar primary beam.

secondary beam	detected rate I = 1.6 pnA	normalysed rate I = pμA
^{35}Ar (8+)	5.4×10^4	3.4×10^7
^{33}Ar (8+)	2.0×10^3	1.3×10^6
^{34}Ar (8+)	2.8×10^1	1.7×10^4

Table VI : Production rate in SIRa with a ^{36}Ar primary beam (95 MeV/nucleon) on a C target.

The present production rate for a ^{35}Ar secondary beam is a factor 10 below the projected final intensities predicted in the NUPECC concerning European Radioactive Beam Facilities (May 1993). By solving the problems listed above this factor would be largely overcome.

- Collaborations

Many contacts have been made and collaboration protocols signed with four other laboratories. It should be noted that there is a great deal of interest in the R & D work that we are undertaking in this field and that we receive very positive contributions from our partners. A framework for discussions between specialists on questions of radioactive beam production and ECR ion sources has been set up in the form of "workshop" days.

The follow are those laboratories with which we have established collaborations:

- France :   IPN-Orsay, CSNSM-Orsay, LPC-Caen, DRFMC/PSI-Grenoble, ISN-Grenoble
- Belgium :   UCL-Louvain-la-Neuve and KUL-Leuven
- CERN :   ISOLDE
- Italy :   INFN-Catania
- Russia :   JINR/FLNR-Dubna

2 - ACCELERATION OF THE RADIOACTIVE IONS

2.1. GENERAL

2.1.1. Choice of a cyclotron

This choice correspond to the best possible way of meeting the physics requirements the costs and the schedule.

It has been envisaged for the following reasons:

a) **The energy/mass range** requested is rather well suited to the rapid energy decrease in $(Q/A)^2$ of the cyclotron with higher masses.

As mentioned in the preceding section, the optimum of the ionisation states for mass as up to 100 obtained with the 14.5 GHz ECR sources corresponds to a Q/A between 0.1 and 0.2 with good ionisation efficiency. The experiments made on the test bench for radioactive beams show that the charge states are only slightly affected when the production target is in position and that the resulting gas flow is difficult to monitor.

It is, therefore, reasonable to base a project on a ratio between 0.15 and 0.20 for mass A = 100.

b) The cyclotron is itself an excellent mass separator capable of selecting ions with neighbouring Q/A with a resolution of 2 to 3.10^{-4} which is useful for isobars particularly.

c) The results obtained with the GANIL injector cyclotron with axial injection (75 % transmission between the injected and ejected beams) now make the cyclotron very competitive as to transmitted **intensities** with the non-negligible advantage of having the target-source ensemble for the production of the secondary beams at voltages of only 25 to 30 kV.

d) The beam characteristics (radial emittance, energy spread, phase extension) have reasonable values with respect to the experimenters' requests.

e) GANIL has a great deal of experience in the design and the operation of this type of machine.

f) It can be placed in the present building.

2.1.2. Basic parameters

The criterion selected for the specification of the post-accelerator is to reach 6 MeV/nucleon for the masses A ≤ 100 that can be obtained with charge states such as Q/A ≥ 0.15.

To reach this objective, the post-accelerator selected is a compact cyclotron K = 265 ($\overline{BR}_{ejec} = 2.344$ T.m) whose working diagram is shown on Figure 14 and energies in figure 15 with the following main parameters, the choice of which is explained below :
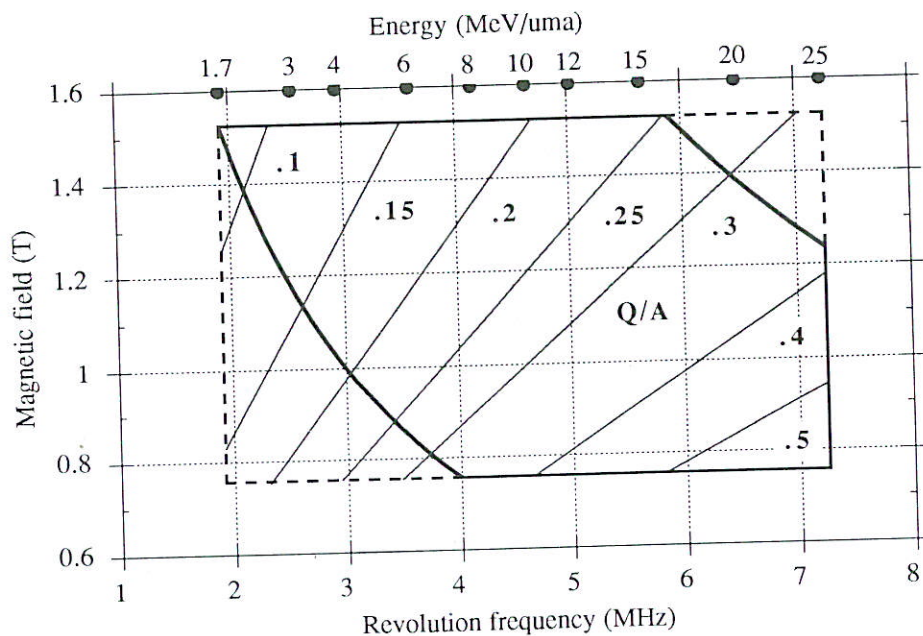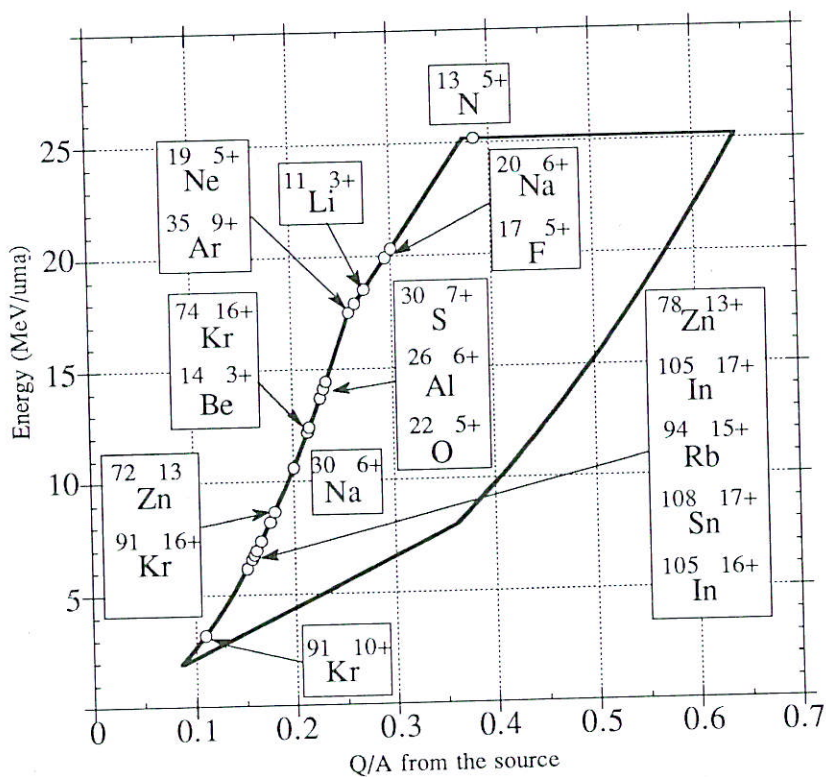

Figure 14.

Figure 15.

- Frequency range and the harmonics

Frequency range	9.6 - 14.5 MHz
Harmonics	2 - 3 - 4 - (5)
Maximum dee voltage	100 kV
Maximum average field	1.56 T
Minimum average field	0.75 T
Exit radius	1.5 m
Maximum injection voltage	30 kV

For the heavy ions the difficulty with cyclotrons lies in the HF system, with the production of low frequencies being the most critical point.

By choosing a minimum frequency of the order of 9.5 to 10 MHz and a frequency range where $F_{max} \cong 1.4$ to 1.5 F_{min}, the RF system remains at a reasonable cost with a coaxial line that is not greater than 1.5 to 2 m long and a variation in frequency that is easy to produce.

The consequences are a limitation of the low energy reached and the obligation to work with higher harmonics to cover the wanted energy range. It is not desirable to use harmonics above $H = 4$, as the transit time between the first gaps becomes too high.

The list of radioactive ions recommended by NuPECC shows that only a few light ions ($^{13}N^{5+}$, $^{7}Be^{3+}$, $^{14}O^{6+}$) that are already highly ionised, with $Q/A \geq 0.35$, would be able to benefit from energies ≥ 20 to 30 MeV/nucleon. It was therefore agreed that the highest energy initially selected (29 MeV/nucleon) could be reduced.

On the other hand, there were strong requests that the low energy should be revised downwards : 2 MeV/nucleon is desired for the light ions.

As a result
The energy range 2.7 - 25 MeV/nucleon, corresponding to the revolution frequency range 2.4 - 7.25 MHz, will be produced by the HF frequency range 9.6 - 14.5 MHz with the harmonics 2, 3, 4 whose use does not present any particular problem in our case.

The range 2 - 2.7 MeV/nucleon will be produced with the 5th harmonic, recognising that in this case :
- the acceptance of the machine is lower and it will be necessary to reduce the intensity of the injected beam (reduce the emittance) which is not too disadvantageous with light ions. It will also be necessary to accept a poorer quality beam (cf. §.II.5).
- the Q/A ratios obtained for the light ions will not always allow a continuous coverage of the 2 - 3 Mev/nucleon energy range (cf.§.V.).

Maximum average field
The deliberate choice not to exceed 1.6 T is justified by the following reasons:
- In staying in a domain outside of the saturation (2 T) in the magnet, the polar

profile can be optimised and the problem of field corrections, the technology of which is always difficult, remains simple (cf.§.II.3).

- The other alternative, also studied, and even of more interest, since it makes it possible to decrease the cyclotron radius ($\approx$ 1 m), is to work in a completely saturated domain. In our case, the ratio B_{max}/B_{min} = 2, required by the variable energy does not allow this possibility and results in too high field corrections.

In addition, the reduction of the radius entails the reduction of the turn separation, which goes against the desired objective at the ejection (cf.§.II.6).

HF voltage and the maximum injection voltage

The dee voltage-injection voltage pair must vary proportionally to the field and the frequency for operation at "constant orbits".

The maximum voltage of 100 kV on the dee, a value quite attainable at the technical level (cf. §.4), was selected as a function of the requirements of the injection of the beam in the cyclotron (cf.§.5.). This value makes it possible to benefit from sufficient acceleration on the first revolution, to effectively clear the central region while having around 250 revolutions before the ejection, which allows a good mass separation.

To avoid the installation of the source-target ensemble on a HV platform, the source body will be directly raised to the potential. The maximum injection voltage is limited to 30 kV, which allows the installation of a hyperboloid type inflector.

To avoid going to too low injection voltages, the operating point 100 kV/30 kV has been fixed at the maximum energy obtained for Q/A = 0.25.

The following limits are shown in figures 1.1 and 1.2 :
- frequency and magnetic field,
- choice of the maximum dee voltage (100 kV), maximum (30 kV) and minimum (10 kV) source extraction potentials.

2.1.3. Objectives

During this study, the participants took particular care to meet the following objectives :
- To ensure the beam qualities requested, to determine the limits of these
- To verify the feasibility of the ensemble (to study particularly the more expensive components and those with a long lead time like the magnet and the HF).

The view of the ensemble of the CIME cyclotron with its main components (magnet, HF, vacuum chamber, ejection system,...) is shown in figure 16.

Its implantation and its connection to the low-energy and medium-energy beam lines are shown in figure 7.

The description of the machine and the beam characteristics (intensity, mass separation, emittance, energy spread, bunch length) are developped in the following sections. The block diagram in figure 17 shows how these studies are connected.
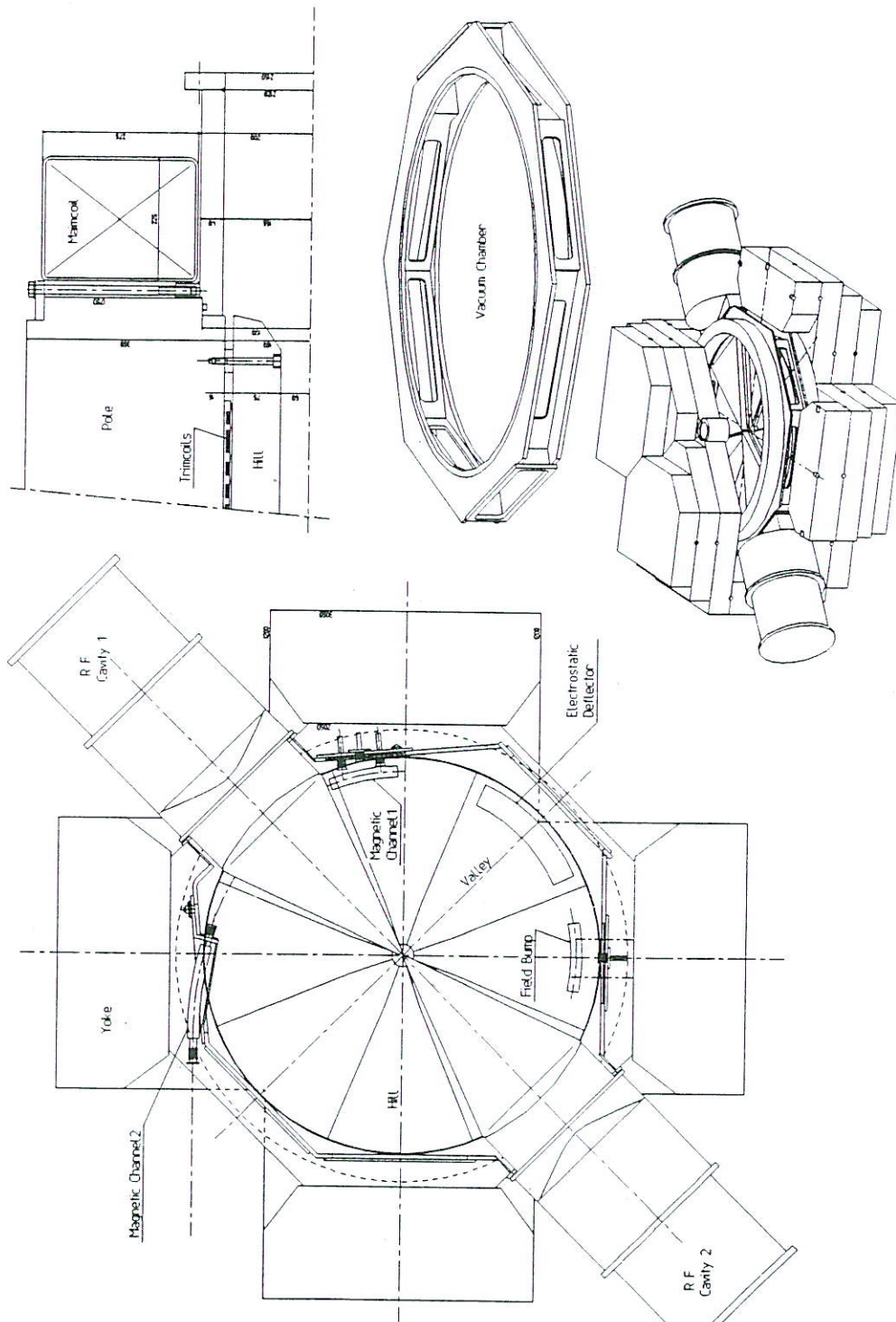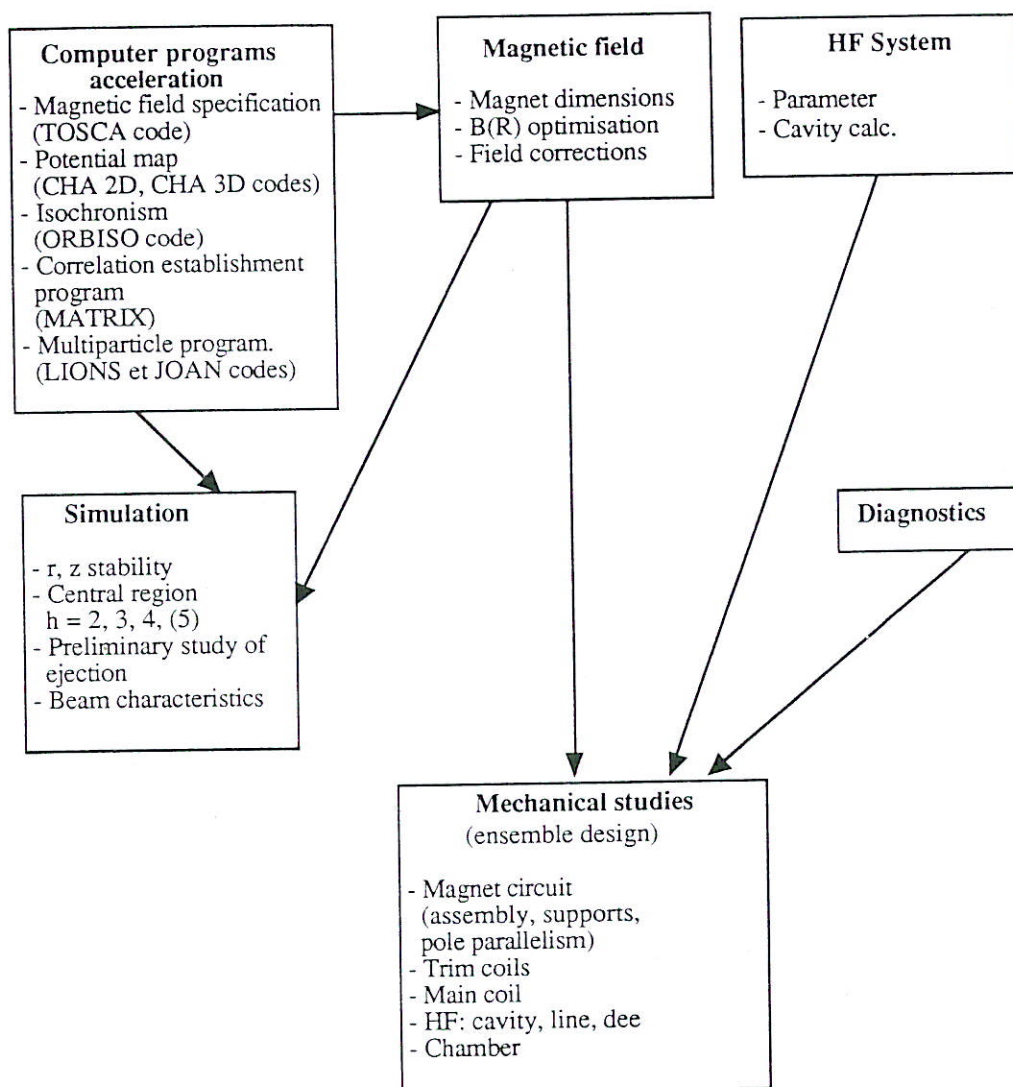
Figure 16 : Overall views of the CIME cyclotron

```
┌─────────────────────────────┐   ┌──────────────────────┐   ┌──────────────────────┐
│   Computer programs         │   │   Magnetic field     │   │     HF System        │
│   acceleration              │──▶│                      │   │                      │
│ - Magnetic field specification│  │ - Magnet dimensions  │   │ - Parameter          │
│   (TOSCA code)              │   │ - B(R) optimisation  │   │ - Cavity calc.       │
│ - Potential map             │   │ - Field corrections  │   │                      │
│   (CHA 2D, CHA 3D codes)    │   └──────────────────────┘   └──────────────────────┘
│ - Isochronism               │
│   (ORBISO code)             │
│ - Correlation establishment │
│ program                     │
│   (MATRIX)                  │
│ - Multiparticle program.    │
│   (LIONS et JOAN codes)     │
└─────────────────────────────┘
```

Figure 17 : Cyclotron feasibility studies
(Sept. 92 - May 93)

2.2. SIMULATION PROGRAMS

Due to the high accuracy required in the study of the CIME cyclotron, it appeared necessary to develop a new program of particle dynamics and to increase the capabilities of some of the existing programs.

In the following, we describe the essential aspects of this new set of software (figure 18).

2.2.1. Magnetic field calculations

The magnetic field of the cyclotron is evaluated using TOSCA[5], a 3D magnetostatic program, which GANIL has owned for several years.

The SUN station dedicated to the TOSCA code has been boosted (sparcstation 10) made faster and equipped with a memory of 32 MB and two 1 GB disks.

─────────────────

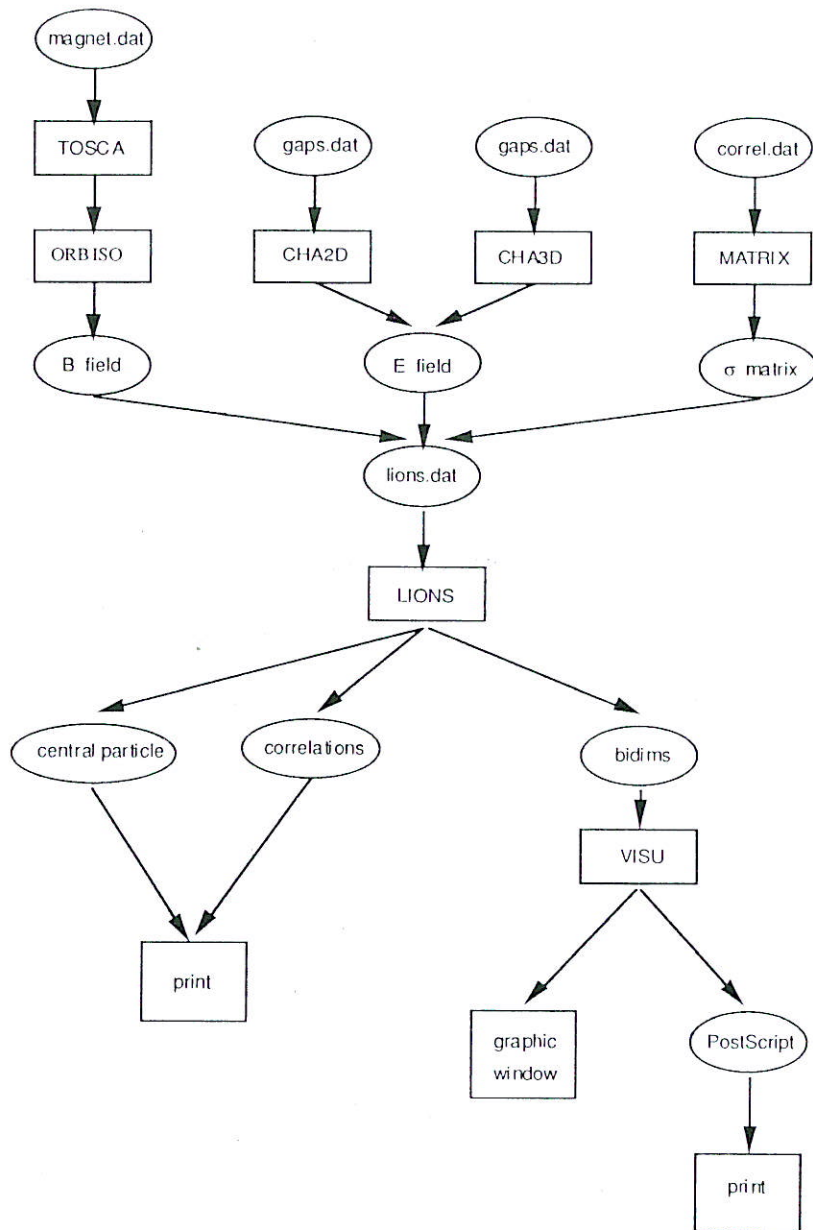[5] *TOSCA, by Vector Fields, OXFORD (U.K)*

Figure 18 : Flow chart software

These new capacities make it possible to run TOSCA in an extended version with the possibility of defining up to 150000 nodes. The accuracy thus obtained is sufficient for optimising the magnet poles, the correction coils, the centre configuration, etc.

For the particle dynamics, a map in polar co-ordinates of the B_z component is extracted from the "finite elements" data of TOSCA.

This map can eventually be isochronised using the standard ORBISO program.

A 720 * 100 size 2D map is obtained which corresponds to a value at around every 0.5° and at around every 2 cm.

For the 3D dynamics calculations, an evaluation of the 3 components of the magnetic field is necessary on both sides of the median plane. This calculation is made starting with two extracted 2D maps using the equations div $(\vec{B}) = 0$ and curl $(\vec{B}) = 0$.

We have verified that the magnetic field values thus obtained outside of the median plane are very close to those provided by TOSCA, which justifies a posteriori that it is sufficient to extract B_z for the median plane only.

2.2.2. Calculation of the RF potential

Several cases arise :

For the calculation of the central geometry potential, due to the presence of the posts, a 2D calculation in the median plane is considered sufficient. On the other hand, the lattice must be extremely fine.

The calculations are carried out with the CHA2D program, in a 30 cm x 30 cm square which allows to include the gaps of the first two revolutions. The lattice has 1024*1024 unknowns, which corresponds to a 0.33 x 0.33 mm cell.

Due to the large number of unknowns, the CHA2D program was revised and now uses the conjugated gradient algorithm. The solution converges in a few hours on a SUN Sparcstation 10.

For the calculation of the gaps outside of the centre there are 2 cases:

If the gap is rectilinear, CHA2D is used with a 2D lattice (1024*1024) in the vertical plane perpendicular to the gap, in taking the rounded shape of the electrodes into account.

Subsequently, the values of the potential in the median plane are extracted to construct a "horizontal" rectangular map along the gap by radial duplication.

For the evaluation of the potential on both sides of the median plane, the calculation is carried out according to the same principles as those for the magnetic field.

2.2.3. Calculation of the trajectories

To study the dynamics, we use the new LIONS (launching of ions) program, which has the following main characteristics :

First of all, it is written in FORTRAN 90, a new language with multiple advantages, among others :

- Compatibility with FORTRAN 77, which facilitates the formatting and the exchange of data with the upstream or downstream programs.

- A very condensed and much more legible method for writing the instructions, making maximum use of the parallelism of the selected algorithms.

The consistent use of double precision is required for an accurate study of the mass separation.

The relative motion equations are time-stepped, with a step that is constant and can be parametrised, and an interpolation in the field maps.

The program is reversible and allows to go backwards in time.

The correlations in 6 dimensions, possibly brought back to 4, are established previously by the MATRIX program. A special effort was made to select the initial conditions of the ion bunch in any part of the cyclotron, taking the effects due to the curvature of the ambient magnetic field into account.

As of now, LIONS generates 4 files of results:
- the file giving the variation of the central particle parameters (which is always the 1st particle of a given bunch);
- the file of the values characteristic of the bunch (position, radial emittance, energy spread, phase spread, etc.);
- the file of these same values decorrelated;
- the file of the variation of the correlation matrix.

LIONS also makes it possible to generate very high accuracy two-dimensional plots to study graphically the variation of some correlations, of the motion of the bunch in the (x,y) plane, etc.

These plots are visualised with the interactive VISU program, which allows a variable display, zooms and black and white or colour Postscript outputs. VISU is also used for verifying the shape of the calculated electric and magnetic field maps.

2.3. MAGNET SYSTEM

The magnet is made up of four independent cruciform yokes and common circular poles with a diameter of 3.5 m, each equipped with 4 sectors (hill/valley gaps of 12 and 30 cm, respectively, hill/valley maximum fields 2T and 1.1 T, respectively) (figure 19).

The choice of a cruciform yoke has the advantage of providing greater accessibility, and above all makes it possible to limit the span of the upper and lower traverses. It also allows to respect 4th order symmetry for the flux return.

2.3.1. Calculation of the magnetic field

The calculations carried out with the TOSCA code made it possible to provide the dimensions of the magnet and to fix the hill geometry (thickness and azimuthal extension), to obtain configurations of the optimum average field B(R) between 0.75 T and 1.56 T, ensuring good vertical focusing and minimising the required field corrections.

- The (horizontal) cross-section of the magnet quadrant is shown in figure 20.

- The sides of the magnet and the geometry of the hill with the dimensions of its azimuthal extension as a function of the radius are shown in figure 19. It can be

seen that the hill is inscribed in a limited angle, called the "HF limit", imposed at the beginning to leave the place required for the HF system in the valleys. The thickness of the hills is kept at 75 mm over all the extent of the sectors. A damping gap of 15 mm is positioned between the hills and the poles. This allows a better flux distribution in the centre and contributes to making the radial field distribution more uniform at different field levels.

- **The curves of the average field B(R)** are shown in figure 21 and the **field corrections** to be carried out with trim-coils at different field levels are shown in figure 22. It is seen that these corrections do not exceed ± 200 G and the gradients to be corrected are lower than 5 G/cm.

The central region (up to a radius of 20 cm) where the sectors join the central plug still requires a little further study. Due to the constraints imposed by the axial injection and the emplacement of the inflector at the machine centre (cf.§.V), the gap at the centre must be maintained at 17 cm and the height of the central plug at not more than 6.5 cm.
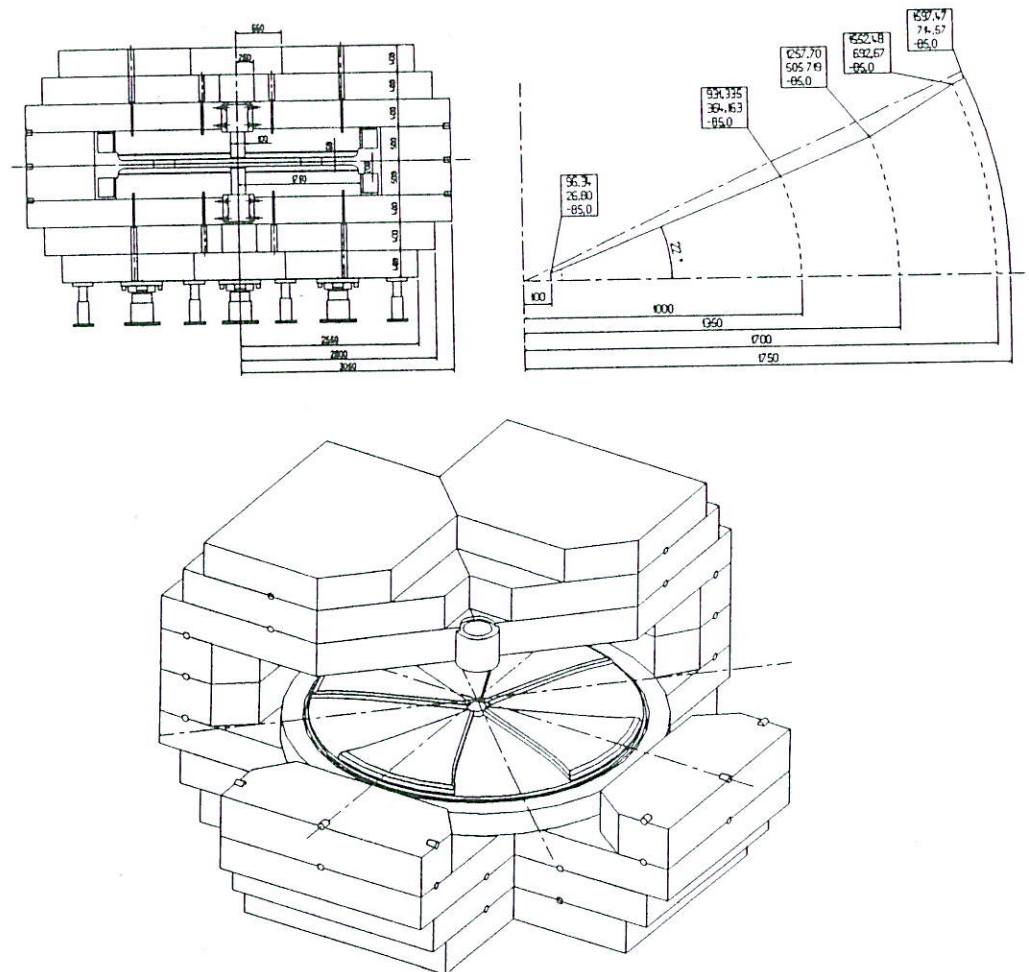

Figure 19.

The damping gap of 15 mm between pole and hills plays an important role in the central region where, initially, the effects of the sector tips had too strong a relative weight with respect to the central plug inducing a "field hole" at low inductions.
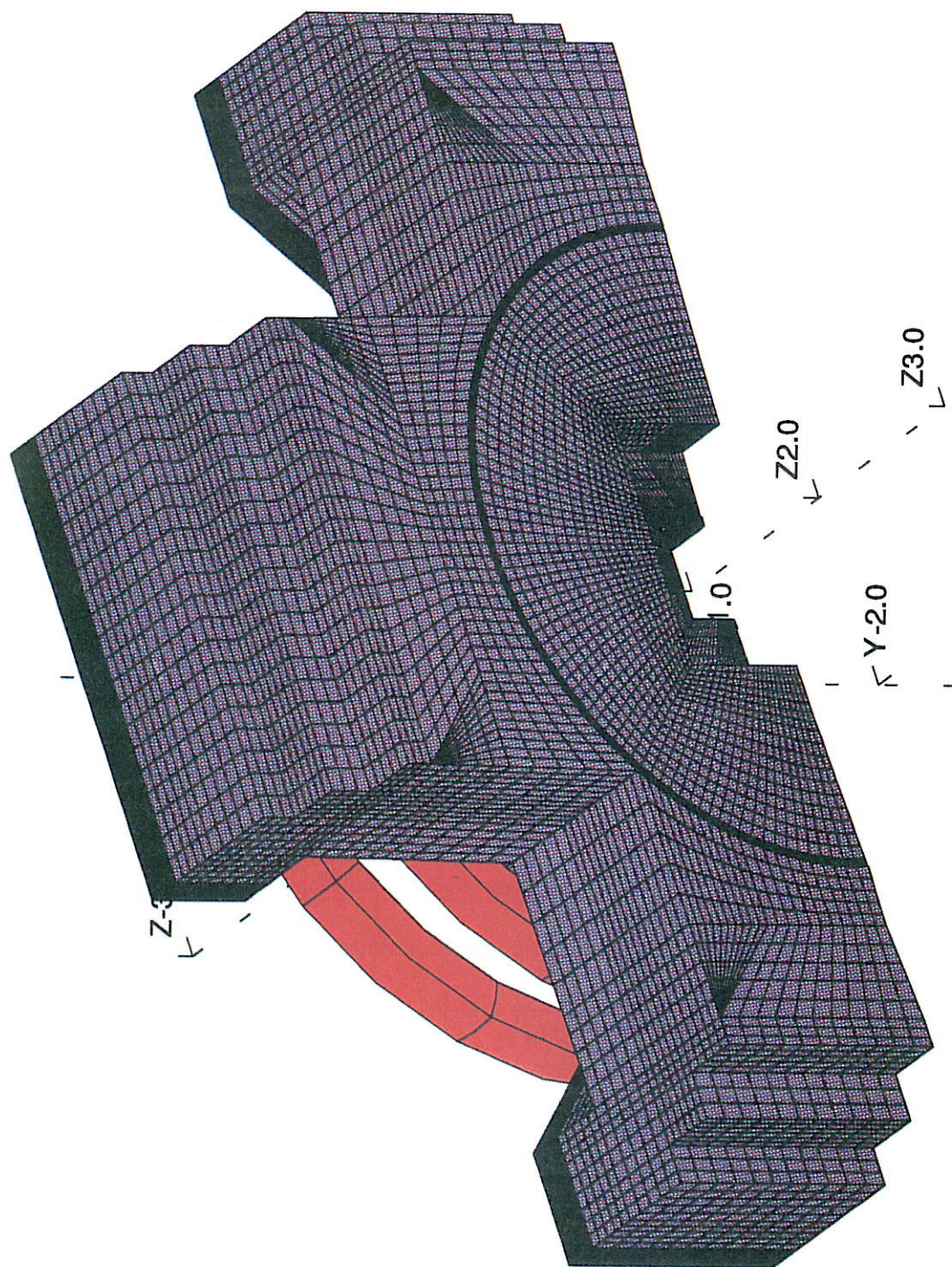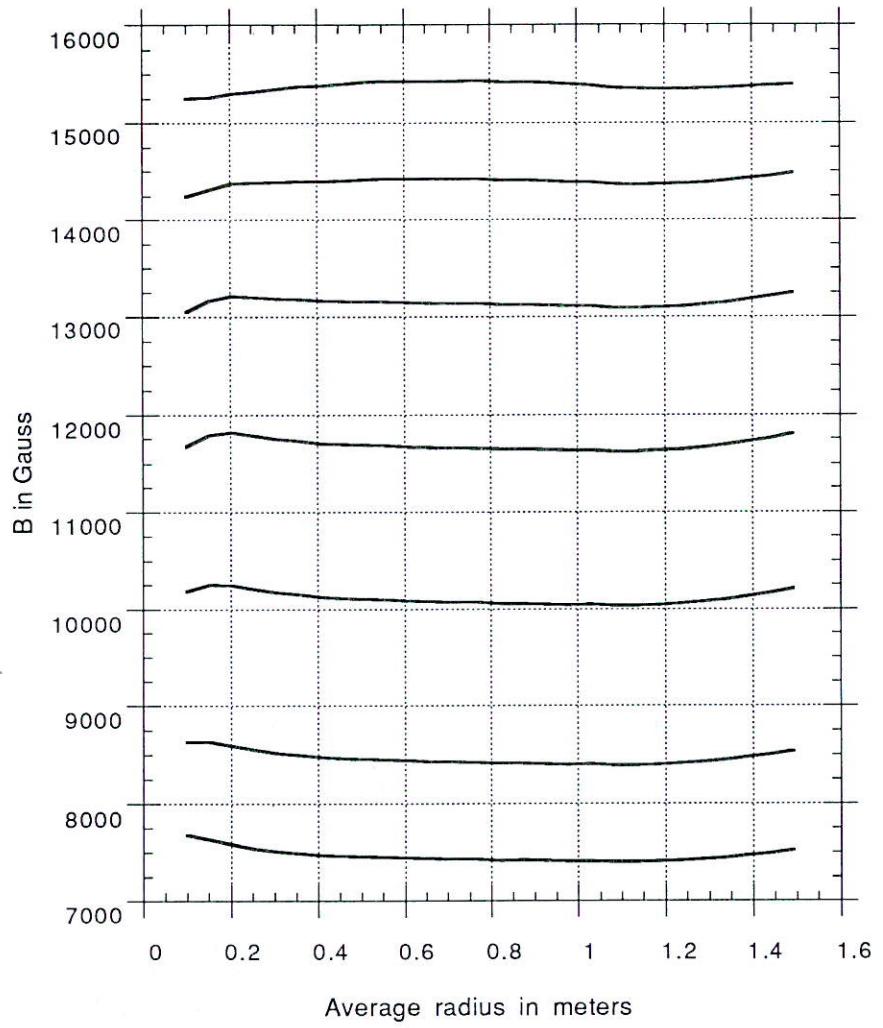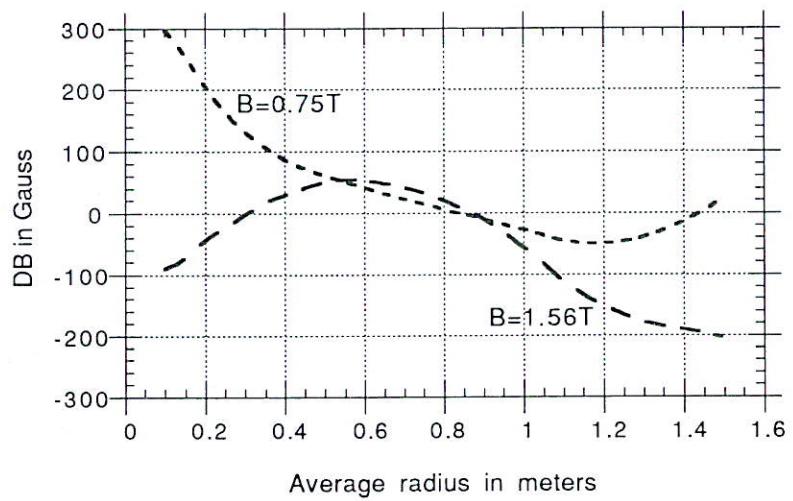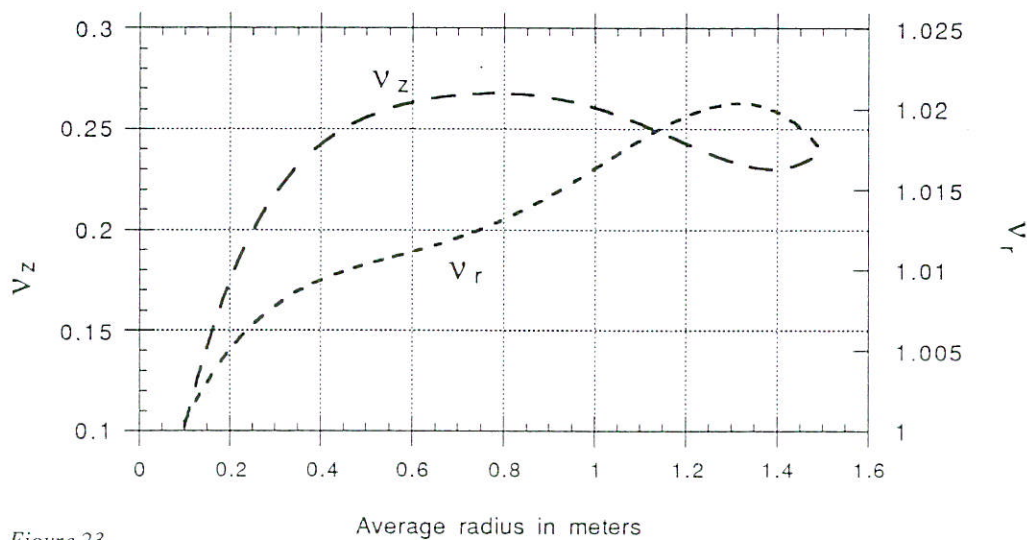

Figure 20.

Figure 21.

Figure 22.

Figure 23.

The stability ν_r, ν_z of the closed orbits in the corrected isochronous field is shown in figure 23.

3.3.2. Magnetic field corrections

The computer calculations have shown that the required **field corrections** defined above, (figure 23), can be ensured by **a set of circular coils** placed directly on the pole, and under the hills, in the damping gap. Each coil provides $7.5.10^{-2}$ G/AT and $2.5.10^{-3}$ G/cm/AT over $\Delta R = \pm 10$ cm.

Thus, a circular coil, made up of 4 windings (o.d. = 5 mm, i.d. = 3 mm) carrying a current of 250 A , gives alone a correction of 75 gauss and a gradient of 2.5 g/cm.

It is therefore envisaged to place 10 to 15 coils in a vacuum tight, stainless steel housing analogous to that used in the GANIL CO1 and CO2 injectors.

The NAPOL program makes possible the calculation of the distribution of currents in these coils at different field levels.

Coils for harmonic corrections are also to be foreseen, for equilibrating the sectors.

3.3.3. Main coils

The main coils of the magnet (width 220 mm, height 275 mm) positioned at 200 mm on both sides of the median plane make it possible to provide the maximum induction with 240.10^3 AT. The power required is 170 kW.

3.3.4. Mechanical studies

The mechanical studies are in progress.

Each of the four independent yokes rests on 3 jacks (identical to those of the

CSS). The upper and lower yokes each consist of 3 plates with a thickness of 40 cm.

A centring ring ensures the joining of the plates on which the pole is to be fixed (330 mm thick).

The 2D code (ACCORD code) has shown that the rigidity of the ensemble is ensured and that the extent of displacement from the centre is .06 mm for the upper pole and .02 mm for the lower pole.

The total weight of the magnet is $\cong$ 530 tonnes, and the maximum weight of the plates is 20 tonnes, making it possible to facilitate the machining, transport and mounting operations.

2.4. HIGH-FREQUENCY SYTEM

2.4.1. General

The acceleration systems cover the frequency range 9.6 to 14.5 MHz. They include two acceleration electrodes of 40° each which allows to use the 2nd, 3rd, 4th and 5th harmonics for constant orbit operation with around 250 orbits and a turn separation at ejection of 3 mm per turn for a maximum peak RF voltage of 100 kV.

The use of the 5th harmonic makes it possible to reduce the frequency range and thus the volume of the resonators.

The acceleration gap is 15 mm at the exit of the inflector and it varies linearly up to 30 mm at the extraction radius (R = 1500 mm).

Due to the electrode dimensions and the maximum possible aperture of the resonator in the valley (200 mm), only a "quarter-wave" type resonator with a variable short circuit can be envisaged.

By optimising the dimensions of the coaxial line and the electrode-line connection, it is possible to reduce the radial dimensions to construct a "cantilever" type rigid structure, without insulator, as the coaxial line-electrode ensemble is under vacuum.

The view of the ensemble of the resonator is shown in figures 24 and 25.

- Frequency range	9.6 - 14.5 MHz
- Dee angle (gap to gap)	40°
- Acceleration gap	Variable from 15 mm at the injection to 30 mm at the extraction
- Maximum peak HF voltage	106 kV
- Nominal peak HF voltage	100 kV
- Dee aperture	30 mm
- Radius at the vacuum chamber-coaxial line connection	2200 mm
- Dee height	100 mm
- Dee-shielding distance (vertical)	50 mm
- Voltage stability	$\cong 10^{-4}$
- Phase stability between resonators	$\pm 0.2°$

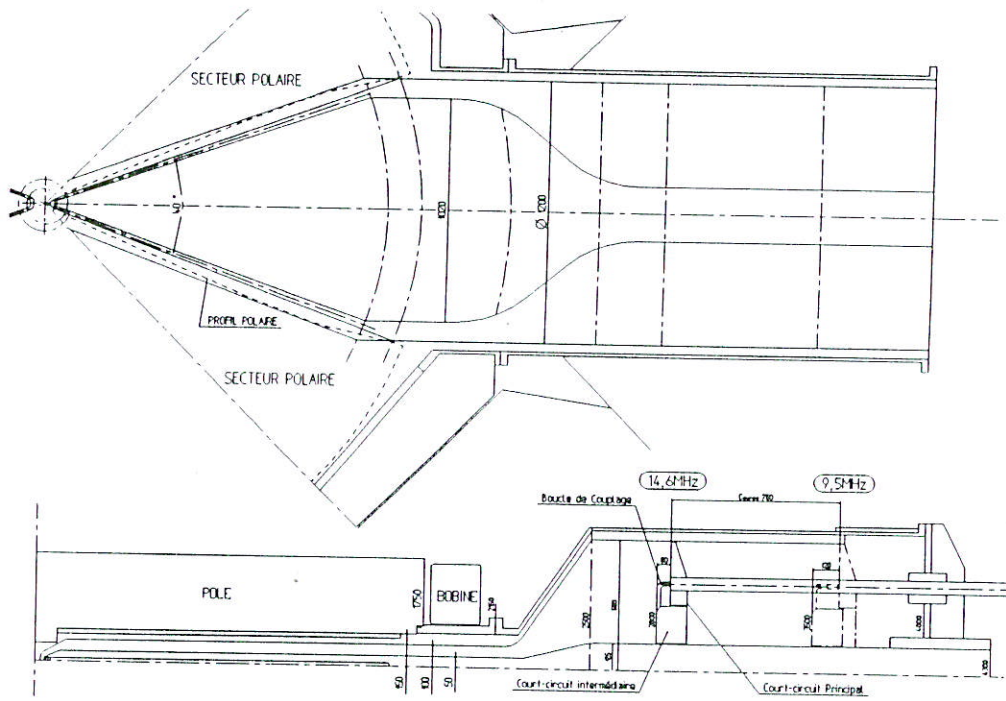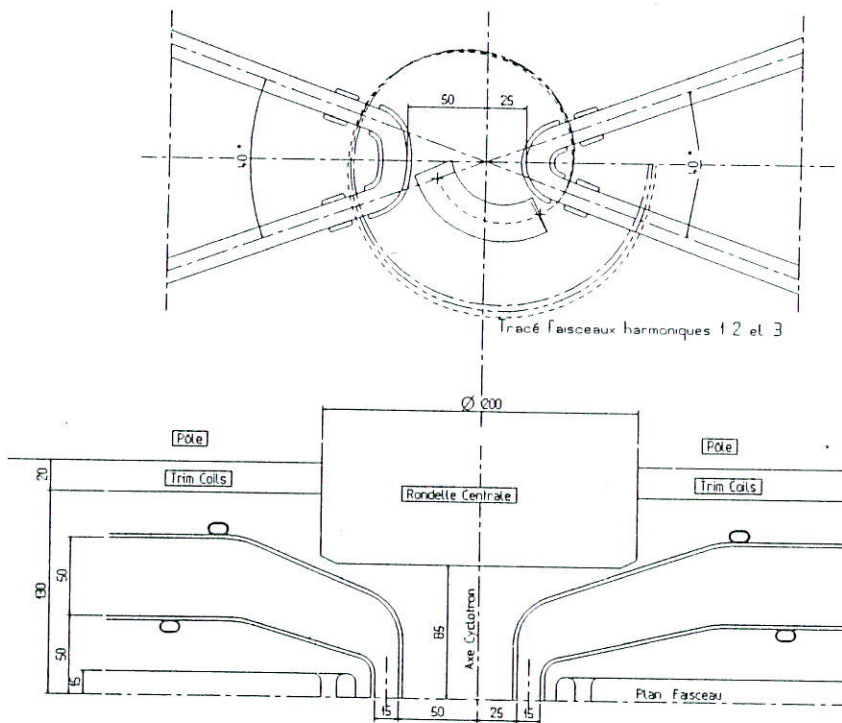## 2.4.2. HF parameters

Figure 24.

Figure 25.

2.4.3. Optimisation of the shapes of the resonators

The studies carried out allow one to reduce the radial dimensions of the resonator while at the same time minimising the RF powers required to obtain 106 kV peak on the dee. Subject to mechanical studies of the electrode structure, we obtain, in the direction of the magnetic field, electric fields limited to 25 kV/cm.

It was also verified that the current densities in the contact rings of the short circuits are compatible with the use of sliding spring-loaded RF contacts already used at GANIL. The height of the electrode is limited to 100 mm with the azimuthal form given for the central region in figure 25. Detailed mechanical calculations will have to be made to show if it is possible to place a prestressed structure sufficient to attain the accuracies requested in the electrode.
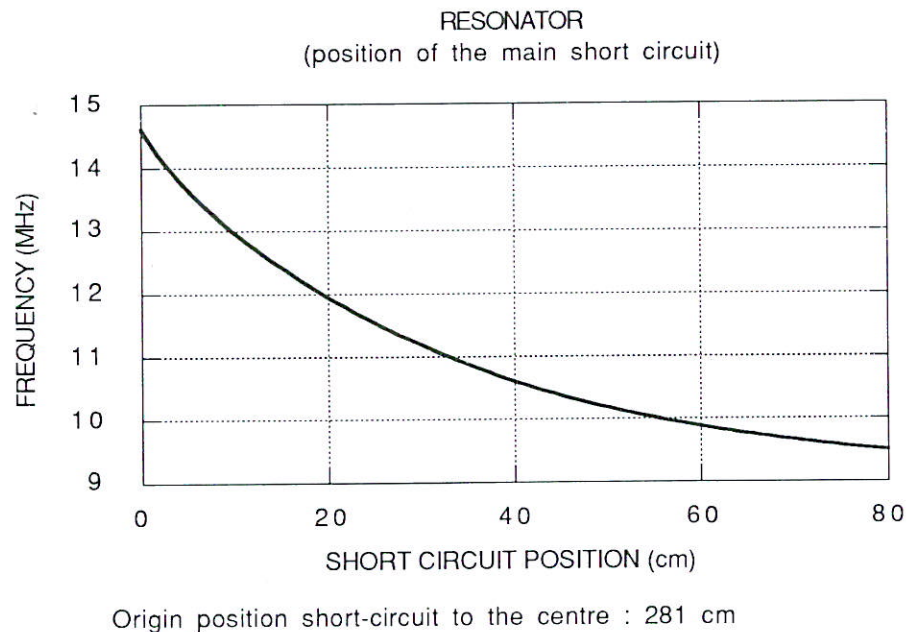
RESONATOR
(position of the main short circuit)

Origin position short-circuit to the centre : 281 cm

Figure 26.

2.4.4. Tuning-coupling

The conical connection of the resonator to the vacuum chamber does not leave enough space to simultaneously house :
- the fine-tuning capacitive device
- the variable magnetic coupling loop
- the pumping systems
- the mechanical fittings for the chamber resonator coupling.

This is why we have adopted an arrangement identical to the AGOR cyclotron , which includes two short variable short circuits, on one of which the coupling loop is fixed. The supply for the RF power passes by one of the control rods of the short circuit. The operating principle is the following :

- the two short circuits are displaced together for the rough tuning due to the low characteristic impedance of the variable length coaxial line formed (figures 26 and 27).

- The intermediate short circuit, whose variation $\Delta f/\Delta x$ is small and which carries the coupling loop is pre-adjusted according to a rating which gives (at the working frequency) a loop impedance of 50 ohms (figure 27).

- This same short circuit is used for fine tuning (essentially the correction of the thermal drifts) with a negligible perturbation of the loop impedance.
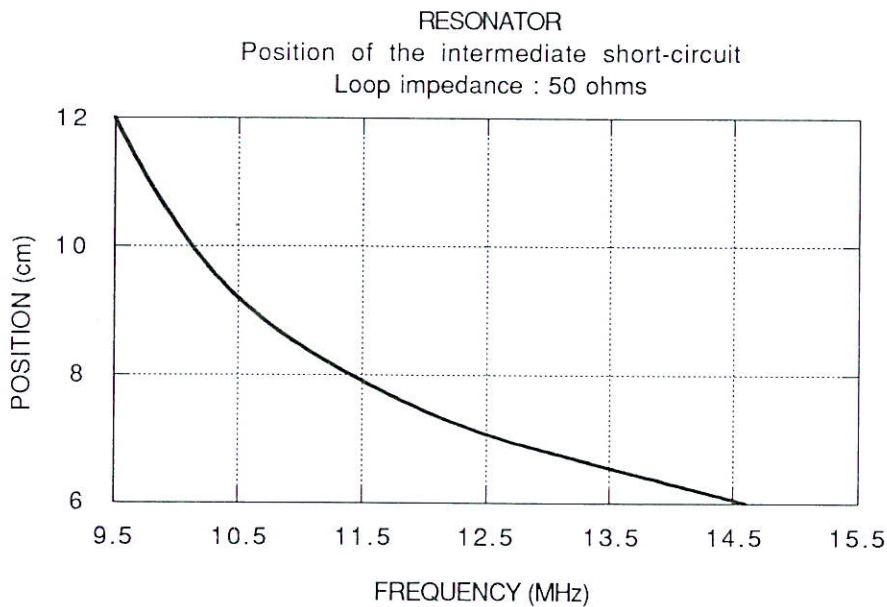
RESONATOR
Position of the intermediate short-circuit
Loop impedance : 50 ohms

Figure 27.

Rough tuning
The initial adjustment of the main short circuit must allow tuning the resonator within a phase interval of $\pm 200°$RF degrees around the selected resonance frequency.

The phase variation, around the resonance frequency is given by :
$$\Delta\phi = 2 * Q * \Delta f/f_0 * 180/\pi$$

At 14.6 MHz, the variation of the main short circuit frequency has the value :

$$\Delta f/\Delta x = 200 \text{ kHz/cm and } \frac{Qc + Qo}{2} = 4400$$

This leads to an uncertain positioning of the main short circuit of $\pm 2/10$ mm which does not present any problem.

Fine tuning
At the working frequency, the fine matching must allow tuning the resonator

83

within a phase interval of ± 5° RF around the resonance frequency and to maintain it as a function of the mainly thermal drifts.

The frequency variation slope of the intermediate short circuit is 60 kHz/cm, which gives for ± 5° RF degree an increment of ± 2.5/100 mm, a value which is quite acceptable for this type of mechanism.

2.4.5. RF power

From the data given above, we have carried out, using the RESHIF program, the general resonator calculations and, in particular :
- the RF power required as a function of the frequency for 106 kV peaks at the injection (figure 28). It is to remain below 40 kW.
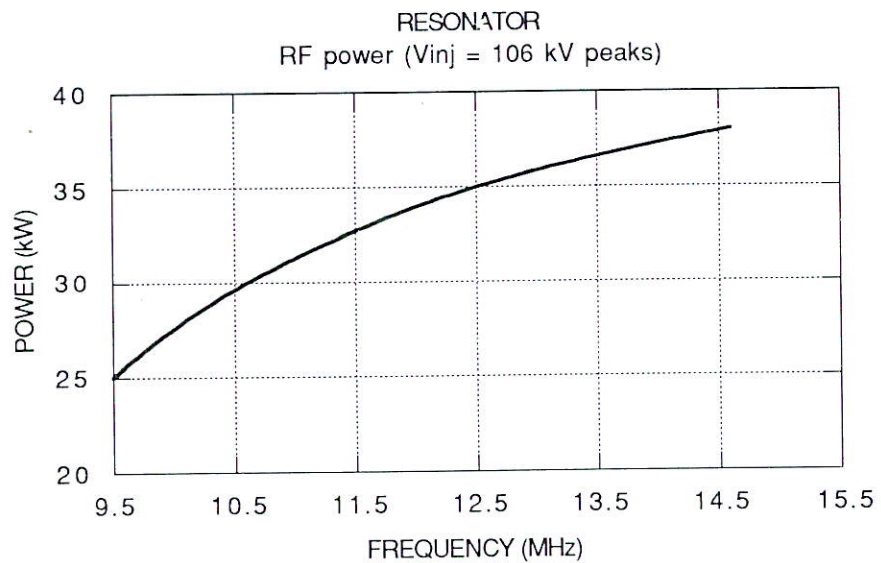- the Q factor (figure 29),

RESONATOR
RF power (Vinj = 106 kV peaks)
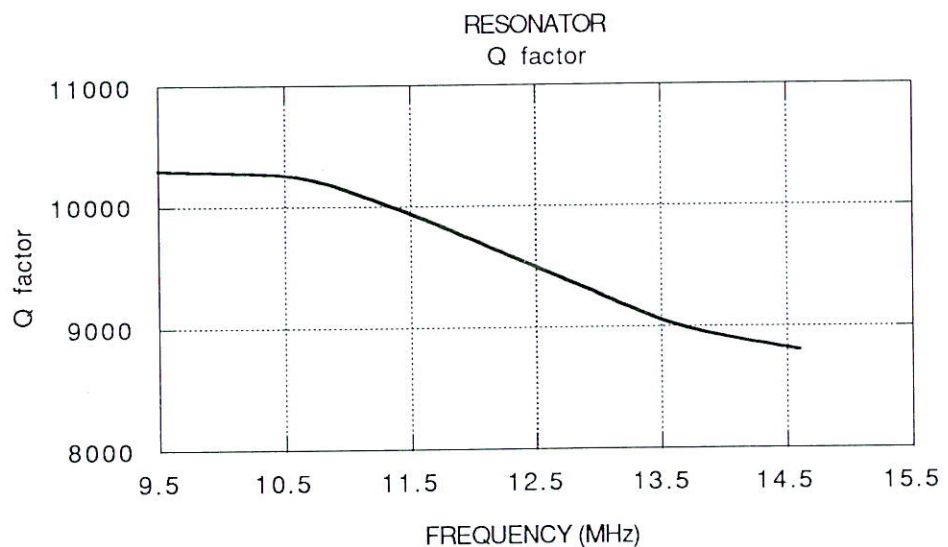
Figure 28.

RESONATOR
Q factor

Figure 29.

84

- the radial voltage distribution at 14.6 MHz (figure 30.a),
- the current density in the RF contacts (figure 30.b).

2.5. INJECTION AND CENTRAL REGION

The beam coming from the source is injected axially with a maximum voltage of 30 kV.
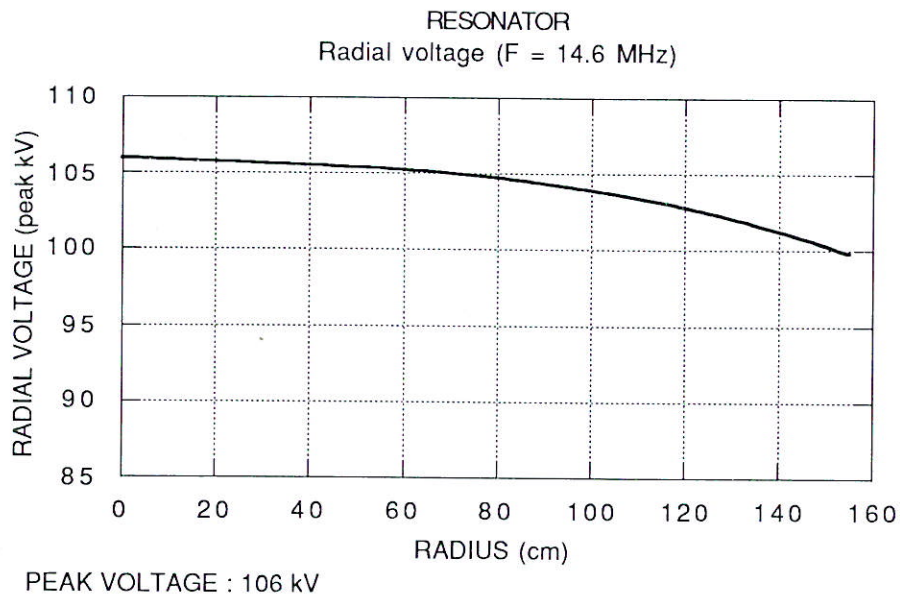
RESONATOR
Radial voltage (F = 14.6 MHz)

PEAK VOLTAGE : 106 kV

Figure 30a.

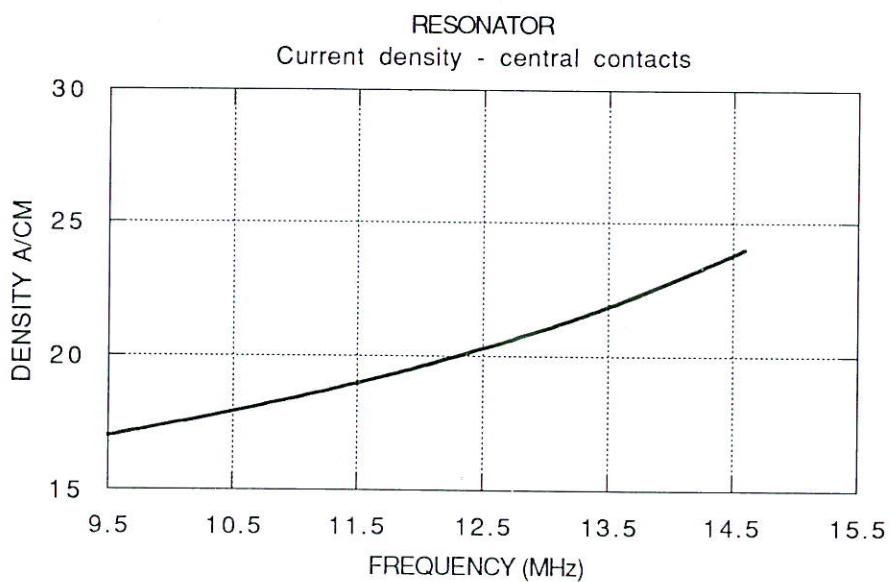**RESONATOR**
Current density - central contacts

Figure 30b.

2.5.1. Inflector

Due to this condition and the clearance of the magnet at the centre (17 cm) a Mueller-type hyperboloid inflector can be inserted. The characteristics of this inflector are summarised in the following table.

Inflector characteristics	
Magnetic radius	3.2 cm
Height	7.84 cm
Ro	15.67 cm
Rs	19.2 cm
ES distance	2.193 cm
EC distance	1.739 cm

The axial injection line, which will be described in section III, is identical to that constructed for the GANIL CO1 injector which allows the adaptation of the beam in 6D at the inflector exit.

This type of inflector is particularly well suited to the cyclotron : it makes it possible to obtain a low divergence in the vertical plane, at the inflector exit, in a region where the magnetic focusing is still inoperative.

A spiral-type inflector, of the same height, would allow higher injection voltages but would have to be followed by an electrostatic quadrupole, which would be quite difficult to position between the inflector exit and the first acceleration gap.

2.5.2. Central geometry

The beam qualities requested lead to the following analysis : the centre of the cyclotron must be of the same quality as the present centre of the GANIL injectors with :
- a well-centred reference trajectory,
- a motion of the centres of the trajectories around the central ray, contained in an extension of ± 2 to 3 mm,
- a correlation (r_0, ϕ_0) in ± 6° phase extension and a betatron adaptation produced in the axial injection (similar to that of the CO1 injector).

Due to the wish (not to say the necessity) of operating with the same central geometry for all the harmonics resulting from intervention problems (activity and reduced accessibility), it was judged that it was indispensable to start the studies of the central region and to study the motion of the particles in the actual fields although these are not yet definitive, to allow a complete simulation of the beams.

The potential maps were calculated with the CHA2D code, the field maps with the TOSCA code and the trajectories with the new multiparticle dynamics LIONS program.

2.5.2.1. Results for the 3rd harmonic

The two 40°-dees contain posts in the first 4 gaps whose position was determined previously with the "hard-edge" approximation.

The beam is injected at the point E (entry of the inflector), decentered by 31 mm with respect to the machine axis and exits from the inflector at the point S (x = 35 mm, y = - 33 mm) with an angle $\dot{r}_0$ and a phase ϕ_0 with respect to the 0°RF phase. The latter were optimised for the operation with the 3rd harmonic (corresponding to the 5 - 10 MeV/nucleon energy range).

The movement of the barycentre of the centres of curvature obtained by following the central particle for 20 revolutions (R ≈ 45 cm) as well as the motion of the centres of the trajectories around the central ray are shown in figure 31.
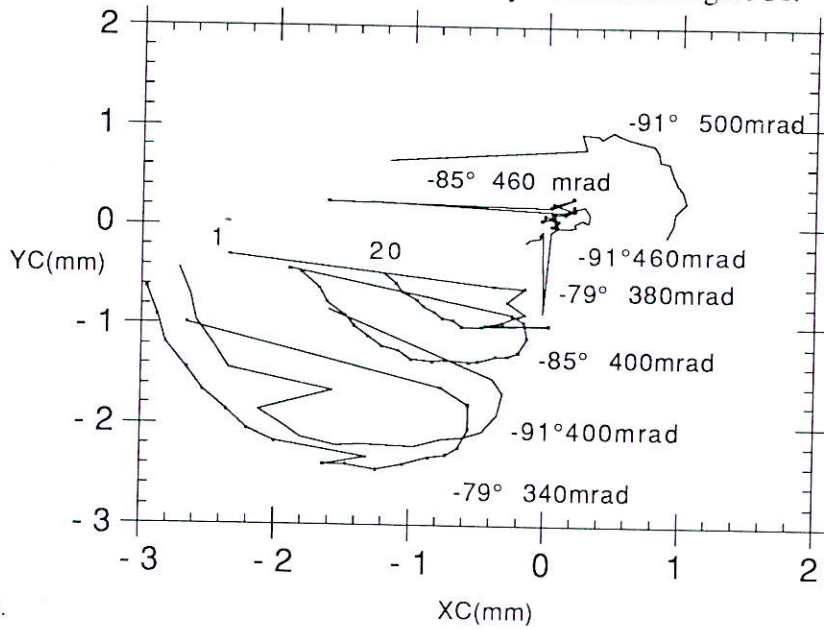

Figure 31.

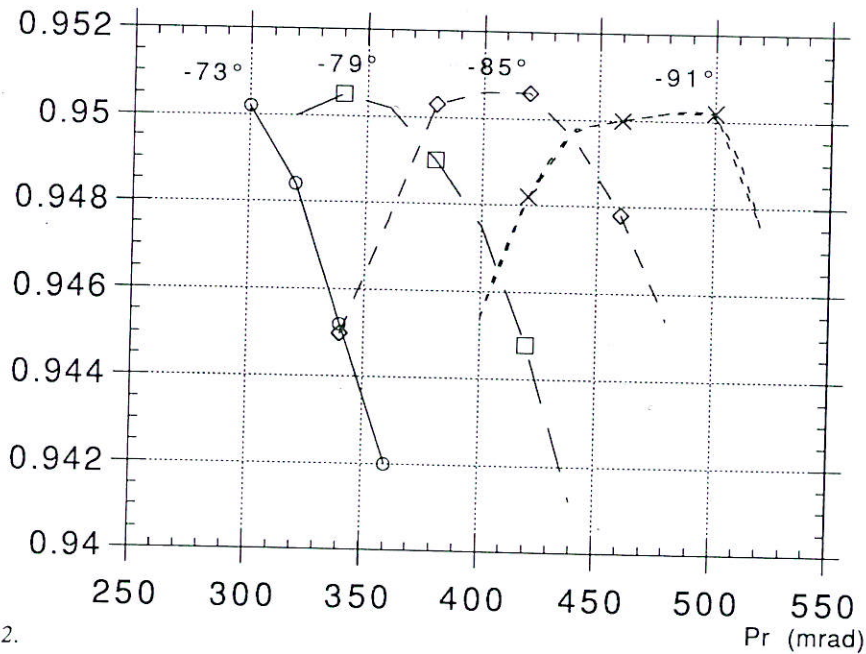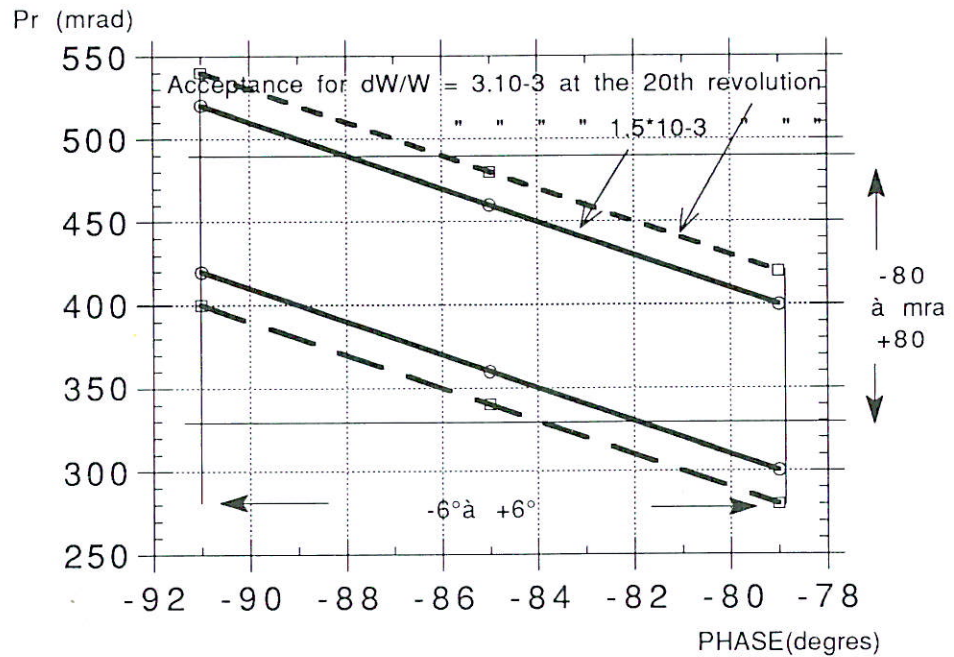The energies reached at the 20th revolution are shown in figure 32.

Figure 32.

Figure 33.

The acceptance ($\dot{r}_0$, ϕ_0) of the cyclotron as a function of the energy spread at the 20th revolution and the correlation ($\dot{r}_0$, ϕ_0) to be obtained at the injection are shown in figure 33.

- A simulation of the beam was subsequently carried out with the LIONS program for a beam having the initial conditions determined previously, by optimising the correlation:

For : $r'_0 = \pm 80$ mrad and a phase extension : $\Delta\phi = \pm 6°$
the figures 34 and 35 show, respectively :

- the variation of the bunches with time,
- the instantaneous centres of curvature,

2.5.2.2. Behaviour with the other harmonics

- Provided that the voltage is adjusted to take account of the transit time, which increases with the degree of the harmonic, and to thus compensate for the loss of energy, and also, of course, that the phase is adjusted, the central particle coming out of the inflector passes correctly through the windows of the 1st revolution.

- By following the central particle for 20 revolutions, the motion of the centres differs with h (which appears to be normal, since V_{HF} is not strictly homothetic) but it appreciably converges in all cases towards the centre of the machine (figure 36).
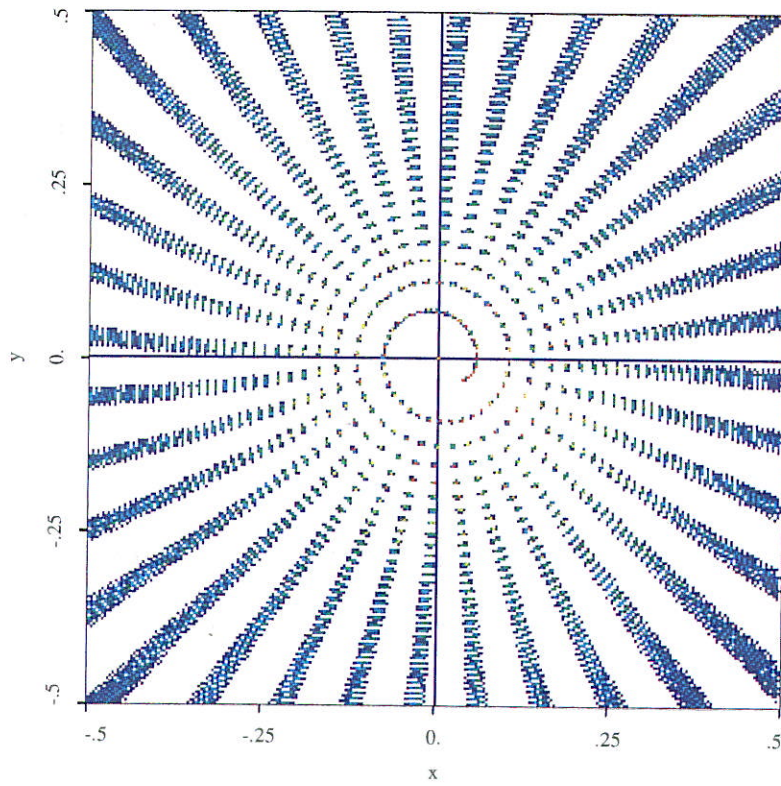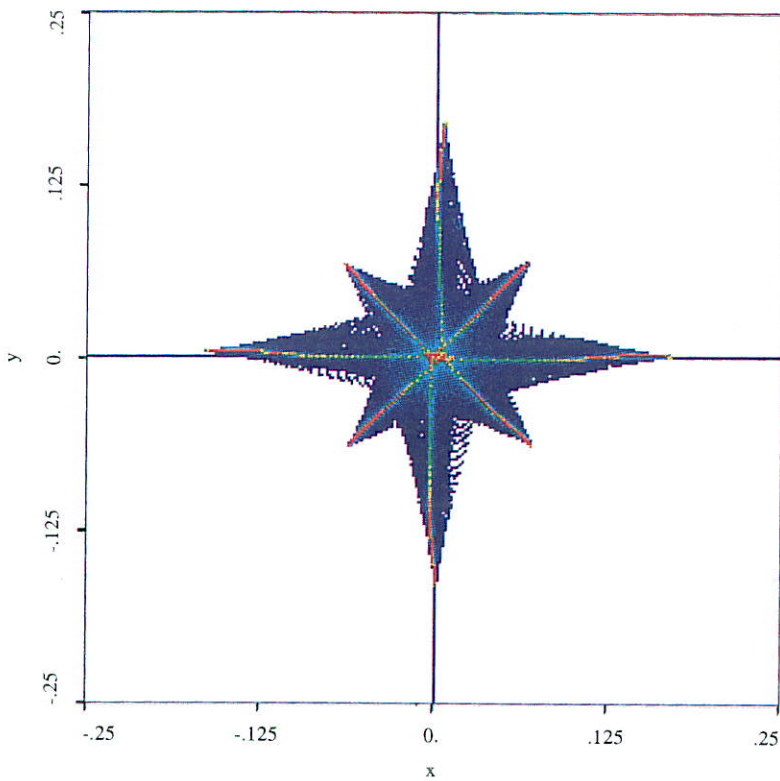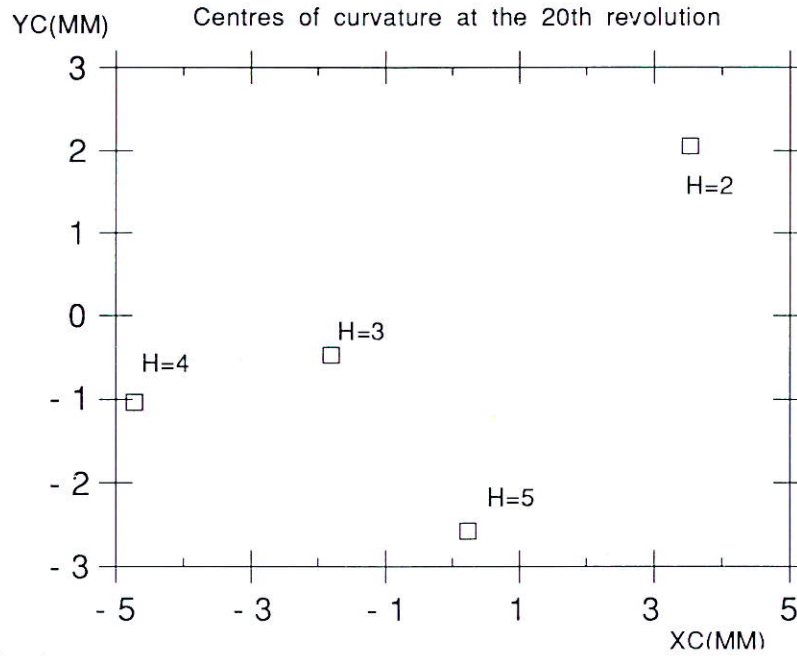
88

Figure 34.

Figure 35.

Figure 36.

- The divergence acceptance around the central ray depends strongly, on the other hand, on the harmonic. In a $\pm 6°$ phase extension at the injection, it varies as follows :

r'_0	$\Delta W/W$ (20th revolution)
> 100 mrad for h2 and h3	$\pm 3.10^{-3}$
$\approx$ 80 mrad for h4	$\pm 3.10^{-3}$
$\approx$ 20 - 30 mrad for h5	$\pm 10^{-2}$

As the maximum divergence of the injected beam is around 80 mrad, it can, therefore be concluded that the operation in the 2 - 25 MeV/nucleon energy range with the same central geometry can be envisaged provided that a current decrease is acceptable, as well as a greater energy spread between 2 and 2.7 MeV/nucleon in the operation with the 5th harmonic.

2.6. EJECTION

2.6.1. Principle

As shown in the overall view presented in section 2.1 (figure 7), the shortest. possible trajectory for the ejection of the beam occupies 180° of the azimuthal extension : starting in one of the two free valleys, it must cross a RF system, avoid the return yoke and exit in the opposite free valley.

The most desirable direction for the ejected beam, both for the positioning of the machine in the building and for the beam transport to the α spectrometer, is found to be that parallel to the yoke.

The preliminary study showed that an ejection of this type can be ensured by a normal standard system, including an electrostatic deflector placed in the free valley, followed by magnetic-gradient compensation channels (cf. §. 6.2 and 6.3).

As the central region ensures the qualities of the internal beam, the ejection ensures those of the extracted beam (emittance and energy spread) which can be seriously degraded since the turn separation (2.8 mm) does not lend itself to a single-turn ejection.

The preliminary study also includes, therefore, the simulation of the extracted beam with the conditions required to meet the desired characteristics (cf. §. 6.2 and 6.4).

2.6.2. Assumptions

As the calculations of the magnetic field as well as those of the central region were in progress when the preliminary study was made and the LIONS program does not yet include the ejection elements, we have made certain assumptions :

a) The calculations are made starting from the radius R = 50 cm with the conditions obtained at the ejection of the GANIL injectors, i.e., without taking account of the phase correlation, which is pessimistic.

εr	25π mm.mrad
$\Delta\varphi$	$\pm 6°$
$\Delta W/W$	$\pm 3.5.10^{-3}$
Δr_c	± 3.4 mm
Δr_{dc}	± 3.3 mm
Δp_r	± 7.6 mrad

b) Magnetic field map given by TOSCA and field correction computed by ORBISO.

c) Analytic fringe field

d) Calculations of the trajectories and the radial motion with the NAJO code (used for the CSS).

At the entry of the deflector placed in the free valley, at $=160°$ at a radius of 1.49 m (R = 150 mm), **the characteristics of the internal beam** are then the following :

r_{DC}	8.5 mm.mrad
εr_c	10.2π mm.mrad $\pm$
Δr_{DC}	4.4 mm
Δr_c	± 3.8 mm
ΔP_r	± 2.6 mrad
$\Delta W/W$	$\pm 3.10^{-3}$
$\Delta\phi$	$\pm 6°$

2.6.3. Characteristics found for the ejection elements

Electrostatic deflector	
Extension	40°
Field	70 kV/cm
Channel width	≈ 12 mm
Θ entry	160°
Θ exit	200°

CM1 Magnetic channel	
Extension	16°
Gradient	3.5 T/m
Channel width	≈ 12 mm
Θ entry	230°
Θ exit	246°

CM2 Magnetic channel	
Extension	30°
Gradient	9 T/m
Channel width	≈ 12 mm
Θ entry	300°
Θ exit	330°

These are altogether standard values and the production of these elements does not present any particular problems.

The CM1 channel can be made up of soft iron bars with a few correcting windings.
The gradient reached with this type of channel is easily 7.5 T/m.

In addition, it will likely be possible to position the CM2 channel outside the vacuum chamber and a quadrupole could probably be substituted for it.

2.6.4. Evolution of the beam

The variation in the radius $\overline{R}$ of the central trajectory and that of the beam amplitude during the ejection are shown in figure 37.
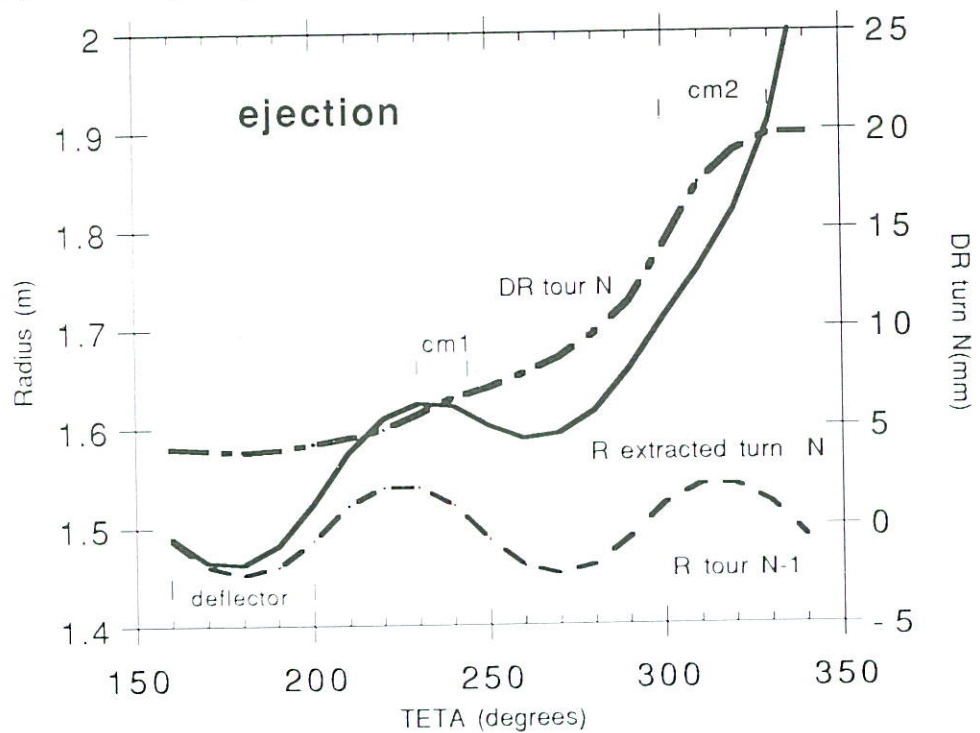

Figure 37.

The central trajectory, extracted at the radius $\overline{R} = 1.50$ m, is $\overline{R} = 2.0$ m with the direction parallel to the desired yoke.
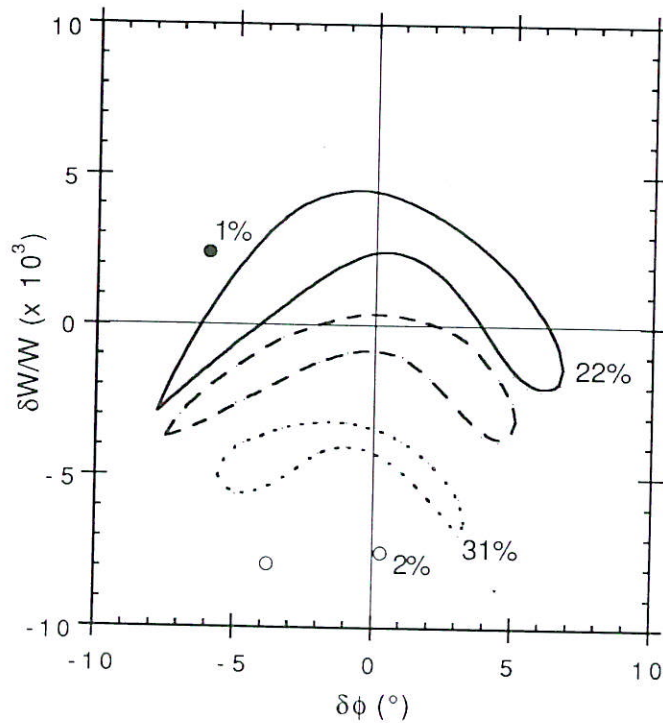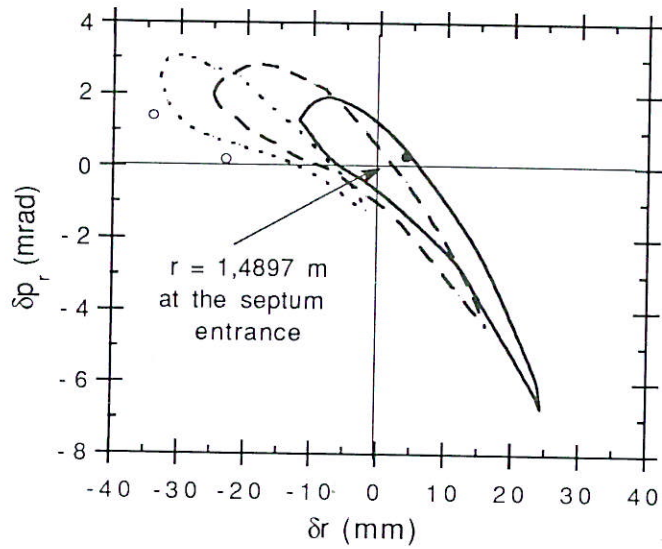
Figure 38. Characteristics of the beam in the space ($\delta pr \times \delta r$) and ($\delta W/W \times \delta \phi$). The curves correspond to the limits for the N-2 revolution(open circles), N-1 (dotted line), N (dashed line), N+1 (solid line), N + 2 (solid circles). The parameters at the exit of the ejection system (R = 2 m, ϕ = 340°) are :

$\Delta r_{out} = \pm 27.6$ mm ; $\Delta p_{rout} = \pm 4.2$ mrad

$\varepsilon r_{out} = 54.9\pi$ mm.mrad ; $\Delta W/W_{out} = \pm 5.07$ %

$\Delta\phi_{out} = \pm 6.5°$; $\varepsilon l_{out} = 32.3$ $\pi‰$.

The CM1 and CM2 magnet channels make it possible to compensate for the radial defocusing of the beam due to the fringe field and to limit the extension Δr at the exit window. This is a first approach: it is seen that the gradient of CM1 should be increased and that of CM2 could be decreased to optimize this extension, as a function of the optics of the downstream beam lines.

2.6.5. Characteristics of the ejected beam

The characteristics of the beam in the space $(r, \dot{r})$, $(\Delta W/W - \Delta \phi)$, at the exit of the ejection system $(R = 2 \text{ m}, \Theta = 340°)$ are shown in figure 38.

The separation per revolution $(\sigma = 2.8 \text{ mm})$ does not allow the single turn extraction. The result is that the energy spread of the beam reaches $\pm 5.10^{-3}$ with the multiturn ejection and the radial extension $\cong 28 \text{ mm}$.

To improve this separation, we introduced a field "bump" (extension $= 10°$, $\Theta e = 130°$ or $295°$, $B = 1000$ Gauss). The improvement obtained in the energy spread, which is reduced to $3.5.10^{-3}$, and in the radial extension at the exit which is decreased to less than 15 mm, are shown in figure 39a. To improve on these performances the beam must be bunched in a $\pm 3°$ instead of a $\pm 6°$ phase extension, the ejection can then be carried out in practically one revolution as shown in figure 39b. Under these conditions, the energy spread is reduced to $\pm 10^{-3}$ and the radial extension to $\pm 8 \text{ mm}$.
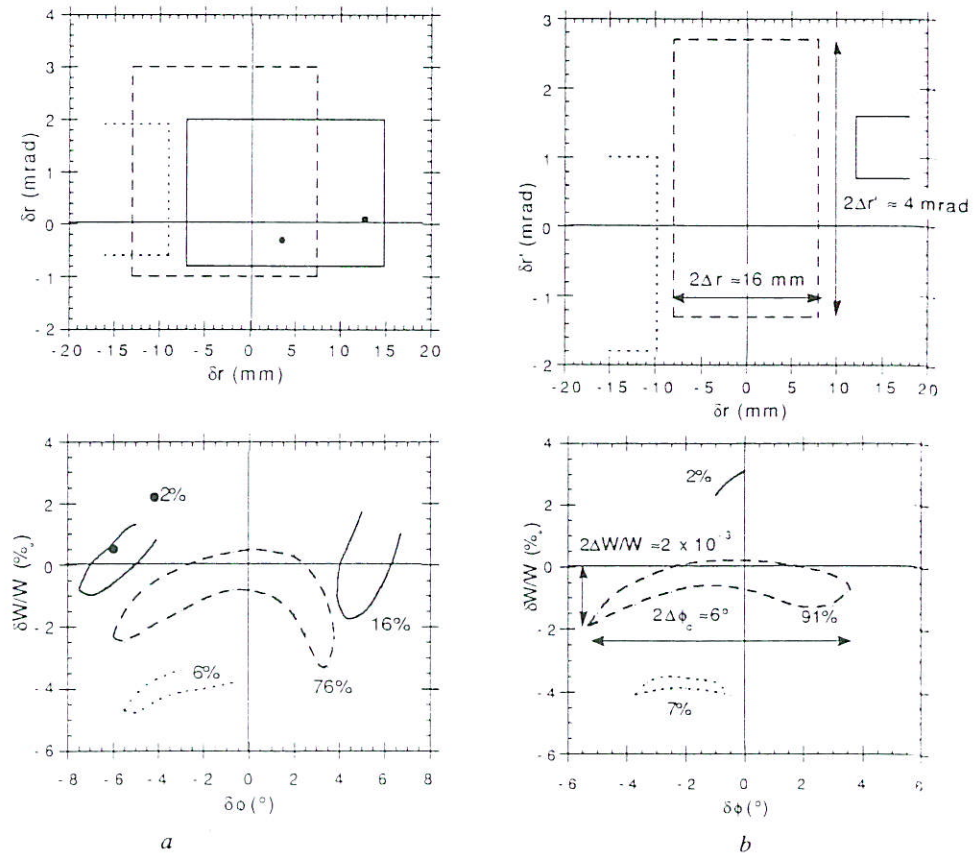
a) Bunched beam in a phase extension $\Delta \phi_{inj} = \pm 6°$

b) Bunched beam in a phase extension $\Delta \phi_{inj} = \pm 3°$ corresponding to erc $< 16\pi$ mm.mrad.

Figure 39.

We have seen in the preceding section that the uncorrelated phase extension of the injected beam is $\cong \pm$ 3.5 to 4° for a total extension of $\pm$ 6°. As a result, we are in a position to produce the conditions required for ejection in a single turn.

2.7. VACUUM CHAMBER

The magnet poles are an integral part of the chamber, a standard solution adopted in all compact cyclotrons.

The version studied, which presents the advantage of a simple mechanical-welded construction produced with 40 mm thick plates, is shown in figure 18.

The closing panels (deflector, RF system) add to the rigidity of the structure. Four holding bolts, inserted between the pole pieces and the main coils, in the axis of each valley, will reduce the sag to .1 mm.

2.8. PUMPING SYSTEM

The experience acquired with the GANIL cyclotrons has shown :
- the necessity of a very low pressure, of the order of 10^{-8} to 10^{-7} for mass 100, to avoid low energy charge exchange,
- relatively few exposures of the components under vacuum to the atmosphere,
- the advantages of having high pumping speed obtained with cryogenic systems.

For the CIME cyclotron, the practical impossibility of finding an orifice in the chamber sufficient for pumping must be taken into account, as must the fact that the ejection components and diagnostics should be reserved as much free access as possible to the exit windows.

The following solution is then proposed :
- a pumping rate of 3000 l/s for each resonator obtained with a turbomolecular pump positioned before the resonator,
- a pumping rate of $\cong$ 10000 l/s for the chamber using cryogenic panels with a useful total surface of around 0.2 m^2, positioned inside the chamber.

A panel is made up of two surfaces at 80 K, cooled either by liquid nitrogen, or by a cryogenerator which constitutes the protective cover of a 16 K panel also cooled by a cryogenerator.

Two 1 x 0.1 x 0.1 m panels placed vertically in the lower part of the two free valleys or better a single horizontal triangular panel with a larger surface (base = 0.7 m, height = 1 m) placed at the base of a valley, are envisaged.

For the cryogenerators, there are two solutions:
- a) An 80 K cryogenerator and a 16 K cryogenerator or just a single 80 K + 16 K cryogenerator, if the power is sufficient.
- b) A 16 K cryogenerator and nitrogen for the panels at 20 K. This arrangement has the advantage of a high pumping speed on H$_2$O but the disadvantage of requiring the installation of a tank and lines for liquid nitrogen, which is burdensome and often

gives operating problems.

- The primary pumping system using a roots pump, is connected to the resonator.

3 - BEAM LINES

3.1. GENERAL

The implementation of SPIRAL requires the construction of three beam lines (figure 7) :

- the primary beam line, by extending the L3 line, by a length of around 14 meters, transporting the beam from CSS2 to the production target.

- the secondary very low-energy beam line, with a length of around 21 meters, transporting the secondary beam from the source to the centre of the "CIME" cyclotron,

- the secondary medium-energy beam line, with a length of around 20 m, transporting the secondary beam from the cyclotron exit to the experimental areas in being connected to the "alpha" spectrometer.

The design of the optical structure of each line is modular, each module (or section) fulfilling only one optical function. The principle of separate functions, a concept already selected for the ensemble of the GANIL beam lines, contributes largely to facilitating the optimisation of the adjustment of the line parameters and to providing good quality beams.

In addition to the optical functions, the layout of these three lines meets a number of criteria of the implantation and of radiation protection of the target-source ensemble and the cyclotron [GAN93].

The main equipment units for the lines (magnetic elements, supplies, diagnostics, vacuum systems, etc.)will be the same type as those on the present lines of the accelerator or in the GANIL experimental areas.

However, with respect to the diagnostics, a special development effort will have to be made notably to provide solutions to the following problems :

- That of very low currents in the very low energy line : CCD cameras. could be used, in the same way as in the medium-energy line, gas profile monitors could be employed in combination with CCD cameras.

- That of the identification of the beam constituents (masses, isobars, etc.) beyond an energy of 3 MeV/nucleon and for an intensity not exceeding 1000 counts/s, silicon detectors could be envisaged.

3.2. PRIMARY BEAM LINE

3.2.1. Beam characteristics

The initial conditions taken for the calculations of the optics of this line are the

characteristics of the beam at the object point of the α-spectrometer, where the beam arriving from CSS2 is achromatic with respect to both position and angle. These characteristics are :

Transverse emittances	$E_h = E_v = 5\pi$ mm.mrad
Transverse dimensions	$\Delta x = \Delta y = \pm 2.1$ mm
Transverse correlations	$\sigma_{21} = \sigma_{43} = 0$ (covariance matrix)
Energy spread	$\Delta W/W = \pm 0.5$ ‰
Max. magnetic rigidity	$B\rho = 2.88$ T.m
Max. beam power	$P \cong 6$ kW

For different emittances, the transverse dimensions are proportional to the square roots of the emittances.

The transverse dimensions expected for the beam at the production target are $\Delta x = \Delta y = \pm 2.5$ to 13 mm for emittances between 2.5π and 6π mm.mrad.

3.2.2. Optical structure of the line

The "production target-source" ensemble will be located in a shielded cave at the -3 m level with respect to the median ramp of the GANIL beam and shifted by the same distance with respect to the L3 line axis.

The beam, after a straight line traversal of the first dipole (L3D31) of the α-spectrometer, will go through an achromatic deviation system -having an anti symmetric plane- located on a plane inclined at 45° and included in a variable magnification system for ensuring the betatron matching on the target.

Although the structures corresponding to these two optical functions are overlapping, the adjustment of their parameters will be made independently within the limits of the line acceptance.

The advantage of this arrangement is to obtain on the production target a stable beam that is free from halo (which is important given the beam powers envisaged), while minimising the vertical beam envelope in the dipoles with a minimum number of parameters.

The achromatic deflection will consist of two magnetic dipoles separated by a quadruple triplet. The system ensuring the betatron matching will be made up of two quadrupole doublets upstream and downstream respectively of the deflection.

3.3. VERY LOW-ENERGY LINE

This line, consisting of six sections is divided into two main parts:

3.3.1. First part

Taking account of the beam characteristics starting from the extraction electrode

- characteristics that depend on the source adjustments - this part transports the beam up to the second part by mainly fulfilling two functions :
- Producing an "on-line" mass analysis
- Characterising the beam at the beginning of the second part.

It includes three sections :

Section 1 - Betatron adaptation at the object point of the spectrometer. The structure will be identical to that developed for the SIRa project (see appendix).

Section 2 - "On-line" achromatic mass spectrometer. It will be made up of two magnetic dipoles separated by a triplet of quadrupoles.

The first dipole, the analysing element ($\theta = 90°$, $\rho = 0.5$ m), will be double focusing. It will make it possible to obtain in its image focal plane a mass filter ($\delta m/m$) of $\pm 4.10^{-3}$ for a radial emittance of 80π mm.mrad. For this, it will be preceded by a sextupole compensating for the second order geometrical aberrations.

The second dipole will be a twofold to make it possible to transport the beam from a second source with similar optics. In addition, the beam from the first source will be able to traverse this dipole with being deflected, to be transported, if necessary, to an experimental area at the source energy.

Section 3 - Betatron matching at the object point of the second part. It will have a four quadrupoles structure.

The ensemble of this optics will have an acceptance of 150π mm.mrad. The maximum magnetic rigidity of this part will be at least 0.05 T.m. This value should be increased if it is wished to enlarge the mass spectrum to be measured.

3.3.2. Second part

This part makes up the axial injection of the cyclotron. With a structure similar to that of the GANIL CO1 injector, it will match the beam on the first acceleration orbit in a six dimensional phase space thus making it possible to reach injection yields of the order of 70 %.

The acceptance of the cyclotron is 80 πmm. mrad for the two transverse phase planes and $\pm 6°$ for the longitudinal phase extension.

The maximum magnetic rigidity is 0.05 T.m.

Assuming a Mueller-type hyperboloidal inflector, the solution presently selected, this part will include three sections (from 4 to 6) whose optical functions are :

Section 4 - Betatron matching and bunching.
Section 5 - Radial chromatic matching.
Section 6 - Vertical chromatic matching.
The magnetic components of these sections will be, respectively:
- Two quadrupole doublets for section 4.
- A dipole plus a triplet of quadrupoles for each of sections 5 and 6.
- A solenoid positioned in the cyclotron yoke for adjusting the rotation of the beam at the inflector entry, terminating section 6.

The bunching system has not yet been studied. It will have to allow to work with the 2nd, 3rd, 4th and 5th harmonics. Two systems can be envisaged :

- either an arrangement with two bunchers (similar to that constructed for the CO1 injector), with the second buncher working on the second harmonic of the first.

- or a single buncher giving saw-tooth modulation.

The two systems have essentially the same bunching efficiency but the changing of harmonics would be easier with the second.

The configuration of this line is still liable to be modified to take account both of the possibility of including a higher-performance in-line spectrometer in the first part (now being studied but not evaluated) and of the conditions of access at the cyclotron centre, which are related to the problems of supporting the yokes. The studies of these problems are not yet complete.

3.4. MEDIUM-ENERGY BEAM LINE

This line provides the transport of the beam from the exit from the cyclotron to the experimental area in being connected to the analytical section of the modified α-spectrometer.

3.4.1. Beam characteristics

The main beam characteristics planned are :
- Transverse emittances: $\varepsilon h = \varepsilon v \leq 10 \, \pi mm.mrad$
- Energy spread: $\Delta W/W \leq \pm 3 \, \%o$
- Maximum magnetic rigidity: $B = 2.35 \, T.m$

3.4.2. Optical structure of the line

It will include three optical sections fulfilling the following functions :
- Section 1 - Making the beam achromatic with respect to position and angle.
- Section 2 - Betatron matching of the beam at the object point of the spectrometer analysis section.
- Section 3 - Providing emittance and energy spread filtering and delivering an achromatic beam to the experimental areas.

The magnetic components of the first two sections are:
- two quadrupole doublets plus a dipole for section 1,
- two quadrupole doublets for section 2.

The connection to the α-spectrometer analysing section - section 3 - (figure 7) can be made in several ways. Two solutions are now being studied :
- either carry out a 45° rotation of the ensemble of the first two dipoles of the α-spectrometer,
- or use the second dipole of the α-spectrometer as the first dipole for the new line and replace it by a double magnet.

In addition, as the ensemble of the spectrometer becomes an achromatic system with an antisymmetric plane, there is an increase in the gradients of the triplet.

4 - MASS SELECTION

Three levels of mass selection are presently planned for SPIRAL :

a) At the source extraction energy:
A resolution in δ (Q/A)/(Q/A) of $\pm 4.10^{-3}$ will be given (the separating power is taken at $\pm 2\sigma$), for an emittance of 80 mm.mrad in the two transverse planes, by the spectrometer planned downstream of the source (cf. section 3-§3).

b) During the acceleration in the cyclotron:
In an isochronous cyclotron, the dephasing between two ions with different Q/A is, to a first approximation given by :

$$|\delta\varphi| = 2 \pi h N \delta (Q/A)/(Q/A)$$

h being the harmonic mode and N the number of turns.
As the separation condition is $|\delta\varphi| > \pi/2$ (the ion is then decelerated), the separating power of a cyclotron is approximately:

$$\delta (Q/A)/(Q/A) \leq 1 / (4 h N_T)$$

N_T being the maximum number of turns.
A more accurate study shows that in the case of the CIME cyclotron for which the total number of turns was fixed at $N_T \cong 250$, the separating power (inversely proportional to h) will vary from 1.5. to $3.5.10^{-4}$ over the range of planned harmonics (2- 3 - 4 and 5).

This result concerns only the separation of the central particles relative to each of the masses. The study of the contamination due to other particles in the bunch as well as that of the additional separation that the ejection system (deflector) could bring about, so as to have a more accurate estimate of the actual separating power of the cyclotron has yet to be carried out.

c) In the medium-energy line :
If necessary, if the separation given by the cyclotron is not sufficient and the beam is still contaminated, two alternatives are possible : either there are ions with the same Q/A but different A, or there are isobars.
- In the first case, a thin Al or C foil, with a thickness comparable to that of a stripping foil at the energy considered, will be completely effective for the sorting and the characteristics of the selected beam will be only slightly affected (to within the stripping yield).
- In the case of isobars, it will be made use of the difference of the energy losses of particles with different Z values in their traversal of the target, which is, of

necessity, thick. In this method which, for isobars of a given mass, is only applicable beyond a certain energy, the selected beam will have its characteristics degraded (reduced central energy and intensity, increased transverse emittances and energy spread). However, it will be possible to restore the initial beam qualities at the price of an additional loss of intensity.

The first estimation of the possibilities of this method for SPIRAL are shown in figure 40. In the most favourable cases, this method allows us to obtain a resolution of some 10^{-5}.
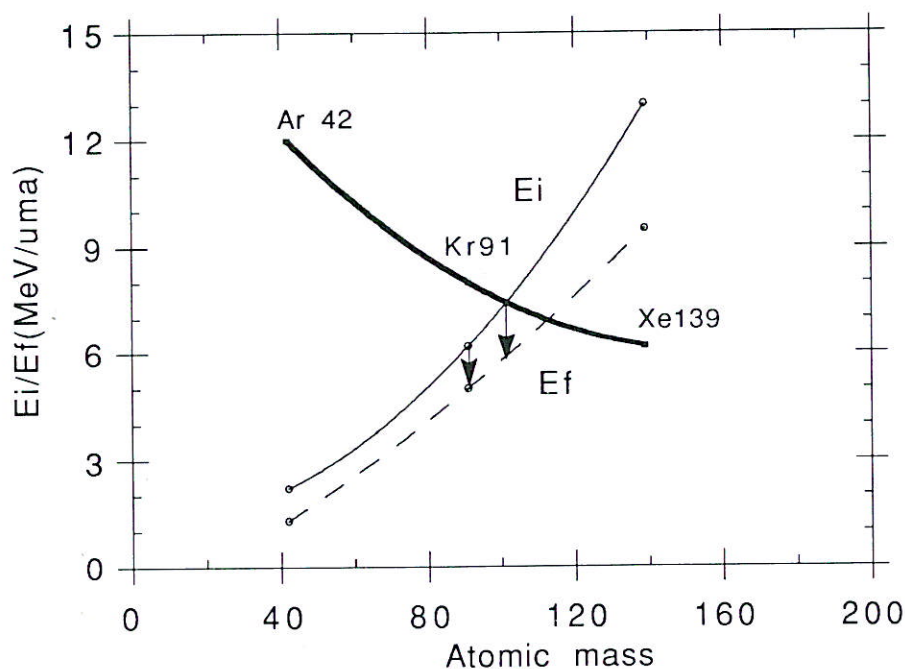

Figure 40 : Minimum incident energy, E_i, allowing the separation of isobars as a function of their mass and the beam energy, E_f, at the target exit.

In both cases the target is positioned at the object point of the α-spectrometer, this selects the desired ion, and if necessary restores the initial beam qualities.

The transmissions that are hoped to be achieved with the proposed system are given in Table VII.

Remark No. 1 :
In the configuration proposed above, the adjustment of the cyclotron should be ensured without any particular problem provided that the field topography is well known and controlled. This can be obtained either by acceleration at the same energy of a stable beam with a Q/A as close as possible to that of the desired beam or directly if there is sufficient knowledge of the trajectories.

Remark No. 2 :
Spectrometers with very high resolving power have been envisaged: a very sophisticated magnetic spectrometer of the type used at ISOLDE or an RF spectrometer as developed at the CSNSM and tested at CERN. However, the cost, the

complexity of the adjustments and the low transmission (for the emittances that we are considering) of these instruments have led us to eliminate them, as high transmission and very easy adjustment are primordial in the case of radioactive ions.

Remark No. 3 :

A new type of spectrometer has been proposed at GANIL and is now being studied. Depending on the results, it could be of interest to use it (in line but with the possibility of a by-pass) as a complement to the very low-energy spectrometer. It appears that it could provide greater facility in the adjustments of the cyclotron in particular by decreasing the number of species injected. Moreover, it could be of great interest to use it in the case where an experiment requiring the energy at the source would be desired (cf. section 3 § 3).

	Resolution $\pm \dfrac{\delta(q/m)}{q/m} * 10^{-4}$	%Transmission *		Beam characteristics	
		Partial	Total "ME"	E_h / E_v $\pi * mm * mrad$	$\pm \Delta W/W$ (‰)
Transport "TBE" from the analysis slits	40.0	80 - 90		80 / 80	0.5
Cyclotron (Inj.+ Acc +Extr.)	1.5 - 3.5	40 - 50		10 / 10	1 ($\delta\phi = \pm 3°$) 3 ($\delta\phi = \pm 6°$)
Experimental areas	"	90	30 - 40	"	"
Separation by ** "Energy loss (Spectro α)	≥ 0.3	3 - 60	1 - 25	$\leq 20 / \leq 20$	≤ 10

* The transmissions given assume that there are not any very major components in the selected range of masses.
** Method usable only for separating the isobars up to mass 100.

Table VII : Planned performances in the mass separation and transmission of the SPIRAL beam

5 - CHARACTERISTICS OF THE POST-ACCELERATED BEAM

Thereafter are summarized he beam characteristics which have, already been given for the most part in the preceding sections.

5.1. ENERGY RANGE

The range of energies that can be obtained is given as a function of Q/A of the accelerated ions in figure 15.

It is to be noted that the very low energies (h = 5; $2 \leq W \leq 4$ MeV/nucleon) are not continuously accessible for the light ions due to the large variation in Q/A between the charge states 1, 2 and 3 required for the masses A ≤ 35. This effect is shown in figure 41, for some typical ions. As a result, operation with the 5th harmonic which generally implies a marked decrease in the overall transmission of SPIRAL, will open only very narrow windows in energy below 2.7 MeV/nucleon for the light ions and will provide energies below the Coulomb barrier for the heavy ions.

5.2. INTENSITIES

The transmissions were given in the table (section 4). The intensities available in the experimental areas will depend on the ion production efficiency, on the acceptance of the cyclotron, and on the "Primary Beam - Target - Source" ensemble.

5.3. EMITTANCES

The results given below correspond to a first simulation carried out with the following assumptions :
- only the motion in the median plan was modelled assuming, in particular, the decoupling of the vertical and horizontal phase planes, which is not strictly correct,
- the initial beam characteristics taken at r = 50 cm are those measured at the exit of the GANIL CO1 injector, assumed to represent the central part of the "CIME" cyclotron, which appears quite realistic in the absence of a definitive study of the centre in 6 dimensions.

5.3.1. Beam extracted from the cyclotron

- Transverse emittances : $\qquad \varepsilon x \cong \varepsilon y \leq 10$ π.mm.mrad
- Longitudinal emittance:
  For $\Delta\varphi = \pm 3°$: $\Delta W/W = \pm 1$ ‰ and only 1 turn extracted (desired objective)
  For $\Delta\varphi = \pm 6°$: $\Delta W/W = \pm 5$ ‰ and 3 turns extracted ($\Delta W/W = \pm 5$ ‰)

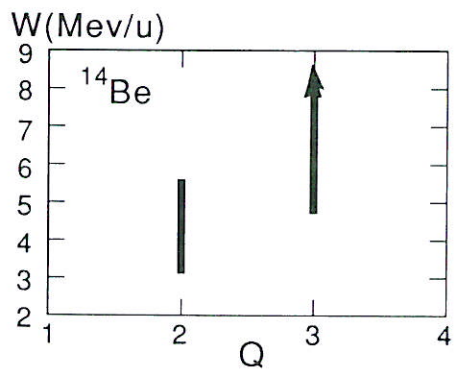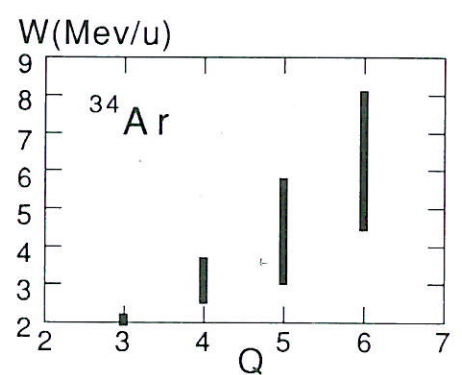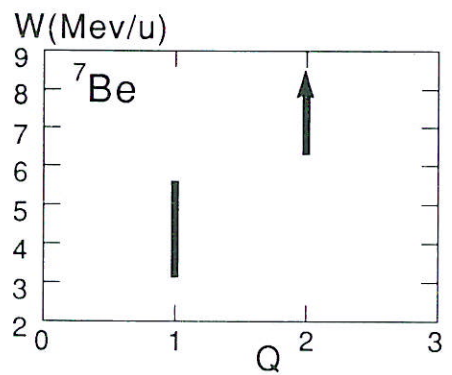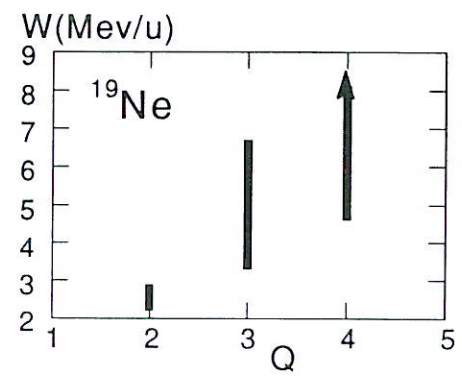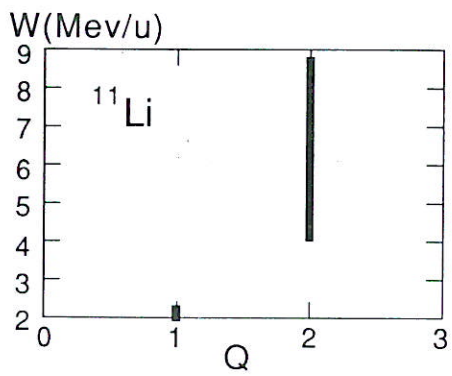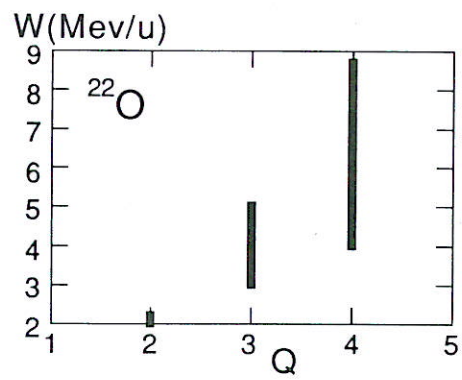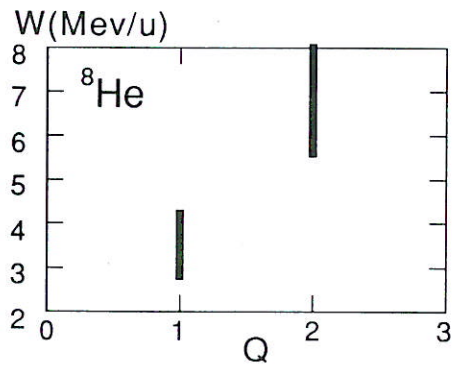Figure 41.

105

5.3.2. Beam delivered to the experimental areas

The spectrometer makes possible the integral transmission of the beam delivered by the cyclotron. However, it can be used, on the condition of a loss of intensity, to reduce the emittance in one or several phase planes.

Let us recall, that, if necessary, the isobar-sorting target will be placed at the object point of the spectrometer, as the spectrometer allows, in addition to restore the characteristics of the beam degraded by the passage through the target.

5.4. TIME STRUCTURE IN THE EXPERIMENTAL AREAS

- It will be possible to obtain a macrostructure by the use of a "bunch suppresser" placed in the beam line upstream of the cyclotron.
- The microstructure is determined by the bunch length (phase extension) at the injection in the cyclotron (± 3 or $\pm 6°$), by the HF frequency ($9.6 \leq F \leq 14.5$ MHz), by the harmonic number ($2 \leq h \leq 5$) and by the drift length between the cyclotron and the physics target.
Let us recall that the drift in a line is given by :

$$\Delta t = \frac{L}{4\pi r} \frac{\overline{h}}{f} \frac{\Delta W}{W}$$

with L, drift length and r cyclotron ejection radius.

For a target placed at 100 metres from the cyclotron and without limitation of emittance at the spectrometer the results for the two extreme energies are the following :

at 2 MeV/nucleon :	for = $\pm 3°$ t = ± 2.8 ns	at the period T = 95 ns
	for = $\pm 6°$ t = ± 13.8 ns	at the period T = 95 ns
at 25 MeV/nucleon :	for = $\pm 3°$ t = ± 0.7 ns	at the period T = 69 ns
	for = $\pm 6°$ t = ± 3.6 ns	at the period T = 69 ns.

5.5. MASS SEPARATION (THIS QUESTION IS DISCUSSED IN DETAIL IN SECTION 4)

6 - RADIATION PROTECTION AND SAFETY

The main radiation protection problems which arise in the SPIRAL project will be in the production cave where there will be the target and source with its extraction system. In fact, the primary beam with a power that can go up to 6 kW, will be completely stopped in the production target. The risks are of three different orders:

1) The "neutron" risk which is completely known and controlled at GANIL and for which we can easily calculate the shielding thicknesses required to obtain dose rates in conformity with the regulations. The calculations carried out for 3.10^{13} of ^{12}C at 100 MeV/nucleon (6 kW) beam show that in the beam direction it will be necessary to have a 4.5 m-thick wall of barytes concrete with a specific gravity of 3.4 to have an equivalent dose rate less than 25 $\mu Sv/h$ behind this shielding (controlled access zone).

In the direction perpendicular to the primary beam axis and for the same dose rate, the wall will have to be made of 1.75 m of the same material. The calculations of the sky shine show that the roof will require a protective layer of 1.25 m of ordinary concrete to give an equivalent dose rate in the limits of the site of less than 0.1 $\mu Sv/h$.

2) The "Gamma" risk is due to the radioactivity induced mainly in the target material by the primary beam. There are different charts given in the GANIL safety report which make it possible to predict the value of the expected dose rates as a function of the primary beam intensity, the target-projectile pair and the irradiation time.

It is already clear that these "hot" components will prohibit the access to this zone.

3) Due to the production of neutrons, the activation of the target and of parts of the source and the extraction system, there will be a contamination risk.

As a result, special care will have to be taken in the construction of this cave (e.g., smooth walls, ceiling and floor with easily decontaminable coatings).

The cave will have to be slightly below atmospheric pressure with a flow of clean air released outside through absolute filters. The pump exhaust will be released only after an initial filtration in a pressurised buffer reservoir followed by passage through an absolute filter system.

All the handling of the active target-source ensembles will have to be carried out with an automated remote controlled system. Every active component from this zone will be stored in the shielded room on the upper floor as long as necessary. Subsequently, the majority of these parts will be considered as radioactive waste and

transferred to the ANDRA[6] disposal sites. It will be possible to recuperate some slightly contaminated parts for further use after a thorough decontamination made in suitable facilities at GANIL.

4) A preliminary technical and cost-estimate study of the system for handling and transport of the active parts from the shielded cave was carried out by Mr. M. Barbier, formerly responsible for CERN radiation protection at Geneva and specialist in the problems of the radioactivity induced around particle accelerators. He is now director of a consulting firm in the nuclear protection field.

He proposes an arrangement designed on the basis of components in the catalogues of specialised manufacturers. It consists of a single travelling crane with two beams, a lift of 7 m and with two trolleys. It will be located in the shielded storage cave on the ground floor.

The first trolley will support the system for raising and replacing the circular hatch providing access to the basement from the ground floor. The second has a telescopic boom with a vertical travel on the order of 8 m. The gripping device, with rotary tongs for seizing and manipulating the different radioactive parts, is mounted at the end of this boom. Radiation-resistant video cameras and a remote control console will make it possible to monitor and direct all the operations.

[6] ANDRA : Agence Nationale pour la gestion des Déchets RAdioactifs

7 - CIVIL ENGINEERING AND SITE LOGISTICS

7.1. MACHINE BUILDING MODIFICATIONS

The work to be carried out does not affect the building itself and all of its present limits will be retained.

The necessity of using the primary beam at the very high intensity coming from CSS2 (6 kW maximum power) and of transporting the accelerated radioactive ion beam to the present GANIL experimental areas leads to installing the SPIRAL ensemble in the zone at the back of the building housing the accelerators. This is now partly occupied by the SPR, in particular for the storage and handling of intense sources for the calibration of detectors. The rest is used as an area for mechanical assemblies and the handling of radiation protection shields.

It was decided to construct initially only a single radioactive ion production station while reserving the room for a second. This option allows to use only the zone occupied by the SPR and leaves the shield handling area free. But this entails, in the immediate future, the construction of a storage area for the SPR, and later when the decision to equip the second station is made, to extend the machine building by a 12 m bay.

In order to minimise the volumes occupied, to position the CIME cyclotron as required (same median plane as the CSS and the beam lines) and to have containment of the radiological risks, it was decided :

- to excavate a 150 m^2 basement at - 3.25 m in the cyclotron zone,
- to excavate a 500 m^2 at -4.25 m for the other zones,
- to prepare these so as to be able to construct an independent block for supporting the CIME by using the same technique as for the CSS,
- to construct the highly shielded cave housing the production target and the ionisation source,
- to construct the technical installations for the distribution of the electric power and part of the power supplies for the target-source ensemble and the beam lines.
There is a space reserved for the installation of the second shielded target-source cave. This basement will be directly connected to the gallery which links the power house basement and the CSS shielded rooms, the electronics gallery as well as the experimental area gallery.

On the ground floor, there will be the CIME cyclotron shielded room with the radioactive beam transport line which is connected to the alpha spectrometer, and, above the radioactive-ion production zone, a shielded room which will be fitted as a temporary storage site for highly radioactive components from the target-source ensemble. The flooring of the latter will be 50 cm thick, a removable hatch will be fitted so as to allow access, using a remote-controlled system, to the target-source

zone for the handling and transport of radioactive components. The walls of the different rooms will be constructed with removable blocks and the ceiling with removable beams.

The civil engineering work does not present any particular problems since it makes use of well-tested standard techniques. It will have, however, repercussions on the operation of the accelerators and especially on that of CSS2 which will have to be stopped during the execution of the excavation work and the construction in the alpha spectrometer zone. To minimise the unavailability of the GANIL beams to the users, the work will have be carried out during a period which includes the winter shutdown . The work involving the emplacement of the mechanical system for displacing the first two magnets of the α-spectrometer should also be scheduled during this period.

7.2. ELECTRICAL SUBSTATION AND REFRIGERATION

7.2.1. Electrical substation

For the SPIRAL project, a power of around 1000 kVA is available on one of the transformers 20/0.4 kV located in the building so-called "bâtiment énergie".
The highest estimate of the power required for the SPIRAL project is 500 kVA.
Therefore, a power reserve of 500 kVA will be available for future extensions.
For the equipments sensitive to perturbations of the 90 kV power line supplied by EDF, we will need two additional inverters with booster battery :
  - the first (20 kVA) for the radiation protection equipements,
  - the second for all other equipments (electronic racks, etc...). Its power is still to be determined.

The installation of the switching station (TGBT) and the inverter will make possible constant access to these without intervention of the SPR for facilitating their maintenance and repair.

Particular care will have to be taken with respect to the operation of the emergency stops for the safety of the personnel in the INB zone.

7.2.2. Refrigeration circuits

The magnets, the RF accelerator cavities and the power supplies require cooling circuits with demineralised water under pressures of 8 and 15 bars.

Due to the positioning of the CIME cyclotron and the supply rooms, it will be possible to make connections to the N° 2 (8 bars) and N° 4 (15 bars) circuits, which supply the ensemble of the equipment in the experimental areas. These circuits have sufficient reserves to meet the estimated requirements and the conduits pass through the gallery connecting the basements of the power house, the CIME and the experimental areas.

However, for the No. 2 circuit it will be necessary to change the temperature control valves in the refrigeration building to meet the HF quality and stability requirements.

APPENDIX

DESCRIPTION OF THE SIRa SEPARATOR

1) The target source ensemble

The target cube is now being studied at Orsay: an internal mechanism will allow the automatic withdrawal of the transfer tube from the ECR source by closing 3 isolating valves (due to contamination risks). Thus the target will be kept under vacuum in a limited volume, with the ensemble being easy to handle.

The first source installed in SIRa will be a Caprice-type standard ECR source operating at 10 MHz which is already available at GANIL.

A new source-target ensemble is being studied, it could be installed in D2 in the second half of 1994.

2) The primary beam line

The quadruplet existing since the start in room D2 (only modification : the second doublet has been moved by 1 m towards the target) makes it possible to obtain a nearly parallel high-energy beam on the target: the spot radius can be modulated from 2.5 to 12.5 mm for emittances between 2.5 and 6π mm mrad.

Two horizontal and vertical steering magnets are positioned at the exit of the quadruplet as well as a profile monitor. Another one is positioned before the target as well as a Faraday cup.

3) The secondary-ion beam line

The maximum magnetic field produced by the analysing dipole can give limits the magnetic rigidity of the beam to 0.136 T.m.

Emittances in their principal axes of $150\ \pi$ mm.mrad- corresponding to the line acceptance - and dimensions of ± 3 mm are taken as initial conditions at the source puller.

The on-line isotope separator includes three sections:

a) The matching section

This is composed of the following magnetic elements :
- a solenoid positioned closest to the source, intended to take up the beam and make it parallel,

- a triplet of quadrupoles as close as possible to the object point O of the analysing magnet.

The distance between the solenoid and the triplet is adjusted depending on the longitudinal size of the source used.

This section, which includes four independent focusing parameters, allows to adjust the radius at the point O between ± 1.5 and ± 10 mm.

The characteristics of the elements are :

Solenoid	
Maximum field	6800 G
Magnetic length	400 mm
Bore diameter	70 mm

It is identical to the yoke solenoid of the axial injection in CO1 but equipped with an iron frame.

Quadrupoles	
Maximum gradient	3.5 T/m
Magnetic length	210 mm
Bore diameter	80 mm

They are identical to the CO1 axial injection quadrupoles: each one contains a dipolar component that is either horizontal or vertical allowing the steering of the beam.

b) The analysis section

It includes :
- the 102° dipole of the previous separator used in this line with a deflecting angle of 90°; a new vacuum chamber was constructed and a set of magnetic measurements made it possible to ascertain the optical parameters of the dipole ; the values of the entry and exit wedge angles show that the dipole is double focusing ($\tan (\varepsilon_i) = \tan (\varepsilon_s) = 1/2$),
- a sextupole placed at 230 mm upstream of the entry of the dipole and intended to correct the second order geometrical aberrations,
- a diagnostics box with radial slits defining the object point O at 830 mm from the entry point of the dipole; these slits as well as the vertical slits allow to eliminate part of the charge states not having the magnetic rigidity for which the line is adjusted, a profile monitor is placed just downstream of these slits,
- a special diagnostics box placed around the image point I (at 830 mm from the exit point of the magnet) containing :
 . adjustable radial slits moving in the focal plane inclined at 27° with respect to the axis,
 . a wire positioned before these slits that can be displaced parallel to the focal plane for rapid acquisition of the ion distribution spectrum,
 . a profile monitor, also parallel to the focal plane, just behind the slits,
 . a faraday cup.

Calculation of the resolution

It was evaluated using the ZGOUBI [MEO93] program for emittances in the main axes of 80 π mm mrad, a radial object 0 ± 13 mm and a vertical object of ± 6.2 mm. 200 particles were taken at random in the 4 dimensional hyperellipsoid defined below and each one assigned a relative shift in momentum of 0, - 2 ‰ and + 2 ‰; therefore a total of 600 particles were plotted in a field map measured for a 2500 G field. The histograms obtained with and without the sextupole are given in figures 41 a and b, they show that a mass resolution of ± 4 ‰ can be reached (we recall that $\delta m/m = 2 \, \delta p/p$).

A better resolution can be obtained, at the detriment of the intensity, by carrying out a matching with a low radial angle at the object point and by redefining the size of this object with the radial slits.

The characteristics of the elements are :

Analysing dipole	
Maximum field	3400 G
Radius of curvature	400 mm
Gap	70 mm
Pole face rotation (entrance and exit)	27°
Horizontal size of the vacuum chamber at the middle of the dipole	± 120 mm

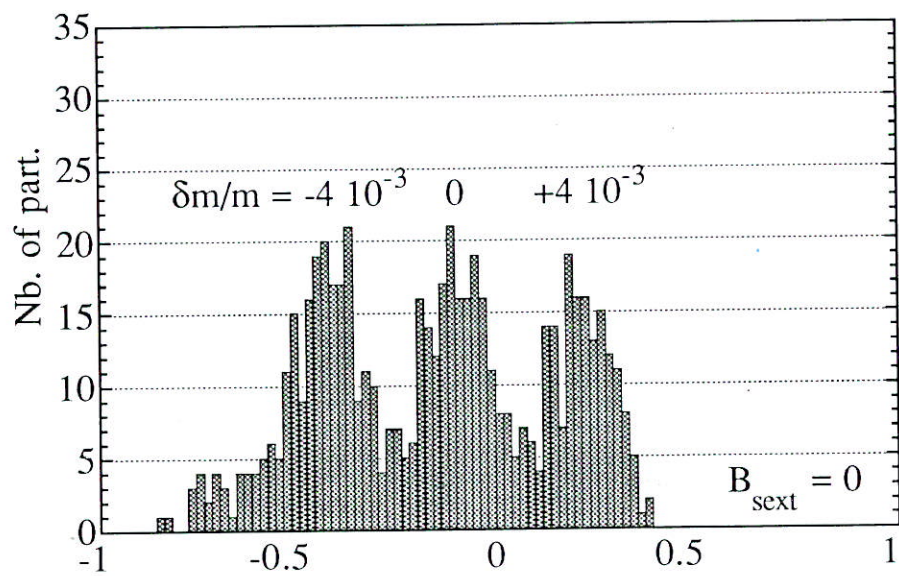| Sextupole	
Maximum field	700 G
Magnetic length	170 mm
Bore diameter	140 mm

c) The transport section up to the detector

The transport of all the emittance is ensured by a doublet then a triplet of electrostatic quadrupoles on the detector D placed outside of the wall of the room D2. The diameter of the spot in D is 10 mm; it is moreover possible to be achromatic only with position at this point.
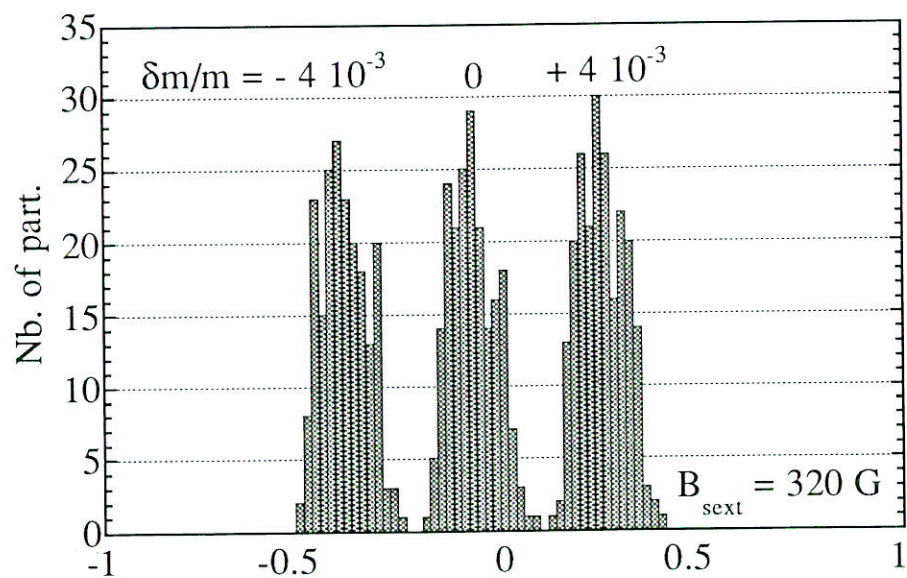
As the electrodes of a quadrupole may be independently polarized, vertical and horizontal steering can be carried out.

The characteristics of these electrostatic quadrupoles are :

Electrostatic quadrupole	
Maximum voltage	2.5 kV
Electric length	210 mm
Bore diameter	110 mm

a : Histogram showing the mass resolution without the sextupole

b: Histogram showing the mass resolution with the sextupole

Figure 42.

REFERENCES

[ALE90]   K. Aleklett et al, Phys. Lett. B236 (1990), 404.
            W. Loveland et al, Phys. Rev. C41 (1990), 973.

[ANN93]   R. Anne et al, GANIL preprint A93 05, presented at the Particle
            Accelerator Conference, Washington (USA) May 1993.

[ANN93]   R. Anne et al, GANIL preprint A93 02, presented at the Int.
            E.C.R.I.S. Conf., Groningen (Pays-bas) May 1993..

[BER93]   P. Bertrand, GANIL Report R93 08

[BER93]   P. Bertrand et al, Internal GANIL Report 93/Dev/19.

[BJO81]   Bjorstad et al, Z. Phys. C41 (1990).

[BOU93]   M.P. Bourgarel et al, NIM A328 (1993), 321.

[CHA93]   A. Chabert et al, GANIL Report R93 10.

[DOM90]   M. Domdsky et al, NIM A295 (1990), 291.

[DOU92]   H. Doubre, Proc. "Franco-japanese colloquium.6" (1992), 370.

[EIS92]   Proc. of the Int. Conf. on Electromagnetic Isotope
            Separators and Techniques Related to their Applications,
            Sendai (Japan) 1991, NIM B70 (1992).

[ERB93]   Proposals in "European Radioactive Beams
            Facilities" NUPECC Report, May 1993.

[ECR90]   R. Geller, Ann. Rev. Nucl. Part. Sci. 40 (1990),15.
            P. Decrock et al, Int. Workshop on the Physics and
            Tecniques of secondary Nuclear Beams, Dourdan (France), 1992,
            eds : J.F. Bruandet, B. Fernandez and M. Bex.

[FUJ81]   M. Fujioka et al, NIM A186(1981), 409.

[JOU93]   A. Joubert et al, GANIL preprint A93 04, presented at the Particle
            Accelerator Conference, Washington, May 1993.

[KIR92]   R. Kirchner, NIM B70 (1992),186.

[MEO93]   ZGOUBI users guide F. Méot and S.Valéro
            Saturne LNS/GT/93-10.

[MUE89]   A.C. Mueller and R. Anne, Proc. of Radioactive
            Nuclear Beams Conference, California (USA) 1989,
            eds. : W.D. Myers, J.M. Nitschke and E.B. Norman.

[RAV93]   H.L. Ravn et al, CERN PPE/93-10.

[SAI82]   M. de Saint Simon et al, Phys. Rev. C86 (1992), 2447.